ISSN 1331-1611
9 771331 161005

KoG

SCIENTIFIC - PROFESSIONAL JOURNAL
OF CROATIAN SOCIETY FOR GEOMETRY AND GRAPHICS

No. 29. (2025)
ISSN 1331-1611

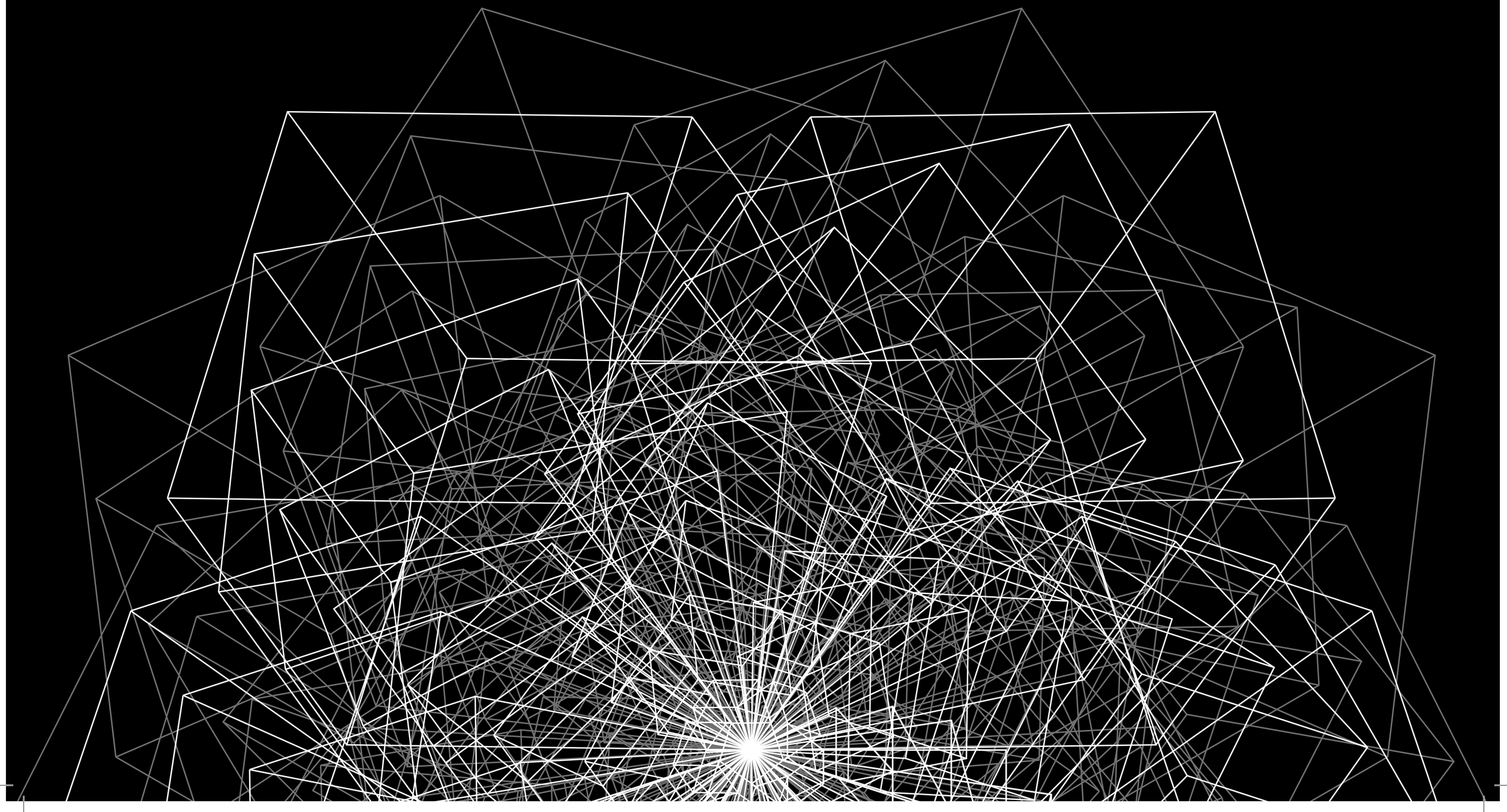

Official publication of the Croatian Society for Geometry and Graphics publishes scientific and professional papers from the fields of geometry, applied geometry and computer graphics.

Founder and Publisher

Croatian Society for Geometry and Graphics

Design

Miroslav Ambruš-Kiš

Layout

Sonja Gorjanc, Ema Jurkin

Cover Illustration

Iva Kodrnja

Print

SAND d.o.o., Zagreb

URL address

http://www.hdgg.hr/kog
http://hrcak.srce.hr

Edition

150

Published annually

Guide for authors
Please, see the page 81.

KoG is reviewed by zbMATH and Scopus.

This issue has been financially supported by the Ministry of Science, Education and Youth.

https://doi.org/10.31896/k.29.1
Original scientific paper
Accepted: 9 July 2025

HELLMUTH STACHEL
GUNTER WEISS

Stellae Octangulae in Motion Revisited

Stellae Octangulae in Motion Revisited

ABSTRACT

It is well-known that two congruent regular tetrahedra T_1 and T_2 forming a Stella Octangula allow a continuous motion of T_2 relative to T_1 such that each edge of T_2 slides along an edge of T_1. Recently the same property has been confirmed for pairs (T_1, T_2) of indirect congruent tetrahedra of general form. It turns out that this overconstrained kinematical systems admits besides some special one-parameter motions also two-parameter motions. We provide a synthetic analysis of the problem. Based on involved quadrics, we study in depth the two-parameter motions and their boundaries. Moreover, we present some generalizations of Stellae Octangulae.

Key words: tetrahedron, Stella Octangula, Euclidean motion, two-parameter movements

MSC2020: 51N20, 51N30

Zvjezdasti oktaedari (Stellae Octangulae) u pokretu – ponovno razmatranje

SAŽETAK

Dobro je poznato da dva tetraedra T_1 i T_2 koji tvore zvjezdasti oktaedar (Stella Octangula) dopuštaju neprekidno gibanje tetraedra T_2 s obzirom na tetraedar T_1 takvo da svaki brid tetraedra T_2 klizi duž brida tetraedra T_1. Nedavno je isto svojstvo potvrđeno za parove (T_1, T_2) indirektno sukladnih tetraedara općeg oblika. Pokazuje se da taj prenapregnuti kinematički sustav, osim nekih posebnih jednoparametraskih gibanja, dopušta i dvoparametarska gibanja. Dajemo sintetičku analizu problema. Na temelju uključenih kvadrika detaljno proučavamo dvoparametarska gibanja i njihove granice. Osim toga, predstavljamo neka poopćenja zvjezdastih oktaedara.

Ključne riječi: tetraedar, zvjezdasti oktaedar (Stella Octangula), euklidsko gibanje, dvoparametarski pomaci

1 Introduction

As reported in [8], during the assembly of a physical model of the classical Stella Octangula in 1982, L. Tompos Jr. discovered the relative movability of two regular tetrahedra T_1, T_2 with permanent edge-contacts. Note that at this physical model one tetrahedron encloses the other, and the exterior tetrahedron consists of edges only (Figure 1).

Though generically six edge-contacts fix the pose of one tetrahedron relative to the other, in the case of regular tetrahedra T_1, T_2 one tetrahedron can slide along the other such that each edge of T_1 keeps contact with an edge of T_2. According to [11] in 1988, this overconstrained kinematic structure admits four one-parameter motions and three two-parameter motions that all share the initial Stella-Octangula pose.

Later the question arose, whether the regular Stella Octangula is the only one with movable tetrahedral parts. Answers were given in [8, 12, 13]: Starting with a generalized

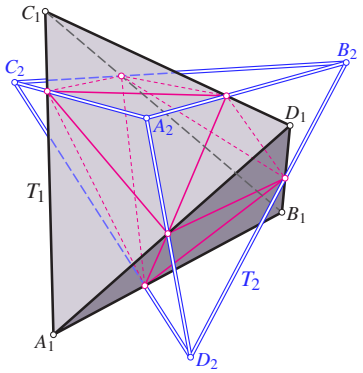

Figure 1: *Two congruent regular tetrahedra T_1 and T_2 with crossing edges, i.e., with six edge-contacts. The magenta lines represent the octahedron $O = T_1 \cap T_2$*

Stella Octangula consisting of congruent tetrahedra T_1 and T_2, one was looking for an at least one-parameter motion of T_2 relative to T_1, where the six edge-contacts are preserved.

In [8], the authors describe analytically six distinct types of such constrained motions in the case where the convex hull of the Stella Octangula is a box, i.e., a rectangular parallelepiped. Most of these motions are rotations about axes in particular position relative to the given box.

Below we present a synthetic approach, where one-sheeted hyperboloids of revolution and orthogonal hyperbolic paraboloids play an essential role. After discussing some basic properties of such pairs of tetrahedra, we analyse in the Sections 3 and 4 two special cases, namely two congruent right three-sided pyramids and, in alignment with [8], equifacial tetrahedra. As main topic, we focus in Sections 5 to 6 on generic tetrahedra T_1 and their indirect congruent copies T_2. For tetrahedra with acute-angled faces and others, there exist even two-parameter motions of T_2 against T_1 that preserve all edge-contacts. We study necessary and sufficient conditions and the boundaries of these motions. Moreover, we describe included one-parameter movements where all points' trajectories are located in parallel planes. Similar to the generalizations presented in [8], we finally provide in Section 7 further examples.

2 Basic properties of two tetrahedra with six edge-contacts

For the sake of simplicity, we introduce the following notion.

Definition 1 *Two tetrahedra T_1 and T_2 are said to have* crossing edges*, if they have six mutual edge-contacts and each contact point is an interior point of both involved edges.*

With regard to a generalization of the cube circumscribed to a regular Stella Octangula, we can state:

Lemma 1 *Two tetrahedra T_1 and T_2 have crossing edges if and only if their convex hull $\mathcal{H}$ is a convex cuboid, i.e., a hexahedron with six quadrangular faces.*

Proof. The vertices of two tetrahedra T_1, T_2 with crossing edges are already the eight vertices of their convex hull $\mathcal{H}$. Each of the six faces of $\mathcal{H}$ has a pair of intersecting edges as diagonals.
Conversely, the two tetrahedra T_1, T_2 arise by truncating the cuboid $\mathcal{H}$ in the way that the edges of the tetrahedra are diagonals of the faces of $\mathcal{H}$. At a convex cuboid each quadrangular face is convex, too, so that the point of intersection between the two diagonals is an interior point of the edges, as required in Definition 1. □

The following lemma can be seen as a dual counterpart.

Lemma 2 *If two tetrahedra T_1 and T_2 have crossing edges, then the intersection of the solids $O := (T_1 \cap T_2)$ is a convex octahedron. Conversely, each convex octahedron O is the intersection of two tetrahedra with crossing edges, but not all tetrahedral vertices need to be finite.*

Proof. The intersection O of the two convex solids T_1 and T_2 must be convex, too. Each of the eight faces of T_1 or T_2 intersects the other tetrahedron along a triangle with vertices at the coplanar contact points. Thus, the six contact points are the vertices of O (see Figure 1).
Conversely, the eight bounding planes of any convex octahedron O can be separated into two quadruples such that any two planes ε, φ of the same quadruple contain octahedral faces that share exactly one vertex. The line $\varepsilon \cap \varphi$ must be a (proper) support line of O, i.e., it meets O only at a single point since otherwise, due to the convexity of O, the octahedral faces in ε and φ would share a line segment.
Each bounding plane ε contains a triangular face of O. Let us assume that the four planes of the quadruple through ε have a point P in common. Then ε intersects the three remaining planes along lines that connect P with the coplanar vertices of O. At least one of them cannot be a (proper) support line of O as it meets the closed triangular face along a line segment. This contradiction with our assumption reveals, that each quadruple defines a tetrahedron, provided that also vertices at infinity are admitted. □

2.1 A kinematic analysis

Suppose that T_1 and T_2 are two tetrahedra with crossing edges. Each single edge-contact reduces the degree of freedom ('dof', for short) of T_2 relative to T_1 by 1. Therefore, the Chebychev-Grübler-Kutzbach formula yields $\text{dof} = 0$. In other words, T_1 is generically rigid relative to T_2. The following kinematical statement shows that in general T_1 is even infinitesimally rigid relative to T_2.

Theorem 1 *Given two tetrahedra T_1, T_2 with crossing edges, let P_i for $i = 1, \ldots, 6$ be the six points where an edge e_{i1} of T_1 meets an edge $e_{i2} \subset T_2$. Then T_2 is infinitesimally movable relative to T_1 if and only if the six perpendiculars n_i through P_i to the planes spanned by e_{i1} and e_{i2} belong to a linear complex of lines.*

Remark 1 *By virtue of Lemma 1, the contact points P_i are the crossing points of the diagonals in the quadrangular faces of the convex hull $\mathcal{H}$, and the normals n_i at P_i are orthogonal to the faces.*

Proof. The tetrahedron T_2 is *infinitesimally movable* relative to T_1, if and only if one can assign to each point attached to T_2 a velocity vector such that for any two points X, Y their mutual distance remains infinitesimally constant, i.e., for the respectively assigned velocity vectors $\mathbf{v}_X, \mathbf{v}_Y$ the difference vector $\mathbf{v}_X - \mathbf{v}_Y$ is perpendicular to the line XY.[1] This is equivalent to the statement that for all points X in space the lines through X orthogonal to $\mathbf{v}_X$ belong to a linear complex of lines (see, e.g., [1, p. 162] [3, p. 292] or [6, p. 219]). The axis of this linear complex coincides with the instantaneous screw axis of the motion of T_2 against T_1.
Suppose that there exists such an infinitesimal motion of T_2 relative to T_1. Then, in order to preserve the edge-contact between e_{i1} and e_{i2}, the velocity vector $\mathbf{v}_i^r$ of the point of contact P_i relative to T_2 must be parallel to e_{i2}, while relative to T_1 the velocity vector $\mathbf{v}_i^a$ of P_i is parallel to e_{i1}. The edge-contacts preserving motion of T_2/T_1 assigns to P_i the velocity $\mathbf{v}_{P_i} = \mathbf{v}_i^a - \mathbf{v}_i^r$ ('absolute' minus 'relative') parallel to the plane connecting e_{i1} with e_{i2}. Consequently, the line n_i through P_i and orthogonal to e_{i1} and e_{i2} belongs to the linear complex of path-normals. This argumentation works also in the converse direction. □

It needs to be noted that the characterization presented in Theorem 1 makes no difference whether the meeting point between e_{i1} and e_{i2} lies on the edges or outside on the extending lines.

Remark 2 *Referring to Theorem 1, let the set of linear line complexes through the six perpendiculars n_i, $i = 1,\dots,6$, be one- or two-dimensional. Then the local dof of infinitesimal motions of T_2 relative to T_1 equals two or three.*

If T_2 is continuously movable against T_1 like in the regular case, then it is infinitesimally movable in each pose. In particular, in the regular Stella-Octangula pose, the six path normals $n_1,\dots,n_6$ coincide with three mutually orthogonal diameters of a regular octahedron O. This implies that even each infinitesimal spherical motion of T_2 about the common center O preserves all edge-contacts with T_1 since $\mathbf{v}_O = \mathbf{0}$.

In the following sections we only focus on pairs of **congruent** tetrahedra (T_1, T_2) with crossing edges. This means that in each pose of T_2 relative to T_1 there is a displacement $\alpha\colon T_1 \to T_2$. We recall from the classification of congruences in the Euclidean 3-space (see, e.g., [10]): If α is orientation preserving, then it is either a translation or a rotation or screw motion. Otherwise, α is either a reflection in a plane σ or the commutative product of this reflection with a translation parallel to σ or with a rotation about an axis orthogonal to σ. The only involutive displacements are reflections in a point, in a line or in a plane; only the second one is orientation preserving.

3 Stellae Octangulae formed by right three-sided pyramids

Let T_1 and T_2 be two congruent right three-sided pyramids in a Stella-Octangula position, i.e., with edge-contacts at all midpoints of edges (Figure 2, top). Then there exists a one-parameter motion with permanent edge-contacts while the axes of rotational symmetry are coinciding in the line a which is supposed to be vertical. This mobility arises from the case of regular tetrahedra treated in [11] by an affine transformation, an appropriate scaling along the axis a. But this time we move simultaneously both tetrahedra T_1 and T_2, while the common axis a and two planes of symmetry between T_1 and T_2 remain fixed, namely one plane φ_0 orthogonal to a, hence horizontal, and the other φ_1 passing through a. Therewith, the two tetrahedra remain symmetric with respect to (w.r.t., for short) a fixed axis, the intersection $s = \varphi_0 \cap \varphi_1$ of the two planes of symmetry (see Figure3).

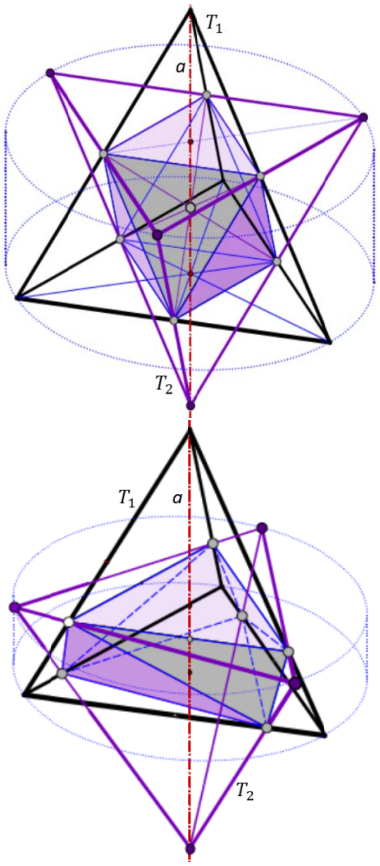

Figure 2: *Stella Octangula consisting of two right tetrahedra T_1 and T_2 in the highly symmetric start position (top), and in an intermediate position (bottom).*

[1] Throughout the paper, XY denotes the line connecting the two points X and Y, while the symbol $[XY]$ stands for the segment bounded by X and Y.

During this one-parameter motion, one vertex of each tetrahedron moves on the axis a, while the other vertices trace algebraic curves on a coaxial cylinder (see Figure 4). The octahedron O of contact points shows up in form of an antiprism with regular triangles as base and top face (see Figure 2, bottom). In the initial pose the six remaining faces are congruent isosceles triangles.

For a detailed analysis of the movements of the two pyramids we denote the vertices of the basis of T_i with A_i, B_i, C_i and the apex with D_i, $i = 1, 2$. We introduce cylinder coordinates with the vertical altitude a as z-axis, with the origin O in the fixed plane φ_0 and the zero-direction along s in the fixed plane φ_1 and pointing to the right in Figure 3. The circumcircles of the base triangles of the two coaxial tetrahedra T_1 and T_2 are assumed as unit circles.

Let $(1, \alpha, -h_\alpha)$ be the cylinder coordinates of A_1 and $(1, -\alpha, h_\alpha)$ that of A_2. Then, the point of intersection P_1 between the edges $[A_1D_1]$ and $[A_2B_2]$ (see Figure 3) has coordinates (ρ, α, h_α). The point of intersection $Q = \varphi_0 \cap A_1D_1$ gets – because of $\overline{QA_1} = \frac{1}{2}(1-\rho) =: \overline{\rho}$ – the cylinder coordinates $(1-\overline{\rho}, \alpha, 0)$, where

$$\rho = \frac{1}{2\cos(\pi/3 - 2\alpha)}, \quad \overline{\rho} = \frac{\cos 2\alpha + \sqrt{3}\sin 2\alpha - 1}{2(\cos 2\alpha + \sqrt{3}\sin 2\alpha)}, \quad \text{for} \quad 0 \le \alpha \le \pi/3. \tag{1}$$

The choice $\alpha = \pi/6$ yields the Stella-Octangula position. For $\alpha = 0$ the two tetrahedra are placed face to face sharing the base triangles.

If h denotes the altitude of the two pyramids, then follows from the proportion $h : (h - 2h_\alpha) = 1 : \rho$

$$h_\alpha = h \cdot \overline{\rho}, \tag{2}$$

and furtheron with $t := \tan\alpha$ the algebraic expression

$$h_\alpha(t) = h\,\frac{t\,(2\sqrt{3} - t)}{2(1 + 2\sqrt{3}\,t - t^2)}, \quad 0 \le t \le \sqrt{3}. \tag{3}$$

The trajectory c_{A_1} of A_1 has the cylinder coordinates $(1, \alpha, -h_\alpha(t))$ by (3).

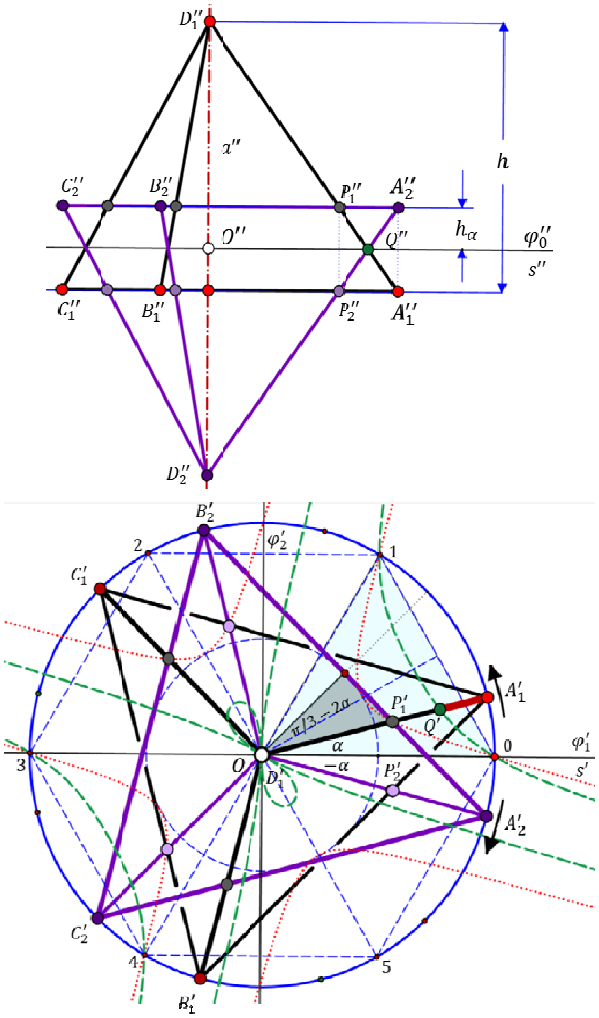

Figure 3: *Front- and top-view of the right pyramids T_1 and T_2 from Figure 2. Here both, T_1 and T_2, translate symmetric to the plane φ_0 along a through h_α, while rotating about a in opposite directions through α. The top-view (bottom) shows the images of the paths of the contact points P_1 (red) and Q (green) without restriction to the parameter interval $0 \le \alpha \le \pi/3$.*

Theorem 2 *Two congruent right three-sided pyramids T_1 and T_2 admit a one-parameter relative motion with six permanent crossings while the axes of symmetry of the two pyramids coincide.*

Remark 3 *Since in each pose the pyramid T_1 is symmetric to T_2 w.r.t. the axis $s = \varphi_0 \cap \varphi_1$, the relative motion T_2/T_1 is a* symmetric roll-sliding *as studied by J. Krames in [7]. The locus of s relative to T_1, called base surface, is the right conoid defined by the equation $z = h_\alpha(\alpha)$ according to eqs.* (2) *and* (1).

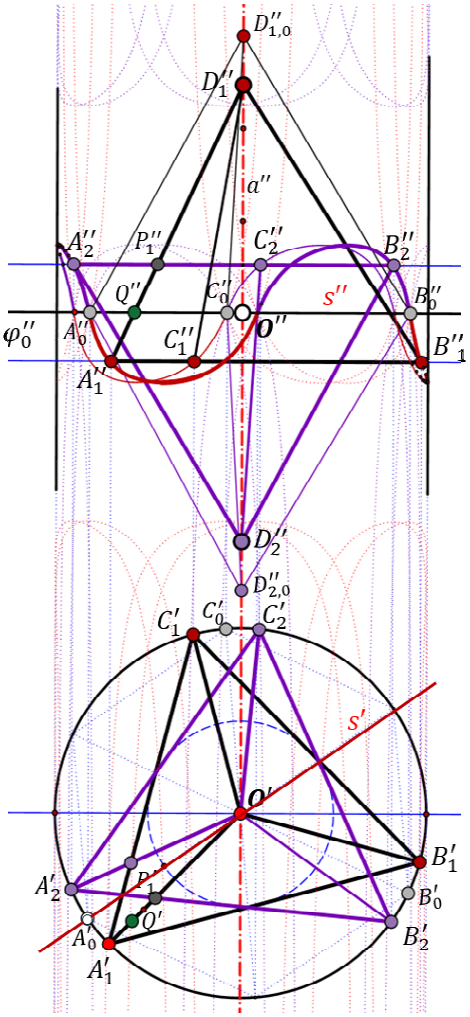

Figure 4: *Top- and front-view of intermediate positions of the right pyramids T_1 and T_2, together with the trajectories of the vertices of T_1 and T_2, shown as formally closed curves on the unit cylinder with axis a (red: paths of vertices of T_1, purple: paths of vertices of T_2).*

In each pose, the reflection in s exchanges T_1 and T_2. Therefore, s is also an axis of symmetry of the octahedron $O = T_1 \cap T_2$ with vertices at the contact points (see Figure 2). This symmetry exchanges in particular the regular triangles, along which each tetrahedron intersects the base of the other and which is inscribed in this base.

If the tetrahedra T_1 and T_2 are regular, then we have four possibilities to choose an axis a and a fixed plane φ_0 for performing the one-parameter motion described above. So the question arises, whether these in fact independent motions can be embedded in a two-parameter motion. However, according to [11] this is not the case.

4 Stellae Octangulae formed by equifaced tetrahedra

Now the initial Stella Octangula is formed by the two tetrahedra T_1 and T_2 that can be inscribed in a rectangular box $\mathcal{H}$ (Figure 5, top). This case was also extensively studied in [8].

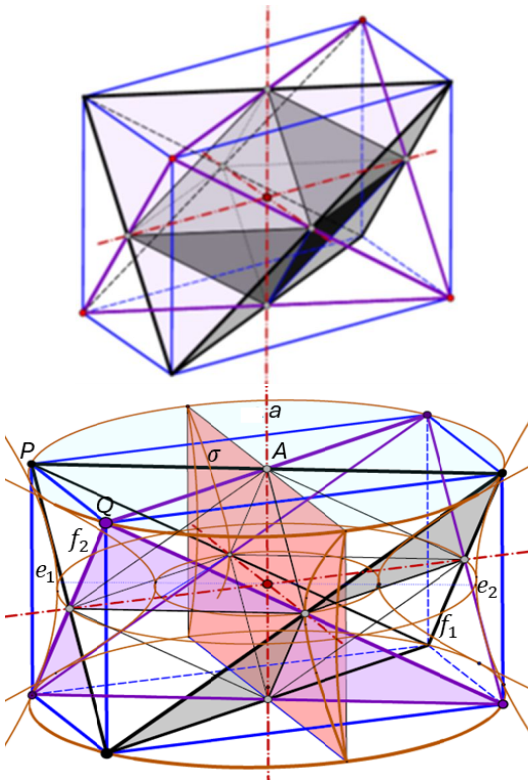

Figure 5: *The Stella Octangula based on equifaced tetrahedra T_1 and T_2 has a rectangular box as convex hull (top). The contact points form an equifaced octahedron. Edges of T_1 that are skew to the vertical diameter a are generators of two hyperboloids of revolution with axis a.*

The two tetrahedra are *equifaced* (or *isosceles*), i.e., all faces are congruent (see, e.g., [5]). The reflection in the center O of $\mathcal{H}$ as well as the reflections in a diameter plane σ parallel to one face of $\mathcal{H}$ exchanges T_1 and T_2 (Figure 5, bottom). Every edge of T_1 has a parallel counterpart at T_2. Reflections in the three mutually orthogonal axes of symmetry of the box $\mathcal{H}$ send each tetrahedron onto itself.

The convex octahedron $O = T_1 \cap T_2$ is equifaced with diagonals parallel to the edges of the box $\mathcal{H}$. We keep one diagonal a of O fixed and assume that a is vertical as shown in Figure 5, bottom. Now we focus on the quadrangle of edges of T_1 that are skew to a.

Two extended opposite edges of this quadrangle are generators of the same regulus of a hyperboloid of revolution Φ_1 with the axis a. The other pair of edges defines a second coaxial hyperboloid of revolution Φ_2. If we reflect T_1 in any plane σ through a, then Φ_1 and Φ_2 remain fixed while the two reguli are exchanged. The tetrahedron T_1 is sent to a pose T_2, where each extended edge of T_2 intersects an extended edge of T_1. Two of these edge-contacts are fixed on a; the other four are intersections between generators of different reguli of one of the hyperboloids.

For a suitably chosen σ all intersection points are indeed inner points of the edges. Thereby "suitably" means that the plane σ through a must be chosen within a restricted angle-interval to ensure that it intersects the edges at inner points. For example, in Figure 5, bottom, this angle interval equals $\sphericalangle PAQ$, provided that PQ is a shorter side in the top rectangle of $\mathcal{H}$. If T_1 remains fixed while σ rotates around a within that angle interval, then T_2 performs a continuous rotation about a.

Since there are three possibilities to choose the axis a, we can recall from [8]:

Theorem 3 *The Stella Octangula based on equifaced tetrahedra T_1, T_2 allows three one-parameter motions of T_2 against T_1 that preserve the six crossings. The relative motions T_2/T_1 are terminated rotations about the common perpendiculars of opposite edges of T_1.*

In the initial position, the octahedron O of contact points is centrally symmetric with mutually orthogonal diagonals (see Figure 5, top). In the other poses O has a pair of skew, but mutually orthogonal horizontal diagonals. They are orthogonally intersected by the axis a being the third diagonal (see Figure 6). Note that parallels of these diagonals through the center O are the axes of line reflections that exchange T_1 with T_2.

Can we generalize the statement of Theorem 3? Can also other lines a through the center of the box $\mathcal{H}$ serve as axes of rotations that preserve the six edge-contacts between T_1 and T_2 in the Stella-Octangula pose?

Two parallel lines are generators of a one-sheeted hyperboloid of revolution with axis a if and only if there is a common perpendicular that intersects a orthogonally in the middle between the two lines. Parallel edges of the two tetrahedra are located in opposite faces of the box $\mathcal{H}$, and the common perpendiculars of the edges are parallel to an axis of symmetry of the box. This implies that the axis a of any rotation in question must coincide with one axis of symmetry of $\mathcal{H}$, and one of the three hyperboloids degenerates in two pencils of lines. In other words, there are no other axes of rotations passing through the center of the box.

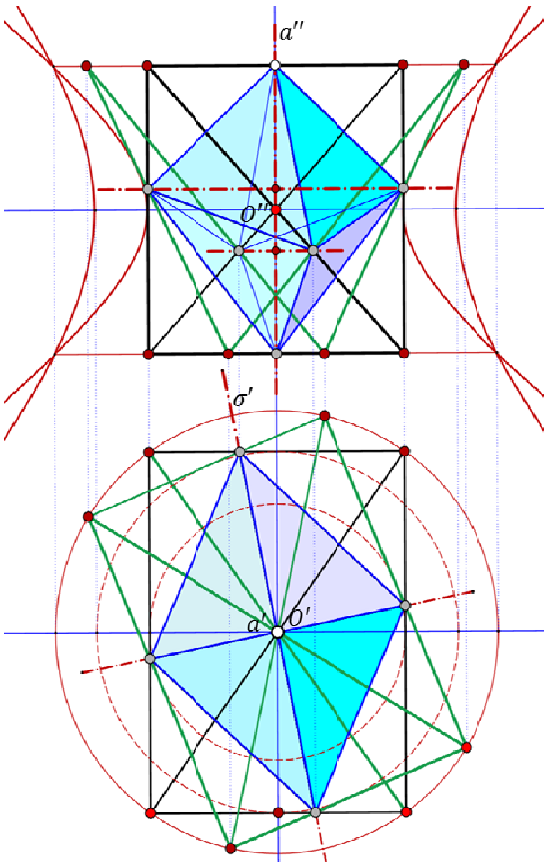

Figure 6: *Front view (top) and top view (bottom) of two equifaced tetrahedra T_1 (black) and T_2 (green) with crossing edges. The octahedron of contact points has a pair of skew orthogonal diagonals with the common perpendicular a as third diagonal. Only in the initial pose the octahedron is centrally symmetric, and all diagonals pass through the center.*

The coming Section 5 will reveal that, contrary to Section 3, the three rotations mentioned in Theorem 3 are included in two-parameter motions which preserve all edge-contacts. Moreover, according to Theorem 5 and in agreement with [8], these two-parameter motions contain infinitely many rotations about axes that no longer pass through the center O of the box $\mathcal{H}$.

5 Stellae Octangulae formed by tetrahedra with acute-angled faces

Now we consider the general case of a Stella Octangula, where a tetrahedron T_1 is mapped to T_2 by reflection in the barycenter O of T_1. Consequently, the two tetrahedra T_1 and T_2 share the midpoints of their edges. We aim at other positions of T_2 having crossing edges with T_1 and obtained by a reflection in a plane σ. Since a plane cannot meet more

than four edges of T_1 at inner points, edge-contacts at two additional points away from σ are necessary.

In the following we explain this for a given sextuple of lines $\mathcal{L}_1 = (a_1, b_1, \ldots, f_1)$. We choose a pair of points $P \in e_1$ and $Q \in f_1$ and their bisecting plane as reflection plane σ (see Figure 7). Then, the reflection of all six lines of $\mathcal{L}_1$ in σ yields a new sextuple $\mathcal{L}_2 = (a_2, b_2, \ldots, f_2)$, which is indirectly congruent to $\mathcal{L}_1$. Obviously, each line of $\mathcal{L}_1$ meets its image in the plane σ. However, in addition the image e_2 of e_1 passes through $Q \in f_1$ and, vice versa, f_2 meets e_1 at P.

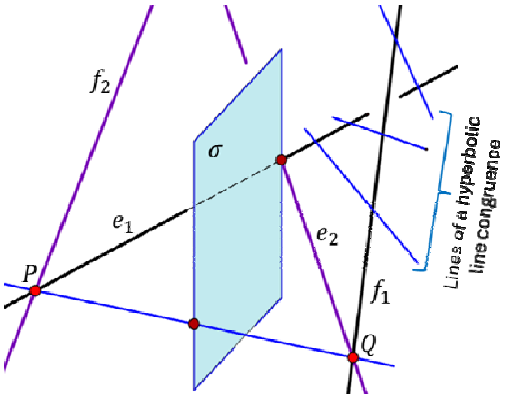

Figure 7: *After reflecting a sextuple of lines $\mathcal{L}_1$ in the symmetry plane σ of two arbitrary points $P \in e_1$ and $Q \in f_1$ we obtain an indirect congruent sextuple $\mathcal{L}_2$ and two additional intersections at P and Q.*

If e_1 and f_1 are skew, we get a two-parameter set of possible lines $g = PQ$ forming a hyperbolic congruence of lines, and thus a two-parameter set of reflection planes σ. With regard to our goal, we need to make sure that
(i) the reflection plane σ intersects four edges of T_1 at inner points and
(ii) the corresponding points P, Q are inner points of the remaining two edges.
Reflection planes σ satisfying (i) and (ii) are called *admissible*.

If the six lines of $\mathcal{L}_1$ are the extended edges of the tetrahedron T_1 and if the bisecting plane σ of two points P and Q is admissible, then there exists in a neighbourhood a two-dimensional domain of congruence lines $g = PQ$ and of admissible reflection planes σ. We will consider the envelope of these planes in Section 5.1.

At a general Stella Octangula, the points of contact between T_1 and T_2 are midpoints of the edges. They form three parallelograms with sides parallel to pairs of opposite edges of T_1 and T_2. There is a central symmetry between T_1 and T_2, but in general no planar symmetry like at the equifaced case of Section 4. In general, the octahedron O of contact points has no mutually orthogonal diagonals (see Figure 8).

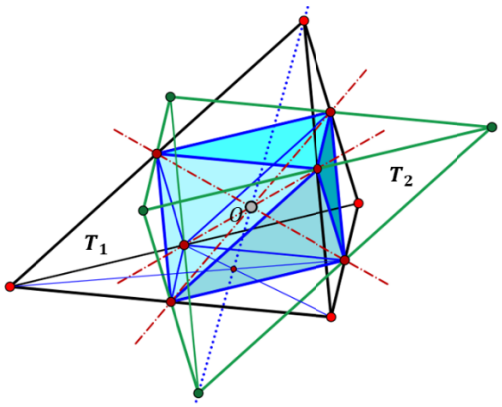

Figure 8: *At a Stella Octangula with general tetrahedra T_1, T_2 the octahedron O of contact points is centrally symmetric, and its diagonals are not mutually orthogonal.*

Each plane of a diagonal parallelogram is parallel to a pair of opposite edges of T_1. This means that also the common normal n of a pair of extended opposite edges (e_1, f_1) has foot points (P, Q) symmetric to the corresponding plane (see Figure 9). Therefore, there exists a certain open two-parameter neighborhood of these foot points and thus a two-dimensional manifold of planes σ, where the contact restrictions (i) are fulfilled. One must only make sure that (ii) both foot points (P, Q) are inner points of the corresponding edges. The contrary situation, where one foot point lies outside, is shown in Figure 10. The following theorem presents a sufficient condition.

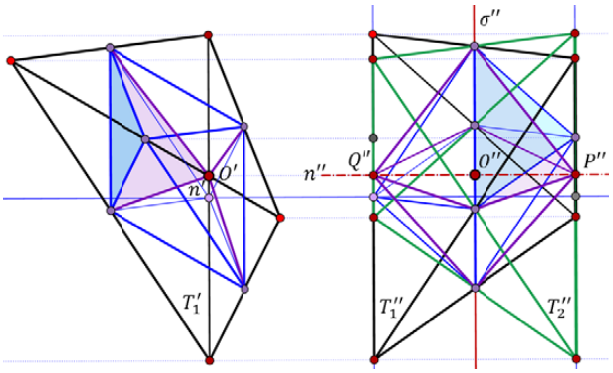

Figure 9: *Front view (left) and side-view (right) of a general tetrahedron T_1, whereby four coplanar midpoints of edges span the projection plane σ for the front view. The reflection in σ transforms T_1 (black) in a tetrahedron T_2' (green) that in general is different from the centrally symmetric T_2 forming the Stella Octangula.*

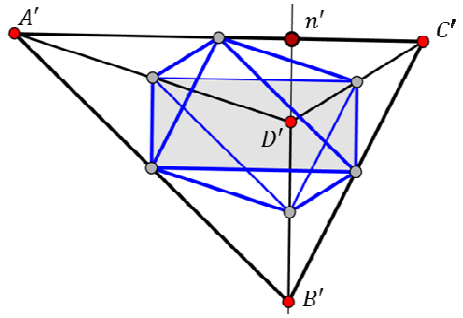

Figure 10: *Top-view of a general tetrahedron T_1 with a pair of opposite edges $[AC]$ and $[BD]$ parallel to the projection plane σ which contains the parallelogram of midpoints (shaded) of the other four edges. Since the common normal $n \perp \sigma$ of $e_1 = AC$ and $f_1 = BD$ intersects $[BD]$ at an exterior point, T_1 has obtuse angled faces. Reflecting T_1 in σ gives a tetrahedron T_2, where the image f_2 of f_1 intersects e_1 in an exterior point.*

Theorem 4 *Each tetrahedron T_1 with only acute-angled faces allows three two-parameter motions T_2/T_1 preserving six edge-contacts. In each of the three motions the poses of T_2 arise from T_1 by reflections in a two-parameter set of planes σ. In general, the three motions have no pose of T_2 in common.*

Proof. We assume that the edges $[A_1C_1]$ and $[B_1D_1]$ of T_1 are horizontal. This means for the top view that these edges are parallel to the projection plane. The interior of T_1 should lie under the face $A_1B_1C_1$. Then the convexity of T_1 implies that in the top view the signed angle between $C_1'A_1'$ and $B_1'D_1'$ lies between $0°$ and $180°$. Let n denote the common perpendicular of the lines A_1C_1 and B_1D_1, and suppose that its top view n' lies outside the segment $[A_1'C_1']$, but closer to A_1' than to C_1' (Figure 11, left).

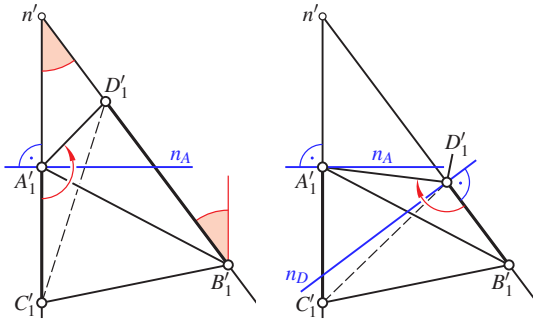

Figure 11: *Illustrating the proof of Theorem 4.*

If the line n_A through A_1' normal to $A_1'C_1'$ separates C_1' from D_1', then the angle $\sphericalangle C_1'A_1'D_1'$ is greater than $90°$. Consequently, also in space the angle $\sphericalangle C_1A_1D_1$ is obtuse.

In the remaining case n_A separates B_1', D_1' and C_1' from n'. Then the line n_D through D_1' orthogonal to $B_1'D_1'$ separates A_1' from B_1' (Figure 11, right). This implies that the angle $A_1D_1B_1$ is obtuse. In other words: If one pedal point of a common normal between opposite edges lies on the extension of an edge, then the tetrahedron must have an obtuse-angled face. □

Remark 4 *The condition of acute-angled faces in Theorem 4 is sufficient, but not necessary since there exist tetrahedra with an obtuse-angled face which nevertheless has the pedal points of the normals between opposite edges inside the edges. This holds, e.g., for the tetrahedron with vertices*

$$A = (\ \ 0.0,\ 0.0,\ 1.0),\ C = (2.0,\ \ 0.00,\ 1.0),$$
$$B = (-0.3,\ 1.0,\ 0.0),\ D = (0.3, -0.48,\ 0.0).$$

We obtain as pedal points of the common normal between opposite edges

$$\begin{array}{ll} AC \text{ and } BD: & (0.105, 0.000, 1.000),\ \ (0.105, 0.000, 0.000), \\ AB \text{ and } CD: & (-0.041, 0.136, 0.864),\ (0.539, -0.412, 0.141), \\ DA \text{ and } BC: & (0.112, -0.180, 0.626),\ \ (0.569, 0.622, 0.378). \end{array}$$

Apparently, the first two points are inner points of the edges $[AC]$ and $[BD]$, and the latter four points have z-coordinates between 0 and 1. However, there is an obtuse angle $\sphericalangle CAB = 101.98°$. Moreover it needs to be mentioned that for the existence of admissible planes σ for a given pair opposite edges it is not even necessary that the bisecting plane of the foot points of the common perpendicular intersects the remaining edges at inner points (note Remark 6). A necessary and sufficient condition for the existence of the two-parameter motion can be found below in Theorem 6.

Note that for obtaining a standard Stella-Octangula, the reflection of any tetrahedron T_1 in its barycenter produces its mate T_2. The two-parameter motions discussed in Theorem 4 need another initial pose T_2': the acute-angled T_1 is reflected in a plane μ through four coplanar midpoints of edges, and there exist three possibilities.

Lemma 3 *Referring to the previous notation, all three initial poses T_2' of the two-parameter movements coincide with the Stella-Octangula pose T_2 if and only if T_1 is equifaced.*

Proof. For equifaced tetrahedra holds $T_2' = T_2$ as shown in Figure 5, bottom.
Suppose that conversely both the point reflection in the barycenter of T_1 as well as the reflection in the plane σ passing through the midpoints of all line segments $[PQ]$ with $P \in [A_1C_1]$ and $Q \in [B_1D_1]$, take T_1 to T_2'. Since the barycenter as midpoint between the midpoints of A_1C_1 and B_1D_1 belongs to σ, the product of the two reflections

is the reflection in the line a through the barycenter and orthogonal to σ. This product must transform T_1 onto itself. Hence, the halfturn about a exchanges A_1 with C_1 and B_1 with D_1, so that we obtain equal lengths $\overline{A_1B_1} = \overline{C_1D_1}$ and $\overline{A_1D_1} = \overline{C_1B_1}$.
If the same assumption holds for another pair $([A_1B_1], [C_1D_1])$ of opposite edges, then also the last two opposite edges have equal lengths $\overline{A_1C_1} = \overline{B_1D_1}$. In other words, the tetrahedron T_1 is equifaced. □

Lemma 3 means, that only in the particular case of equifacial tetrahedra there exists a single bifurcation between all three two-parameter movements, namely at the common Stella-Octangula pose.

5.1 The role of the bisecting paraboloids

In [8], the authors already proved that equifacial tetrahedra with crossing edges admit infinitely many continuous rotations that preserve the edge-contacts. The following generalization for the generic case describes also the geometric loci of the axes of these rotations.

Theorem 5 *Referring to Theorem 4, for each of the three two-parameter motions T_2/T_1 the admissible reflection planes σ are tangent to an orthogonal hyperbolic paraboloid Ψ_1, the bisector of the extensions e_1, f_1 of opposite edges of T_1 (Figure 12). Each of these continuous motions includes two one-parameter families of bounded rotations. The axes of these continuous rotations of T_2 against T_1 are generators of Ψ_1 and at the same time axes of rotations that send e_1 to f_1.*

Proof. The symmetry planes σ of all pairs of points $P \in e_1$ and $Q \in f_1$ envelop an orthogonal hyperbolic paraboloid Ψ_1, the bisector of the pair of lines (e_1, f_1) (see, e.g., [9, p. 64]). Each plane σ contains two generators p and $\overline{p}$ of Ψ_1. Keeping one of these generators fixed, say p, the tangent planes of Ψ_1 along p form a pencil. Since the product of the reflections in two planes through p is a rotation about p, the admissible planes σ through p correspond to poses of the tetrahedron T_2 which are related by rotations about p. According to [9, p. 64], the lines p on the bisector Ψ_1 are the axes of rotations that send e_1 to f_1. This agrees with previous arguments, since p is the axis of a hyperboloid of revolution through e_1 and f_1, and the reflection in a meridian plane exchanges the reguli. The generators p and $\overline{p}$ in the bisecting plane σ of $P \in e_1$ and $Q \in f_1$ are axes of rotations that take in addition P to Q. □

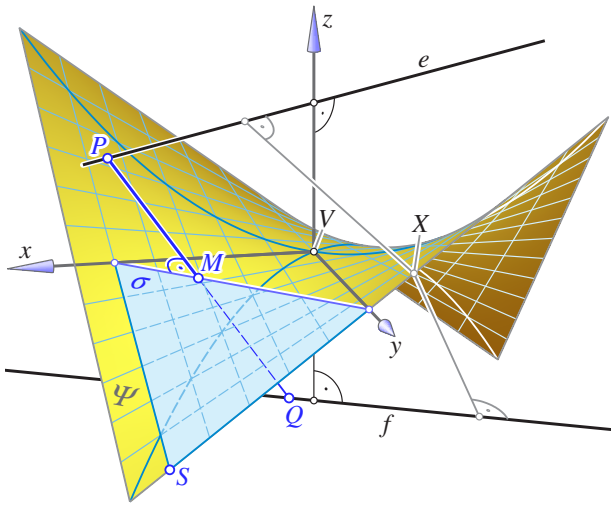

Figure 12: *The orthogonal hyperbolic paraboloid Ψ is the bisector of the skew lines e and f, i.e., the set of points X satisfying $\overline{Xe} = \overline{Xf}$. The plane σ of symmetry of the points $P \in e$ and $Q \in f$ contacts Ψ at the point S.*

Remark 5 *The two-parameter motions according to Theorem 4 are* symmetric rollings *since an orthogonal hyperbolic paraboloid Ψ_2 attached to T_2 is rolling*[2] *on an indirectly congruent paraboloid Ψ_1 such that the two surfaces are permanently symmetric w.r.t. the common tangent plane σ at the point of contact. Note the difference: At the symmetric roll-slidings mentioned in Remark 3 the two base surfaces are directly congruent.*

In the particular case of equifacial tetrahedra, the vertex generators of the three bisecting hyperbolic paraboloids are parallel to the edges of the convex hull $\mathcal{H}$ in the Stella-Octangula pose, i.e., of a rectangular box (see Figure5, top). The rotations about these particular generators are exactly the same as studied in Section 4.

6 The boundaries for admissible reflection planes

A generic plane σ that meets the interior of the tetrahedron T_1 without passing through any vertex, separates either one vertex from the other three or two from two. In the first case we speak of *type-1 planes*, otherwise from *type-2 planes* (see Figure 13). Only type-2 planes are candidates for admissible planes as they meet four edges. We are going to determine the boundaries for the set of admissible planes.

[2] In fact, a rolling of physical models of the paraboloids is not possible since the two surfaces penetrate each other along the common generators in the plane of contact (see Figure 12).

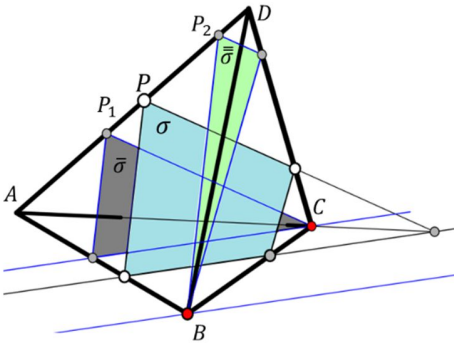

Figure 13: *When intersecting a tetrahedron with parallel planes, one finds two open regions where the intersection is empty, two regions of type-1 planes, and one of type-2 planes.*

At a given tetrahedron T (we suppress the subscripts for a while) with vertices A,B,C,D let $P \in [AC]$ and $Q \in [BD]$ be interior points of their edges. Then their midpoint M on $g = PQ$ is an inner point of T. All possible points M form the interior of an parallelogram in a plane μ with the midpoints of the edges $[AB]$, $[BC]$, $[CD]$, and $[DA]$ as vertices (see Figure 14).

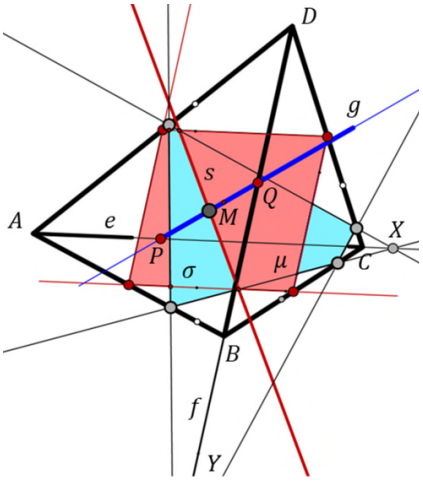

Figure 14: *Segments PQ with their endpoints on opposite edges $[AC]$ and $[BD]$ of the tetrahedron T have their midpoint M in the plane μ parallel to the lines $e = AC$ and $f = BD$. A presumptive reflection plane σ is normal to $g = PQ$ and contains M.*

Now we intersect the plane σ through M orthogonal to g with the extended edges $e = AC$ and $f = BD$. If these intersections are external points, then σ is a type-2 plane as it intersects all sides of the skew quadrangle $ABCD$ at inner points thus satisfying condition (i). In order to satisfy (ii), the midpoint M of $[PQ]$ must be an interior point of the parallelogram $T \cap \mu$. We summarize:

Theorem 6 *Let the lines e and f be the extensions of opposite edges $[AC]$ and $[BD]$ of the tetrahedron T, and let Ψ be the bisecting orthogonal hyperbolic paraboloid of e and f. Then the set of contact points S of Ψ with admissible planes σ related to the edges $[AC]$ and $[BD]$ equals the interior of the intersection of two open domains of Ψ,*
a) the domain enclosed by four conics, the contact curves of the tangent cones of Ψ with apices A,B,C,D, and
b) the domain that results from planes σ corresponding to midpoints M in the parallelogram $\mu \cap T_1$ (Figure 15).

For visualizing the two domains, we assume the lines e and f along with the plane μ to be horizontal and inspect the top view. Note that μ is tangent to the hyperbolic paraboloid Ψ at its vertex V, and the generators through V are axes of symmetry of e and f. Moreover, according to [9, p. 64] the lines e and f are polar w.r.t. Ψ. Therefore, the tangent cones from $A,C \in e$ contact Ψ in the respective polar planes passing through f and, vice versa, the contact curves for $B,D \in f$ lie in planes through e. These four planes enclose the tetrahedron T^* that is Ψ-polar to T. The first domain mentioned in Theorem 6 and corresponding to the condition (i) is the intersection of Ψ with the interior of T^* (see Figure 15). In general, it is bounded by four hyperbolic arcs.

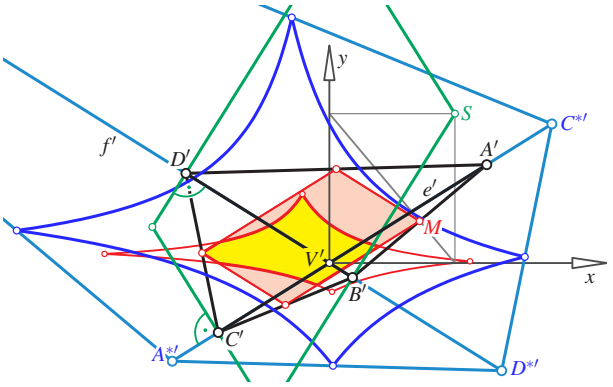

Figure 15: *Top views of the tetrahedron T (black) with the parallelogram of midpoints M (red), the polar tetrahedron T^* with vertices $A^*,\ldots,D^*$ (blue) and the four hyperbolic arcs (red) that enclose the first domain of the hyperbolic paraboloid Ψ as mentioned in Theorem 6. For admissible planes σ the midpoint M has to be chosen in the yellow area. The green parallelogram is the top view of the four parabolas terminating the second domain for the contact points S with Ψ.*

For determining the second domain, we choose the generators through the vertex V of Ψ as x- and y-axis of a coordinate frame and define e and f by

$$z = \pm d \quad \text{and} \quad x\sin\alpha = \pm y\cos\alpha,$$

where $2\alpha = \sphericalangle(e,f)$, and $2d$ equals the orthogonal distance between e and f. This implies

$$\Psi\colon\ 2dz + xy\sin 2\alpha = 0.$$

The polar plane of any point $P = (\xi,\eta,\zeta)$ w.r.t. Ψ satisfies

$$(\eta x + \xi y)\sin\alpha\cos\alpha + dz = -d\zeta. \tag{4}$$

The vertices $A^*, C^* \in e$ and $B^*, D^* \in f$ of the polar tetrahedron T^* are respectively conjugate to $A, C, B, D \in T$ w.r.t. Ψ. Thus, we obtain by (4) for $A = (a, a\tan\alpha, d)$ the vertex $A^* = (a^*, a^*\tan\alpha, d)$ and for $B = (b, -b\tan\alpha, -d)$ the vertex $B^* = (b^*, -b^*\tan\alpha, -d)$, where

$$aa^* = bb^* = \frac{-d^2}{\sin^2\alpha}.$$

For describing the second domain, we check the relation between any midpoint $M \in \mu$ and the contact point S of the corresponding plane σ with Ψ:

Given $M = (\xi,\eta,0)$, we first determine the line g through M meeting e and f. The meeting point $Q \in f$ is the point of intersection between f and the plane connecting M with e, which satisfies

$$(\xi\sin\alpha - \eta\cos\alpha)(z-d) + d(x\sin\alpha - y\cos\alpha) = 0.$$

This yields

$$\begin{aligned} Q &= (\xi - \eta\cot\alpha,\ \eta - \xi\tan\alpha,\ -d) \\ P &= (\xi + \eta\cot\alpha,\ \eta + \xi\tan\alpha,\ d). \end{aligned}$$

The bisecting plane of P and Q is

$$\sigma\colon\ \eta x\cot\alpha + \xi y\tan\alpha + dz = \xi\eta(\tan\alpha + \cot\alpha).$$

We obtain the contact point S of σ with Ψ as its pole by comparing the equation of σ with (4) (see Figure 12). This results in

$$S = \left(\frac{\xi}{\cos^2\alpha}, \frac{\eta}{\sin^2\alpha}, -\frac{\xi\eta}{d\sin\alpha\cos\alpha}\right). \tag{5}$$

The relation between the top views of M and S in the plane $z = 0$ is affine. Hence, the second domain as locus of admissible points $S \in \Psi$ as mentioned in Theorem 6 and corresponding to condition (ii) appears in the top view as interior of a parallelogram. It is easy to verify that the side lines of this parallelogram are respectively orthogonal to e' and f' and pass through the top views $A', \ldots, D'$ of the vertices of T (see Figure 15). After transforming the top views of the four hyperbolas by the inverted affine relation $M \mapsto S$ we find the locus of midpoints M that correspond to admissible bisecting planes σ.

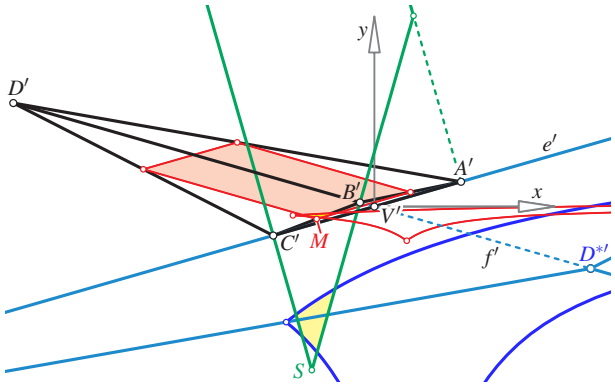

Figure 16: *At this example, the common normal of e and f (with top view V′) has its foot point on f outside the segment [BD]. Nevertheless, there exist admissible reflection planes σ. The top views of the domains for the corresponding midpoints M and for the contact points S with the hyperbolic paraboloid Ψ are shaded yellow.*

Remark 6 *The example displayed in Figure 16 demonstrates that due to Theorem 6 a two-parameter motion can also exist when the common perpendicular of the opposite edge lines e, f has a foot point outside the edge. Thus, interior foot points are a sufficient, but not necessary condition for the existence of a two-parameter motion of the type presented in Theorem 4. In other words, along with Remark 4 this means that the tetrahedra with acute-angled faces are a proper subset of the set of tetrahedra where the foot points of all common perpendiculars are interior points of edges. And this is a proper subset of the set of tetrahedra which admit three two-parameter symmetric rollings.*
Referring to Figure 16, when the common perpendicular of e and f has both footpoints outside the respective edges [AC] and [BD], then the intersection of the two domains mentioned in Theorem 6 must be empty as they are always separated by one coordinate axis.

6.1 Contained planar one-parameter motions

A motion in 3-space is called *planar* if all point trajectories are located in parallel planes. For example, according to Theorem 5 all rotations about generators of the bisecting hyperbololic paraboloids are planar motions. There are still more planar one-parameter movements contained in the two-parameter motions of congruent tetrahedra with crossing edges.

We recall that for each pair of opposite edges $[AC]$ and $[BD]$ of T we find admissible reflection planes σ as planes of symmetry for points $P \in [AC]$ and $Q \in [BD]$. If point Q is kept fixed while P varies (see Figure 17, top), then the corresponding planes σ envelop a part of a parabolic cylinder. This follows from the standard definition of a parabola

(note, e.g., [2, Fig. 2.13]), since this cylinder intersects the plane γ connecting Q with $[AC]$ in an arc of the parabola c with focus Q and directrix $e = AC$ (Figure 17, bottom).

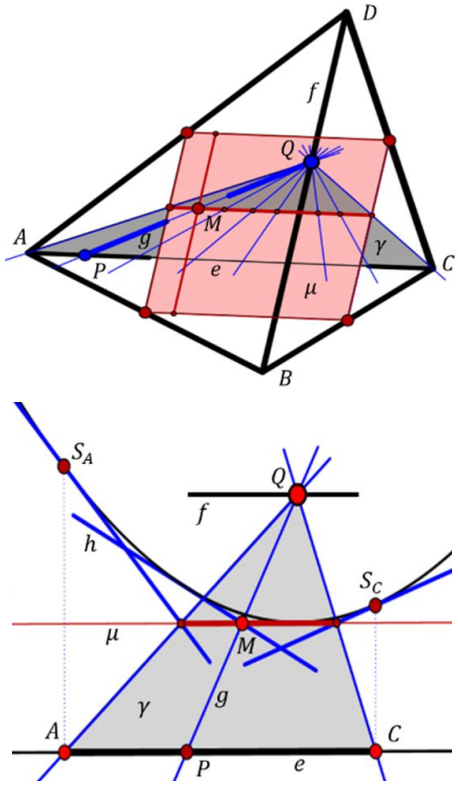

Figure 17: *For given opposite edges $[AC]$ and $[BD]$ the locus of midpoints M of points $P \in [AC]$ and $Q \in [BD]$ is a parallelogram in a plane μ parallel to AC and BD. For fixed Q the planes of symmetry σ envelop a parabolic cylinder.*

We are also able to figure out the boundaries of this parabolic arc c (see Figure 17, top): The plane $\sigma \perp PQ = g$ passes through the midpoint $M \in (\mu \cap T)$ of $[PQ]$ and intersects γ in a tangent h of c. The required arc of c is bounded by the points S_A and S_C because of $P \in [AC]$. Moreover, $h \cap e$ has to be an exterior point of the segment $[AC]$. Hence, in the case shown in Figure 18, the corresponding parabolic arc is limited by S_C and by the contact point T of a tangent of c through C.

In the limiting case $Q = B$, the envelope of the planes σ belongs to a parabolic cylinder with generators orthogonal to the plane spanned by ACB. These generators have top views orthogonal to the top view e' of $e = AC$. The parabolic cylinder contacts the hyperbolic paraboloid Ψ along a parabola that bounds the second domain and appears in the top view as a side of the mentioned parallelogram (green in Figure 15). At each point S of this parabola the tangent must be conjugate w.r.t. Ψ to the generator of the contacting cylinder. Conjugate lines are in a harmonic position w.r.t. the Ψ-generators through S, which have top views parallel to the coordinate axes. As a result, the top view of the contacting parabola must be orthogonal to f', as already documented above (see Figure 15).

When reflecting T_1 on admissible planes σ with fixed point $Q \in f$ we obtain poses of T_2 where the point attached to T_2 trace curves in planes parallel to the plane γ connecting Q with e. At the same time a parabolic cylinder attached to T_2 rolls on a parabolic cylinder attached to T_1 such that the cylinders are permanently symmetric w.r.t. the plane σ of contact. This is again a planar motion contained in the two-parameter motion related to the pair (e, f).[3] The corresponding midpoints $M \in \mu$ trace a segment parallel to e (Figure 17), hence parallel to one side of the parallelogram in μ. The symmetric parabolic-cylinder-rollings corresponding to a fixed point $P \in e$ has similar properties. In comparison, at the contained rotations according to Theorem 5 the point S of contact between σ and the paraboloid Ψ_1 (see Figure 12) traces a generator. In the top view, the point S' runs along a line parallel to one coordinate axis, and the same holds for the midpoint M' due the affine correspondence between these points (Figure 15).

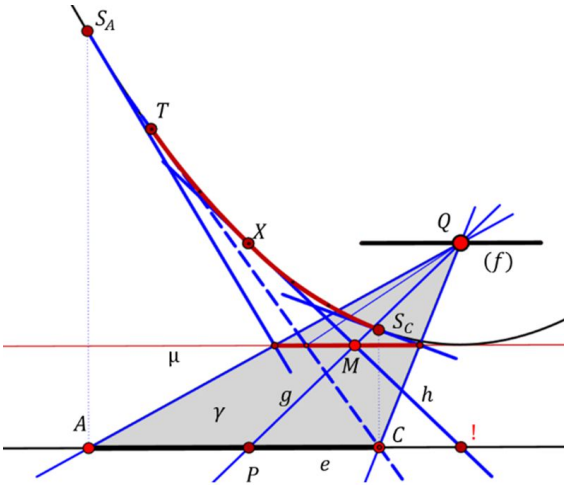

Figure 18: *The parabola's tangent at S_A does no longer belong to an admissible bisection plane σ as it meets the segment $[AC]$ at an interior point.*

7 Further movable pairs of congruent structures with edge-contacts

a) We follow an idea of [8] generalizing an equifaced tetrahedron with isosceles faces to an antiprisma over a regular

[3] In planar kinematics, the symmetric rolling of two parabolas has the property that the focus of the first parabola traces the directrix of the second parabola while the directrix of the first parabola slides through the focal point of the second.

n-gon (see Figure 19). This allows further generalizations, as we only must demand that the pairs of opposite skew edges of a generalized antiprisma are generators of the same coaxial hyperboloid of revolution. Consequently, the regular top- and bottom-polygons can be similar and, to a certain extent, even affine transforms of regular polygons. When we move a planar polygon within its plane to another position, then corresponding edge lines will trivially intersect, and, of course, we can restrict the movement such that all corresponding edges intersect at inner points.

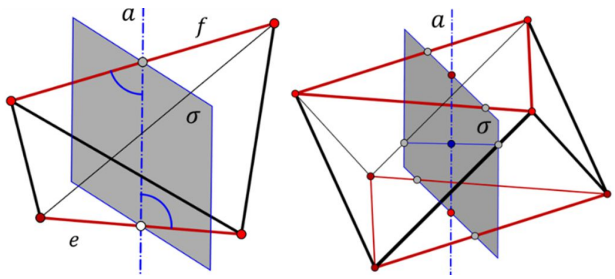

Figure 19: *Pairs of n-sided antiprisms as movable structures include for $n = 2$ equifaced tetrahedra (left) and for $n = 3$ octahedra (right). Also pairs of symmetric tetrahedra with top- and bottom edge of different lengths allow a one-parameter set of motions with fixed axis a, as well as pairs of generalized antiprisms with affine-regular top- and bottom polygons.*

b) When using the last statement for a classical pyramid P_1 with a convex planar basis, then we can, with certain restrictions, reflect it in a plane σ through its altitude a getting a pyramid P_2, which is in edge-contact with P_1. Hence, we can extend an antiprism by two pyramids at the top- and bottom-polygon such that their apices are points of the axis a of the antiprism. Then the reflection of this polyhedron P_1 in any plane σ through a yields a congruent copy P_2, which still can move relative to P_1 while keeping all edge-contacts. For example, a regular icosahedron satisfies these conditions (see Figure 20). A scaling in direction of the axis a will not restrict the mobility.

c) Even congruent pairs of (regular) double pyramids with a non-planar belt-polygon can be considered as movable polyhedral edge structures, as far as the belt polygon also suits to a generalized antiprism. A cube serves as a simple example, when rotated around one of its spatial diagonals. Another example is the regular pentagon dodecahedron, seen as a truncated double pyramid (Figure 21). Obviously the movability remains when such a structure is subjected to a scaling in direction of the fixed axis.

d) The standard case of a pair of coaxial right pyramids over a regular n-gon (see [11] and [12]) allows further generalizations. If h denotes the altitude of the pyramids and they share in the initial position the base n-gons, then the extremal distance t of their base planes is related as

$$t : h = \left(1 - \cos\frac{\pi}{n}\right) : 1\,. \tag{6}$$

These pyramids P_1, P_2 can be embedded in two congruent cones Ψ_1, Ψ_2 of revolution. When we "bend" all non-base edges of P_1 and P_2 to congruent curves on Ψ_1 and Ψ_2, then also these objects will allow a one-parameter set of motions as products of appropriate rotations about and translations along the axis, while the formula in (6) will still remain valid.

As a next step we generalize, with restrictions, the cones Ψ_1, Ψ_2 to smooth surfaces of revolution Φ_1, Φ_2. At first we take their meridians m as replacements of the edges of the pyramids P_1, P_2. Then again, we can replace these meridians by a set of congruent curves on Φ_1, Φ_2, and we will end up with a movable edge-curve structure.

e) We return to **a)** and consider equifaced tetrahedra and regular antiprisms again. There the key property is the existence of coaxial hyperboloids of revolution. Obviously, we can now bend the straight edges to congruent curves on these hyperboloids and receive a movable edge-curve structure. Also here, the hyperboloids can be replaced by more general surfaces of revolution, and, in case of antiprisms, the edges of the top- and base polygon can be replaced by curves, too.

It is easy to imagine such a structure on a sphere: Consider the vertices of a regular n-gon on, say, the two polar circles of the sphere, and connect them with arcs of, e.g., a loxodrome, a curve of constant slope, or simply with arcs of a great circle. In this very special case of a curved edge system the chosen arcs need not even be congruent.

According to these statements, we can replace the edges of the cube, the regular icosahedron and the pentagon dodecahedron (see **b**) by congruent curves and preserve the movability of the curved edge structure.

Nevertheless, an explicit calculation of the motion will depend on the chosen curved edges and might get lengthy. In each pose, the instantaneous behaviour is that of an object with the tangents as edges, and therefore it is locally an edge structure of the types treated in the foregoing chapters.

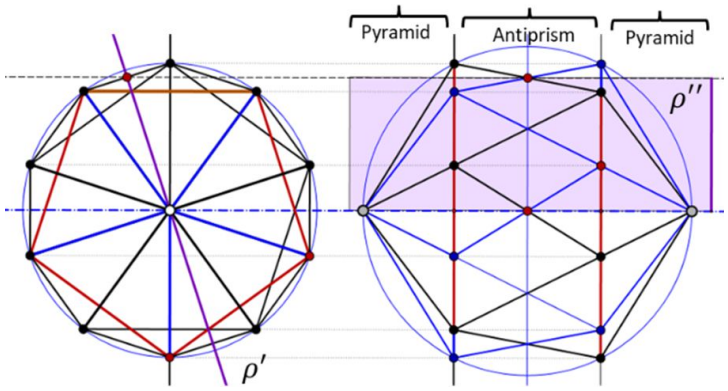

Figure 22: *A regular icosahedron together with its image under a rotation about an axis connecting opposite vertices yields two congruent polyhedral structures which allow a relative movement while all edge-contacts are preserved.*

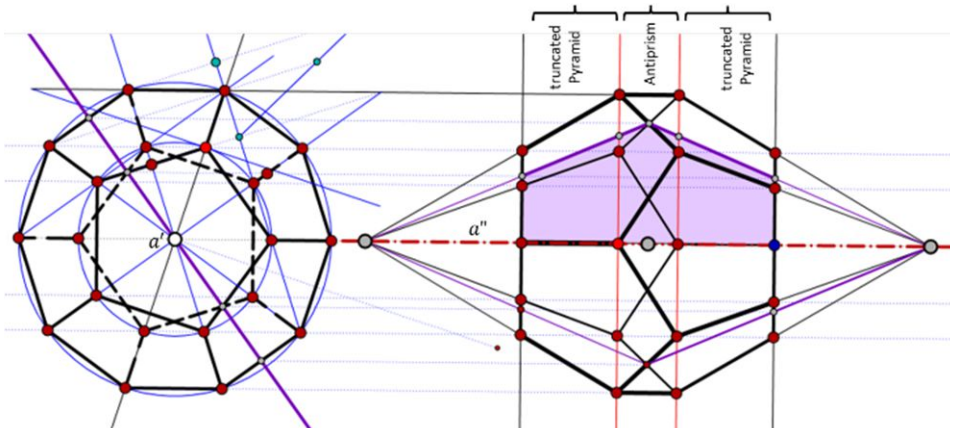

Figure 21: *Another example of a movable polyhedral edge structure consists of two congruent regular pentagon dodecahedra sharing an axis that connects midpoints of opposite faces.*

8 Conclusion

We aimed at a geometric analysis of the sliding motions, which occur at congruent tetrahedra, forming a Stella Octangula in the initial pose. We preferred geometric reasoning against lengthy calculations. The surprising fact that the pair of tetrahedra of a classical Stella Octangula is movable in spite of dof $= 0$ caused the questions "why" and "are regular tetrahedra the only ones with that property". We could show that general pairs of indirect congruent tetrahedra (T_1, T_2) keep their six crossings under three two-parametric motions of T_2 relative to T_1. Each pose of T_2 can be obtained by a reflection of T_1 in a tangent plane of orthogonal hyperbolic paraboloids, and their generators act as axes of possible rotations.

There is kind of hierarchical structure among the tetrahedra T_1, T_2 from the most general ones to those having in the initial Stella-Octangula pose a box as convex hull, and finally those being regular three-sided pyramids. The latter allow motions generated by reflections in axes orthogonal to the common axis of symmetry of T_1 and T_2. The most special case with two regular tetrahedra allows both, the special axial reflections as well as the reflections in planes. In all the discussed cases, the poses of T_2 relative to T_1 are generated by single reflections, i.e., by involutive displacements. Here the question arises: "Is the assumption of tetrahedra T_1, T_2 being congruent a necessary condition for their movability?"

Moreover, one might ask for pairs of other polyhedral structures, which allow such relative motions. Besides generalizations presented in [8], it is possible to find many other polyhedral structures allowing at least one-parameter motions, if trivial edge-contacts are not excluded. In addition, even structures where the edges are bent to congruent curves can admit such sliding motions.

References

[1] BOTTEMA, O., ROTH, B., *Theoretical Kinematics*. North-Holland Publ. Comp., Amsterdam, 1979.

[2] GLAESER, G., STACHEL, H., ODEHNAL, B., *The Universe of Conics*. 2nd ed., Springer Spektrum, Heidelberg, 2024, https://doi.org/10.1007/978-3-662-70306-9

[3] HUSTY, M., KARGER, A., SACHS, H., STEINHILPER, W., *Kinematik und Robotik*. Springer-Verlag, Berlin-Heidelberg, 1997, https://doi.org/10.1007/978-3-642-59029-0

[4] HYDER, A., ZSOMBOR-MURRAY, P., An equilateral tetrahedral mechanism. *Robotics and Autonomous Systems* **9**(4) (1992), 227–236, https://doi.org/10.1016/0921-8890(92)90040-6

[5] KATSUURA, H., Characterization of an Isosceles Tetrahedron. *J. Geom. Graph.* **23**(1) (2019), 37–40.

[6] KRAMES, J.L., *Darstellende und kinematische Geometrie für Maschinenbauer.* 2nd ed., Franz Deuticke, Wien, 1967.

[7] KRAMES, J., Über Fußpunktkurven von Regelflächen und eine besondere Klasse von Raumbewegungen. (Über symmetrische Schrotungen I). *Monatsh. Math. Phys.* **45** (1937), 394–406.

[8] MAKAI, E., TARNAI, T., Generalized Forms of an Overconstrained Sliding Mechanism Consisting of Two Congruent Tetrahedra. *Stud. Sci. Math. Hung.* **60**(1) (2023), 43–75, https://doi.org/10.1556/012.2023.01534

[9] ODEHNAL, B., STACHEL, H., GLAESER, G., *The Universe of Quadrics*. Springer-Verlag, Berlin, Heidelberg, 2020, https://doi.org/10.1007/978-3-662-61053-4

[10] QUAISSER, E., *Bewegungen in der Ebene und im Raum*. VEB Deutscher Verlag der Wissenschaften, Berlin, 1983.

[11] STACHEL, H., Ein bewegliches Tetraederpaar. *Elemente der Math.* **43**(3) (1988), 65–75.

[12] TARNAI, T., MAKAI, E., A movable pair of tetrahedra. *Proc. Royal. Soc. London* A **423** (1989), 419–442.

[13] WEISS, G., Symmetry in motion: Stellae Octangulae, and equifaced polyhedra. *Proceedings of "Symmetry: Art and Science"*, 12th SIS-Symmetry Congress, Porto 2022, 210–217, https://doi.org/10.24840/1447-607X/2022/12-26-210

Hellmuth Stachel
orcid.org/0000-0001-5300-4978
e-mail: stachel@dmg.tuwien.ac.at

Vienna University of Technology
Wiedner Hauptstr. 8-10/104, 1040 Wien, Austria

Gunter Weiss
orcid.org/0000-0001-9455-9830
e-mail: weissgunter@gmx.net

Vienna University of Technology
Wiedner Hauptstr. 8-10/104, 1040 Wien, Austria

https://doi.org/10.31896/k.29.2
Original scientific paper
Accepted: 11 July 2025

QUANG HUNG TRAN
NIKOLAOS DERGIADES

A Generalization of Archimedean Circles on an Arbelos

A Generalization of Archimedean Circles on an Arbelos

ABSTRACT

In this paper, we extend the classical notion of Archimedean circles, originally discovered by Archimedes in the arbelos, to the broader framework of the arbelos with overhang. By means of new constructions, we establish conditions under which circles in this generalized setting retain the characteristic radius property of Archimedean circles. Our results unify and extend previous findings, revealing deeper symmetries and structural invariants within these geometric figures.

Key words: Archimedean circles, Arbelos, Arbelos with Overhang

MSC2020: 51M04, 51N20

Poopćenje Arhimedovih kružnica na arbelosu

SAŽETAK

U ovom radu proširujemo klasičan pojam Arhimedovih kružnica, koji je izvorno otkrio Arhimed na arbelosu, na širi okvir arbelosa s produžetkom. Pomoću novih konstrukcija određujemo uvjete pod kojima kružnice u ovom poopćenom okruženju zadržavaju karakteristično svojstvo polumjera Arhimedovih kružnica. Naši rezultati ujedinjuju i proširuju prethodne rezultate, otkrivajući dublje simetrije i strukturne invarijante unutar ovih geometrijskih figura.

Ključne riječi: Arhimedove kružnice, arbelos, arbelos s produžetkom

1 Introduction

The *arbelos*, or "shoemaker's knife", is a classical figure in plane geometry, first studied by Archimedes. It consists of the region bounded by three mutually tangent semicircles with collinear diameters. One of the most remarkable aspects of the arbelos is the existence of an infinite family of circles that share a surprising property: they all have the same radius as a particular circle introduced by Archimedes. These circles are now known as *Archimedean circles* [2].

Archimedes proved that a specific circle constructed inside the arbelos—the so-called *Archimedes' circle*—has a radius equal to that of another circle tangent to the same boundaries (see Figure 1). Over the centuries, many additional Archimedean circles have been discovered, all exhibiting the same constancy in radius despite being derived from different constructions.

The study of Archimedean circles continues to fascinate geometers, both for the elegance of their construction and for the deeper geometric principles they reveal.

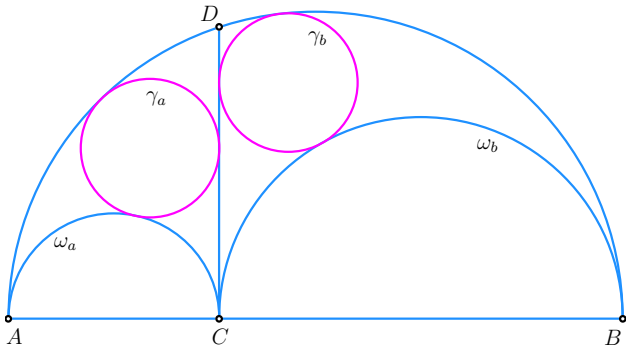

Figure 1: *The twin of the Archimedes' circle on the arbelos.*

A natural generalization of the classical arbelos, known as the *arbelos with overhang*, was introduced by H. Okumura in [7]. Furthermore, Okumura presented several results concerning Archimedean circles within this extended framework [3, 4, 5, 6]. An additional pair of Archimedean circles

in the context of the arbelos was introduced by the present authors in [1].

Theorem 1 *(Archimedes' circle on the arbelos with overhang) Let AB be a segment, and construct the semicircle ω_c with diameter AB. Let C be a point on AB, and let the perpendicular from C to AB intersect ω_c at D. On rays CA and CB, choose points A' and B' respectively. Construct semicircles $\omega_{a'}$ and $\omega_{b'}$ with diameters CA' and CB'. This configuration is called the* arbelos with overhang. *Construct two circles: γ_a tangent to ω_c, $\omega_{a'}$, and CD; and γ_b tangent to ω_c, $\omega_{b'}$, and CD. Then γ_a and γ_b have equal radii if and only if $AA' = BB'$.*

The proof and some applications of Theorem 1 can be found in [6].

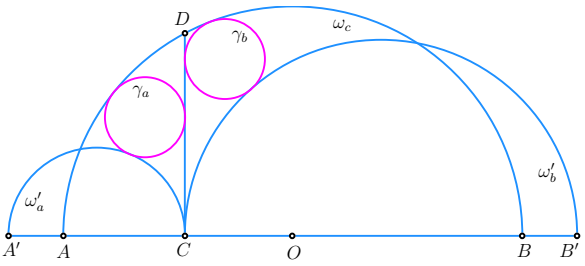

Figure 2: *The twin of the Archimedes' circle on the arbelos with overhang.*

In this paper, we generalize the concept of Archimedean circles to the arbelos with overhang and investigate constructions that preserve the equal-radius property under this extended configuration.

Theorem 2 *Let AB be a segment, and construct the semicircle ω_c with diameter AB. Let C be a point on the segment AB, and let the perpendicular line d from C to AB intersect ω_c at D. Suppose K and L are arbitrary points on the rays CA and CB, respectively. Construct the circles ω_k and ω_l centered at K and L and passing through C. Let A' and B' be the points dividing CK and CL in the same ratio, respectively. Construct the semicircles $\omega_{a'}$ and $\omega_{b'}$ with diameters CA' and CB'. Define $M(r_1)$ to be the circle tangent internally to both ω_k and ω_c and tangent externally to $\omega_{a'}$. Define $N(r_2)$ to be the circle tangent internally to both ω_l and ω_c and tangent externally to $\omega_{b'}$. If the distances from the centers of M and N to the line d are d_1 and d_2, respectively, then:*

i) $\dfrac{r_1}{d_1} = \dfrac{r_2}{d_2}$;

ii) if K tends to infinity, then $r_1 = \dfrac{a'b'}{a+b'}$;

iii) if L tends to infinity, then $r_2 = \dfrac{a'b'}{a'+b}$;

iv) if both K and L tend to infinity, then $r_1 = r_2$ if and only if $AA' = BB'$.

Remark 1 *If both K and L tend to infinity, then the semicircles $\omega_{a'}$ and $\omega_{b'}$ degenerate into the line CD. In this limiting case, we obtain $r_1 = r_2$ if and only if $AA' = BB'$, which means that the semicircles $\omega_c, \omega_{a'}, \omega_{b'}$ form an arbelos with overhang (see [6]). Hence, Theorem 2 naturally generalizes the arbelos with overhang.*

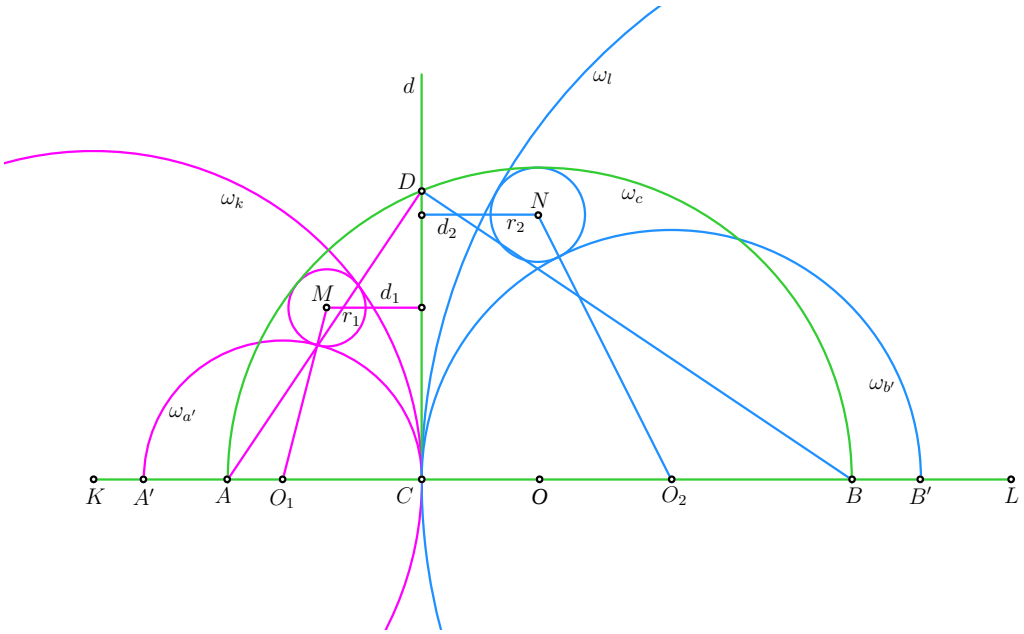

Figure 3: *A generalization of Archimedean circles on the arbelos with overhang.*

2 Proof of Theorem 2

Proof. (See Figure 3.) Assume $a < b$ and denote

$$CA' = 2a, \qquad CB' = 2b, \qquad AC = 2a', \qquad AB = 2b',$$

$$KA = k, \qquad LB = l.$$

Let O_1, O_2, and O be the midpoints of CA', CB', and AB, respectively. In Cartesian coordinates, place

$$O(b'-a',0), \qquad O_1(-a,0), \qquad O_2(b,0), \qquad K(-k-2a,0),$$

$$L(l+2b,0), \qquad M(-d_1,y), \qquad N(d_2,z).$$

Since A' and B' divide CK and BL in the same ratio, the relation

$$\frac{k}{a} = \frac{l}{b} \tag{1}$$

holds.

We now consider the following distance relations:

$$KM^2 = (KC - r_1)^2$$
$$\text{that is, } (-d_1 + k + 2a)^2 + y^2 = (k + 2a - r_1)^2, \tag{2}$$
$$MO_1^2 = (a + r_1)^2$$
$$\text{that is, } (-d_1 + a)^2 + y^2 = (a + r_1)^2, \tag{3}$$
$$MO^2 = (a' + b' - r_1)^2$$
$$\text{that is, } (b' - a' + d_1)^2 + y^2 = (a' + b' - r_1)^2. \tag{4}$$

Subtracting (3) from (2) gives

$$(a+k)d_1 = r_1(3a+k). \tag{5}$$

Subtracting (3) from (4) gives

$$(a - a' + b')d_1 + r_1(a + a' + b') = 2a'b'. \tag{6}$$

Solving equations (5) and (6) for r_1 yields

$$r_1 = \frac{a'b'(3a+k)}{2a(a-a'+2b') + (a+b')k}. \tag{7}$$

From (5), the quotient r_1/d_1 is

$$\frac{r_1}{d_1} = \frac{a+k}{3a+k} = \frac{1+\frac{k}{a}}{3+\frac{k}{a}}. \tag{8}$$

A completely analogous computation with point L gives

$$\frac{r_2}{d_2} = \frac{1+\frac{l}{b}}{3+\frac{l}{b}}. \tag{9}$$

Using relations (1), (8), and (9), we obtain the equality

$$\frac{r_1}{d_1} = \frac{r_2}{d_2},$$

which completes the proof of part (i) of Theorem 2.

We now examine the limit as k tends to infinity. Using (7), the expression for r_1 becomes

$$\begin{aligned} r_1 &= \lim_{k\to\infty} \frac{3aa'b' + a'b'k}{2a(a-a'+2b') + (a+b')k} \\ &= \lim_{k\to\infty} \frac{\frac{3aa'b'}{k} + a'b'}{\frac{2a(a-a'+2b')}{k} + a + b'} \\ &= \frac{a'b'}{a+b'}. \end{aligned}$$

Thus part (ii) of Theorem 2 is established.

A similar limiting argument with l tending to infinity gives

$$r_2 = \frac{a'b'}{a'+b}.$$

Finally, if both K and L tend to infinity, then the expressions obtained above satisfy

$$r_1 = \frac{a'b'}{a+b'}, \qquad r_2 = \frac{a'b'}{a'+b}.$$

The radii r_1 and r_2 are equal exactly in the case where

$$\frac{a'b'}{a+b'} = \frac{a'b'}{a'+b}.$$

Since $a'b'$ is nonzero, the equality of the two fractions occurs exactly when

$$a + b' = a' + b,$$

or equivalently when

$$AA' = BB'.$$

This completes the proof of part (iv) of Theorem 2. □

3 Conclusion

In this paper, we have extended the classical theory of Archimedean circles to the generalized setting of the arbelos with overhang. By introducing suitable constructions, we demonstrated that circles in this configuration retain the defining equal-radius property, analogous to that of the original Archimedean circles.

Our generalizations preserve the elegance and structural harmony of the classical case while also uncovering new symmetries and invariants inherent in the modified figure. These results enrich the study of the arbelos and its extensions, illustrating how classical geometric phenomena persist under broader transformations.

We hope this work encourages further exploration of Archimedean-type configurations in other generalized geometries, thereby contributing to the continuing dialogue between classical and modern geometry.

Acknowledgments. The authors would like to express their sincere gratitude to the anonymous referee for his/here careful reading, insightful comments, and valuable suggestions, which have significantly improved the quality of this paper. We are also deeply indebted to the editor for the kind guidance and support throughout the review process.

References

[1] DERGIADES, N., TRAN, Q. H., An interesting generator of Archimedean circles. *Math. Gaz.* **107**(568) (2023), 155–159, https://doi.org/10.1017/mag.2023.27

[2] DODGE, C. W., SCHOCH, T., WOO, P. Y., YIU, P., Those ubiquitous Archimedean circles. *Math. Mag.* **72**(3) (1999), 202–213, https://doi.org/10.1080/0025570X.1999.11996731

[3] OKUMURA, H., Archimedean circles of the collinear arbelos and the skewed arbelos. *J. Geom. Graph.* **17**(1) (2013), 31–52.

[4] OKUMURA, H., Archimedean twin circles in the arbelos. *M*ath. Gaz. **97**(504) (2013), 512, https://doi.org/10.1017/S0025557200000322

[5] OKUMURA, H., Lamoenian circles of the collinear arbelos. *KoG* **17** (2013), 9–13.

[6] OKUMURA, H., The Arbelos with Overhang. *KoG* **18** (2014), 19–27.

[7] OKUMURA, H., Ubiquitous Archimedean circles of the collinear arbelos. *KoG* **16** (2012), 17–20.

Quang Hung Tran
orcid.org/0000-0003-2468-4972
e-mail: tranquanghung@hus.edu.vn High School for Gifted Students
Vietnam National University at Hanoi, Vietnam

Nikolaos Dergiades
orcid.org/0009-0001-0868-9581
e-mail: ndergiades@yahoo.gr
Thessaloniki, Greece

https://doi.org/10.31896/k.29.3
Original scientific paper
Accepted: 28 October 2025

MANDI ORLIĆ BACHLER

On Fuss' Relations for Bicentric Polygons with an Odd Number of Vertices

On Fuss' Relations for Bicentric Polygons with an Odd Number of Vertices

ABSTRACT

This paper presents novel analytical forms of Fuss' relations for bicentric polygons with an odd number of sides and higher rotation numbers. The method is based on Poncelet's theorem and Radić's theorem and conjecture concerning the connection between Fuss' relations for different rotation numbers. Explicit analytical expressions are obtained for the bicentric triskaidecagon with $k = 2,4,6$ and for the bicentric pentadecagon with $k = 2$, while complete sets of relations are established for the bicentric heptadecagon ($k = 1,2,3,4,5,6,7,8$) and enneadecagon ($k = 1,2,3,4,5,6,7,8,9$). The proposed approach simplifies the derivation and enables a systematic extension of known Fuss' relations to higher-order bicentric polygons and new rotation numbers, confirming the validity of Radić's conjecture.

Key words: bicentric polygon, Fuss' relation, rotation number, triskaidecagon, pentadecagon, heptadecagon, enneadecagon

MSC2020: 51N20, 51M15, 37J45

O Fussovim relacijama za bicentrične poligone s neparnim brojem vrhova

SAŽETAK

U radu su izvedeni analitički oblici Fussovih relacija za bicentrične poligone s neparnim brojem stranica i višim brojevima rotacije. Metoda se temelji na Ponceletovom teoremu te Radićevom teoremu i slutnji u vezi s povezanošću Fussovih relacija za različite brojeve rotacije. Dobiveni su eksplicitni analitički izrazi za bicentrični trinaesterokut s rotacijskim brojem $k = 2,4,6$ i za bicentrični petnaesterokut s rotacijskim brojem $k = 2$, dok su uspostavljeni kompletni skupovi relacija za bicentrični sedamneasterokut (za $k = 1,2,3,4,5,6,7,8$) i devetnaesterokut (za $k = 1,2,3,4,5,6,7,8,9$). Predloženi pristup pojednostavljuje izvođenje i omogućuje sustavno proširenje poznatih Fussovih relacija na bicentrične poligone višeg reda i nove brojeve rotacije, čime se potvrđuje valjanost Radićeve slutnje.

Ključne riječi: bicentrični poligon, Fussova relacija, rotacijski broj, trinaesterokut, petnaesterokut, sedamnaesterokut, devetnaesterokut

1 Introduction

A bicentric n-gon is a polygon with n sides that is both tangential (it possesses an inscribed circle, or incircle) and cyclic (it possesses a circumscribed circle, or circumcircle). These two circles are nested, meaning that one lies entirely within the other.

Let $A_1,\ldots,A_n$ be a bicentric n-gon with an incircle C of radius r centered at point I, and a circumcircle K of radius R centered at point O. Denote by d the distance between their centers, where the circle C lies inside the circle K. Let $T_1,\ldots,T_n$ be the points of tangency of the sides (segments) $A_1A_2,\ldots,A_nA_1$, respectively. The lengths $|A_iT_i|$, $i = 1,\ldots,n$, are called the tangent lengths of the polygon $A_1,\ldots,A_n$. If

$$\sum_{i=1}^{n} \arctan\left(\frac{|A_iT_i|}{r}\right) = k\pi \tag{1}$$

where k is a positive integer satisfying $k \leq \frac{n-1}{2}$, the polygon $A_1,\ldots,A_n$ is said to be k-circumscribed, and k is called its rotation number [8].

The relation connecting the radii of the incircle and circumcircle, and the distance between their centers, is called a Fuss' relation. Throughout this paper, the notation $F_n^{(k)}(R,r,d)=0$ will consistently denote the Fuss' relation for a bicentric n-gon with rotation number k, relating the radii R and r of the circumcircle and incircle and the distance d between their centers.

The problem of determining the relation between the radii of the incircle and circumcircle and the distance between their centers for bicentric polygons is one of the classical topics of Euclidean geometry, originating from the results of Euler and Fuss. Euler first derived the corresponding relation for the triangle, while Nicolaus Fuss (1755–1826) obtained analogous relations for bicentric quadrilaterals, pentagons, hexagons, and heptagons. These expressions are now collectively known as Fuss' relations.

Later authors extended these relations to polygons of higher order, using various analytical, geometrical, and computational approaches. Particularly significant are the results of Mirko Radić, who developed a relatively simple and effective method for establishing Fuss' relations based on Poncelet's theorem. In papers [3]–[7], [9], Fuss' relations were derived for bicentric polygons up to $n=11$, and for certain cases with $n=13,15,17,18$. However, these results do not include all possible values of the rotation number k. Specifically, for the bicentric triskaidecagon (13-gon), only the cases $k=1,3,5$ were known, while for the bicentric pentadecagon (15-gon) the known cases were $k=1,3,4,5,6$. The remaining cases $k=2,4,6$ for $n=13$ and $k=2$ for $n=15$ have not been obtained analytically so far, mainly due to the computational complexity of Radić's classical method, whose algebraic expressions grow exponentially with both n and even values of k.

Recent investigations have further extended the study of bicentric and Poncelet-type polygons using computational and algebraic methods. For instance, Dragović and Radnović [2] analyzed Poncelet's porisms through elliptic and hyperelliptic function theory, establishing algebraic integrability and modular relations for multi-rotational polygons. New algebraic invariants associated with Poncelet–Jacobi bicentric polygons have been introduced and studied in the work of Roitman, Garcia, and Reznik [10], providing additional structural insight into the geometry underlying bicentric configurations. Compared with these works, the present paper emphasizes a purely analytic-geometric derivation of Fuss' relations, providing explicit polynomial forms for higher-order odd bicentric polygons. This complements rather than replaces the modern computational approaches, bridging classical Euclidean geometry with contemporary algebraic methods.

The present paper builds upon Radić's approach and provides new analytical forms of Fuss' relations for bicentric polygons with an odd number of sides and higher rotation numbers. The derivation is based on Poncelet's theorem, Radić's theorem on the connection between Fuss' relations, and Radić's conjecture on their equivalence for different rotation numbers. Detailed statements of these results and references to their proofs are given in Section 2.

The main contribution of this paper is the derivation of previously unknown Fuss' relations for:

- the bicentric triskaidecagon (13-gon) with the rotation numbers $k=2,4,6$,
- the bicentric pentadecagon (15-gon) with the rotation number $k=2$,
- the bicentric heptadecagon (17-gon) with the rotation numbers $k=1,2,3,4,5,6,7,8$,
- and the bicentric enneadecagon (19-gon) with the rotation numbers $k=1,2,3,4,5,6,7,8,9$.

In this way, the paper fills a previously unexplored part of the set of known bicentric polygons and demonstrates the efficiency of a generalized approach that combines Poncelet's theorem with Radić's results on the relationship between the Fuss' relations $F_n^{(k)}(R,r,d)$ and $F_{n/p}^{(q)}(R,r,d)$ where p and q are determined by the greatest common divisor of n and k.

2 Theoretical background

This section provides a concise overview of the mathematical foundations on which the results of this paper are based. It includes the statements of Poncelet's theorem, Radić's theorem on the connection between Fuss' relations, and Radić's conjecture. Proofs of these theorems, and the derivation of the associated algorithms can be found in the cited works; therefore, only the relevant formulations and explanations are given here. Among them, Poncelet's theorem plays a central role in establishing the existence of bicentric polygons. This classical theorem is fundamental in the study of bicentric polygons and underlies the existence of closed polygons tangent to one circle and inscribed in another.

Theorem 1 (Poncelet's theorem) *Let C and K be two circles in a plane such that one lies entirely inside the other. Then exactly one of the following two statements holds:*

a) There exists no bicentric n-gon whose incircle is C and whose circumcircle is K.

b) There exist infinitely many bicentric n-gons whose incircle is C and circumcircle is K. For every point A_1 on the circle K, there exists a bicentric n-gon $A_1, A_2, \ldots, A_n$ whose incircle is C and circumcircle is K.

A detailed proof of this classical theorem can be found in [1] and is not repeated here.

Theorem 2 *Let n and k be positive integers, and let*

$$p = \gcd(n,k), \quad k = p \cdot q.$$

Then the corresponding Fuss' relations satisfy

$$F_n^{(k)}(R,r,d) = F_{n/p}^{(q)}(R,r,d),$$

where n is the number of sides and k the rotation number.

That is, analytically the Fuss' relation for a bicentric n-gon with rotation number k is equivalent to the relation for a smaller bicentric $\frac{n}{p}$-gon and rotation number q. The proof of this theorem is given in [9], where a computational procedure based on tangent lengths and Poncelet's closure condition is also presented.

Conjecture 1 *For an odd integer $n \geq 3$, the following equalities hold for the Fuss' relations of bicentric n-gons:*

$$F_n^{(i)}(R,r,d) = F_n^{(j)}(R,r,d)$$

$$\textit{for all odd } i,j \textit{ with } \gcd(i,n) = \gcd(j,n) = 1,$$

$$F_n^{(u)}(R,r,d) = F_n^{(v)}(R,r,d)$$

$$\textit{for all even } u,v \textit{ with } \gcd(u,n) = \gcd(v,n) = 1.$$

In other words, all Fuss' relations for rotation numbers that are coprime to n are identical within the same parity class (odd or even). The Conjecture 1. has been verified analytically and numerically for numerous values up to $n = 18$, but it remains unproven in the general case. If eventually proven, this Conjecture 1. would reveal a fundamental structural symmetry among Fuss' relations for bicentric n-gons. Although Conjecture 1. has not yet been rigorously established in full generality, the results presented here rely on it as a practical working assumption. Its validity has been confirmed for all tested configurations through both analytical derivations and numerical verification, which supports the conjecture's applicability within the scope of the present study.

Remark 1 *Radić's Conjecture 1. plays a fundamental role in simplifying the classification of Fuss' relations for bicentric n-gons with an odd number of sides [9]. It effectively reduces the number of distinct analytical forms that must be derived, since all relations within the same parity class (odd or even rotation numbers) are conjectured to coincide. In this paper, the Conjecture 1. is adopted as a working hypothesis for the higher-order cases ($n = 13, 15, 17, 19$) of this study, and the obtained results are in complete agreement with its predictions. Although the general proof of the Conjecture 1. remains open, the analytical and numerical confirmations presented here further support its validity and may provide further evidence supporting its eventual formal proof.*

3 Method

The analytical procedure for determining the coordinates of the vertices of a bicentric n-gon $A_1, A_2, \ldots, A_n$, when n is an odd number and the rotation number $k = 1$, was originally presented in [3]. In this section, the method is summarized, further clarified, and extended to cases of higher rotation numbers $k > 1$. The procedure is based on Poncelet's theorem, which guarantees the existence of a closed polygon inscribed in one circle and tangent to another, and on Radić's Theorem 2. and Conjecture 1., which establish the relationships among the corresponding Fuss' relations $F_n^{(k)}(R,r,d) = 0$ for different values of k.

Geometric setup. According to Poncelet's theorem, the choice of initial point and orientation does not affect polygon closure. Therefore, without loss of generality, we consider a configuration symmetric with respect to the x-axis, which passes through the centers of the two circles. The incircle C of radius r is centered at the point $I(d,0)$, while the circumcircle K of radius R is centered at the origin $O(0,0)$. The parameter d denotes the distance between their centers, and the inner circle C lies strictly inside the outer circle K, that is,

$$R \geq d + r > 0.$$

This assumption guarantees that C is completely contained within K and will later justify excluding nonphysical factors in the closure condition.

The polygon vertices $A_1, \ldots, A_n$ lie on K, and the sides A_iA_{i+1} are tangent to C.

Let t_i denote the tangent to the circle C at the point of tangency corresponding to the side A_iA_{i+1}, and let T_i denote the tangency point on C. The coordinates of the first vertex A_1 are obtained as the intersection of the tangent t_1, drawn

at the point $P(x_p,0)$ on the circle C, with the circle K. The abscissa x_p depends on the parity of the rotation number:

$$x_p = \begin{cases} d+r, & \text{if } k \text{ is odd,} \\ d-r, & \text{if } k \text{ is even.} \end{cases}$$

Recursive construction of vertices. Each subsequent vertex $A_i(x_i,y_i)$, for $i = 2,3,\ldots,n$, is determined as the intersection of the tangent t_i drawn from A_{i-1} to the incircle C and the circumcircle K. The equation of the tangent t_i is obtained from two conditions:

1. the line $y = ax+b$ passes through the known vertex $A_{i-1}(x_{i-1},y_{i-1})$, and
2. the line is tangent to the circle C.

From these conditions, the slope a and the intercept b are obtained by solving the system:

$$\begin{aligned} a\,x_{i-1} + b &= y_{i-1}, \\ r^2(1+a^2) - (ad+b)^2 &= 0. \end{aligned} \tag{2}$$

The intersection of this tangent with the circumcircle K gives the coordinates of the vertex A_i.

Since the polygon is symmetric with respect to the x-axis, the vertex $A_{(n+1)/2}$ lies on this axis, with the abscissa $x = -R$.

Closure condition and derivation of the Fuss' relation. In the geometric construction of a bicentric n-gon, we consider two opposite vertices, A_1 and $A_{(n+1)/2}$, on the circumcircle. From each of these vertices, tangents are drawn to an arbitrarily chosen vertex A_i on the same circle. When the point A_i is reached by successive tangent constructions starting from A_1, it is denoted by $A_i^{(1)}$. Likewise, when the same vertex is reached by tangents constructed in the opposite direction, starting from $A_{(n+1)/2}$, it is denoted by $A_i^{((n+1)/2)}$. The superscript therefore indicates the origin of the tangent sequence: $A_i^{(1)}$ corresponds to the forward traversal originating from A_1 (with successive index increments of $+1$), while $A_i^{((n+1)/2)}$ corresponds to the backward traversal originating from $A_{(n+1)/2}$ (with successive decrements of -1). All intermediate vertices generated along these two tangent sequences inherit the superscript of their respective starting vertex.

The closure condition of the bicentric n-gon requires that these two tangent sequences terminate at the same vertex on the circumcircle; in other words, the points obtained from the forward and backward constructions must coincide:

$$A_i^{(1)} \equiv A_i^{((n+1)/2)}.$$

This geometric requirement ensures that the polygon closes after n sides and thus satisfies Poncelet's closure theorem.

By equating the corresponding abscissas (and equivalently the ordinates) of the two coinciding vertices, one obtains the analytical closure equation

$$\rho(R,r,d) \cdot F_n^{(k)}(R,r,d) = 0,$$

where $\rho(R,r,d)$ is a non-vanishing scalar factor, and $F_n^{(k)}(R,r,d) = 0$ represents the analytical form of the Fuss' relation for the given n and rotation number k.

This formulation expresses the precise condition for polygonal closure and provides the foundation for deriving the explicit analytical expressions of the Fuss' relations discussed in the following sections.

Extension to higher rotation numbers. For polygons with rotation number $k > 1$, the construction proceeds analogously, but the initial tangent t_1 is drawn at the point $P(x_p,0)$ chosen according to the parity of k. Each subsequent tangent t_i is determined recursively using (2), while the closure condition is imposed after every k steps, that is, after k successive tangent mappings returning the polygon to the same orientation with respect to the incircle. The resulting equation in (R,r,d) then yields the corresponding Fuss' relation $F_n^{(k)}(R,r,d) = 0$.

The bicentric n-gon constructed from the initial point $A_1\,(x_p,0)$ thus represents the entire family of configurations satisfying Poncelet's closure condition. The same geometric construction, with the choice $x_p = d+r$ for odd k and $x_p = d-r$ for even k, yields all corresponding Fuss' relations for different rotation numbers. In particular, this means that the same analytical form of Fuss' relation $F_n^{(k)}(R,r,d) = 0$ applies to all polygons with rotation numbers of the same parity (e.g., $k = 1,3,5,\ldots$ or $k = 2,4,6,\ldots$), as predicted by Conjecture 1.

This recursive–geometric procedure, combined with algebraic elimination of intermediate coordinates, enables the analytic derivation of Fuss' relations for various odd values of n and rotation numbers k. The method thus provides a unified analytical approach applicable to all bicentric polygons that satisfy Poncelet's closure condition.

Transition to the results. The procedure described above enables the analytical determination of the closure condition for any bicentric n-gon satisfying Poncelet's theorem. By applying the method to specific values of n and k, the corresponding Fuss' relations $F_n^{(k)}(R,r,d) = 0$ can be explicitly derived. In the following section, we present the results obtained for the bicentric 13-gon, 15-gon, 17-gon, and 19-gon, including several previously unknown relations corresponding to higher rotation numbers.

4 Results

Throughout this section we use the shorthand

$$p=\frac{R+d}{r}, \qquad q=\frac{R-d}{r}. \tag{3}$$

For a bicentric n-gon the rotation number satisfies $k \in \{1,\dots,\lfloor (n-1)/2 \rfloor\}$. By Theorem 2. and Conjecture 1., the corresponding Fuss' relations $F_n^{(k)}(R,r,d)=0$ group into two parity classes (odd/even) that are identical within each class when $\gcd(k,n)=1$.

Bicentric 13-gon. For the bicentric 13-gon, the admissible rotation indices are $k \in \{1,2,3,4,5,6\}$. According to Theorem 2. and Conjecture 1., all Fuss relations for the bicentric 13-gon fall into two parity classes (odd and even):

$$F_{13}^{(1)}(R,r,d)=F_{13}^{(3)}(R,r,d)=F_{13}^{(5)}(R,r,d)=0, \tag{4}$$

$$F_{13}^{(2)}(R,r,d)=F_{13}^{(4)}(R,r,d)=F_{13}^{(6)}(R,r,d)=0. \tag{5}$$

The odd-class identity (4) was obtained in [3], here we derive the corresponding even-class relation (5).

Theorem 3 (13-gon, even class) *The bicentric 13-gon with rotation number $k=2$ satisfies*

$$F_{13}^{(2)}(R,r,d)=0,$$

where the explicit polynomial form in p,q is listed in Appendix A, Eq. (A.1).

Detailed proof. We work in the symmetric coordinate setup from Section 3: the incircle

$$C:\ (x-d)^2+y^2=r^2 \quad \text{and} \quad K:\ x^2+y^2=R^2,$$

with C entirely inside K and the x-axis joining the centers $O(0,0)$ and $I(d,0)$. For the even rotation number $k=2$ we start from the tangency point

$$P(d-r,0)\in C,$$

whose tangent to C is the vertical line $x=d-r$. Its intersection with K gives the first vertex

$$A_1=(x_1,y_1)=\big(d-r,\ \sqrt{R^2-(d-r)^2}\big),$$

where the sign of the square root is chosen so that A_1 lies above the x-axis. This choice only fixes orientation and does not affect the final closure condition.

Tangent from a given vertex and the next intersection with K. Let $A_{i-1}=(x_0,y_0)\in K$. A line $t_i: y=ax+b$ passes through A_{i-1} iff $b=y_0-ax_0$. The condition that t_i is tangent to C is

$$\operatorname{dist}\big(I,(t_i)\big)^2=\frac{(ad+b)^2}{1+a^2}=r^2 \iff r^2(1+a^2)-(ad+b)^2=0.$$

Substituting $b=y_0-ax_0$ yields a quadratic equation for the slope a:

$$\big(r^2-(d-x_0)^2\big)a^2-2(d-x_0)y_0\,a+\big(r^2-y_0^2\big)=0. \tag{6}$$

We pick the root that continues the forward traversal of the polygon (the other root corresponds to the opposite tangent).

Once a is fixed, t_i meets K at two points whose x-coordinates are the roots of

$$(1+a^2)x^2+2ab\,x+(b^2-R^2)=0.$$

Since one root is x_0, Vieta's formulas give the other root explicitly as

$$x_i=\frac{(a^2-1)x_0-2a\,y_0}{1+a^2}, \qquad y_i=ax_i+b. \tag{7}$$

Equations (6)–(7) form the closed recurrence for successive vertices.

Three steps from A_1. Applying (6)–(7) first with $(x_0,y_0)=A_1$, and then again from A_2 to obtain $A_3^{(1)}$, we arrive (after clearing radicals by squaring and simplifying) at rational expressions in (R,r,d). It is convenient to use the variables p and q introduced in (3). In these variables, the abscissa of $A_3^{(1)}$ takes the form

$$x_3^{(1)}=\frac{n_3^{(1)}}{d_3^{(1)}}, \tag{8}$$

with

$$\begin{aligned} n_3^{(1)} =& r\Big(-p^7(q-1)^4(q+1)^2 \\ &+p^6(q^2-1)^2(q^3+6q^2+3q+2) \\ &+p^5q(q+1)^2(2q^4-5q^3-4q^2+7q-4) \\ &-p^4q^2(q^5+10q^4-6q^3-12q^2+5q+2) \\ &+p^3q^3(-4q^4+5q^3+6q^2+5q+8) \\ &+p^2q^4(-q^3+2q^2+q-2) \\ &+pq^5(2q^2-3q-4)+q^6(q+2)\Big), \\ d_3^{(1)} =& 2\Big(p^3(-(q-1)^2)(q+1)-p^2q(q+1)^2 \\ &+pq^2(q+1)+q^3\Big)^2. \end{aligned}$$

Four steps from the symmetry point. By symmetry with respect to the x-axis, the middle vertex of the 13-gon is

$$A_{(13+1)/2} = A_7 = (-R, 0).$$

Starting from A_7 and iterating (6)–(7) three times forward (to $A_6^{(7)}, A_5^{(7)}, A_4^{(7)}$) and once more to reach $A_3^{(7)}$, we obtain

$$x_3^{(7)} = \frac{n_3^{(7)}}{d_3^{(7)}}, \tag{9}$$

with

$$\begin{aligned} n_3^{(7)} =& r(p+q)\Big(p^{16}(q^2-1)^4(q^8-20q^6-26q^4-20q^2+1) \\ &-8p^{14}q^2(q^2-1)^4(q^6-5q^4-9q^2-3) \\ &+4p^{12}q^4(q^2-1)^2(7q^8+8q^6+50q^4+40q^2-9) \\ &-8p^{10}q^6(q^2-1)^2(7q^6+29q^4+49q^2+11) \\ &+2p^8q^8(35q^8+60q^6-158q^4-68q^2+99) \\ &-8p^6q^{10}(7q^6-3q^4-31q^2+11) \\ &+4p^4q^{12}(7q^4-18q^2-9)-8p^2q^{14}(q^2-3)+q^{16}\Big), \end{aligned}$$

$$\begin{aligned} d_3^{(7)} =& 2\Big(p^8(q^2-1)^2(q^4+6q^2+1) \\ &-4p^6q^2(q^2-1)^2(q^2+1) \\ &+p^4(6q^8-4q^6+6q^4)-4p^2(q^8+q^6)+q^8\Big)^2. \end{aligned}$$

Poncelet closure and factorization. Poncelet's closure for the bicentric 13-gon with $k=2$ requires that the two constructions agree at the same point on K, hence

$$x_3^{(1)} = x_3^{(7)}.$$

Clearing denominators in (8)–(9) and simplifying, we obtain a polynomial equation in (R,r,d) which factors as

$$(d-r+R)\cdot\left(d^2-2rR-R^2\right)\cdot F_{13}^{(2)}(R,r,d) = 0, \tag{10}$$

where $F_{13}^{(2)}(R,r,d)$ is the polynomial displayed in (A.1).

Excluding extraneous factors. Because C lies strictly inside K, we have $R \geq d+r$ with $r>0$. The factor $d-r+R=0$ would imply $R = r-d \leq r+(-d) < r+d$, contradicting $R \geq d+r$ unless $r=0$ (degenerate). Moreover,

$$d^2-2rR-R^2 \leq d^2-2r(d+r)-(d+r)^2 = -\left(4dr+3r^2\right) < 0,$$

so $d^2-2rR-R^2=0$ is impossible under the nesting assumption. Hence the only admissible factor in (10) is

$$F_{13}^{(2)}(R,r,d) = 0,$$

which is exactly the claimed Fuss' relation for the 13-gon with rotation number $k=2$.

This completes the detailed analytic derivation. □

Graphical examples. For illustration, we present a concrete bicentric configuration corresponding to the analytically and numerically verified configuration of the 13-gon with rotation number $k=2$. With $R=1$ and $d=0.1$, solving $F_{13}^{(2)}(R,r,d)=0$ yields

$$r_{13,2} = 0.856554,$$

while, according to the even-class relations (5), the corresponding radii for higher even rotation numbers are

$$r_{13,4} = 0.561780, \qquad r_{13,6} = 0.119618.$$

Figure 1 illustrates the configuration for $k=2$.

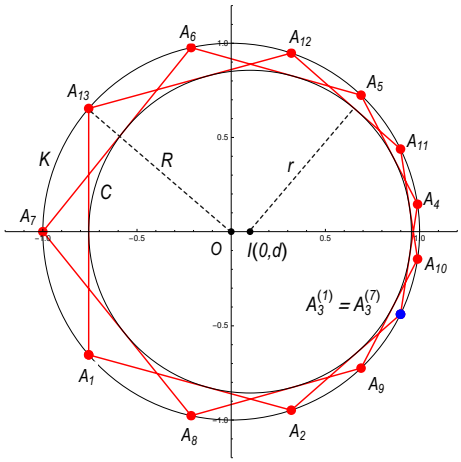

Figure 1: *Bicentric 13-gon for $R=1$, $d=0.1$, $r_{13,2}=0.856554$, and rotation number $k=2$. The incircle C is tangent to all sides of the polygon, and the circumcircle K passes through all vertices $A_1,\ldots,A_{13}$. The centers O and I are aligned on the x-axis. The polygon closes precisely after 13 tangents, confirming the analytical and numerical validity of the derived relation $F_{13}^{(2)}(R,r,d)=0$.*

Bicentric 15-gon. For the bicentric 15-gon, the admissible rotation indices are $k \in \{1,2,3,4,5,6,7\}$. According to Theorem 2. and Conjecture 1., all Fuss' relations for the bicentric 15-gon fall into four parity classes:

$$F_{15}^{(1)}(R,r,d) = F_{15}^{(7)}(R,r,d) = 0, \tag{11}$$

$$F_{15}^{(3)}(R,r,d) = F_5^{(1)}(R,r,d) = 0 \tag{12}$$

$$F_{15}^{(5)}(R,r,d) = F_3^{(1)}(R,r,d) = 0, \tag{13}$$

$$F_{15}^{(2)}(R,r,d) = F_{15}^{(4)}(R,r,d) = 0. \tag{14}$$

Identity (11) was obtained in [3], and the identities (12) and (13) were obtained in [9]. Here we derive the identity (14).

Theorem 4 *For a bicentric 15-gon with circumcircle of radius R, incircle of radius r, and distance d between their centers, the corresponding Fuss' relations satisfy:*

$$F_{15}^{(2)}(R,r,d) = F_{15}^{(4)}(R,r,d) = 0.$$

The explicit analytical forms of these relations are provided in Appendix A, Eq. (A.2).

Proof. The proof follows the same analytic–geometric procedure as in Theorem 3. The coordinates of the vertices $A_i(x_i,y_i)$ are determined recursively from the tangent condition (2) for the bicentric configuration with $n = 15$. The closure condition is imposed by equating the abscissas (and, equivalently, the ordinates) of the vertices $A_3^{(1)}(x_3^{(1)},y_3^{(1)})$ and $A_3^{(7)}(x_3^{(7)},y_3^{(7)})$, obtained from tangents drawn from A_1 and $A_{(n+1)/2}$. Since both $k = 2$ and $k = 4$ correspond to even rotation numbers, the geometric construction and algebraic elimination are completely analogous to those in Theorem 3 (the 13-gon case), differing only in the degree of the resulting polynomial in r. After simplification, the equations $F_{15}^{(2)}(R,r,d) = 0$ and $F_{15}^{(4)}(R,r,d) = 0$ are obtained. □

Bicentric 17-gon. For the bicentric 17-gon, the admissible rotation indices are $k \in \{1,2,3,4,5,6,7,8\}$. According to Theorem 2. and Conjecture 1., all Fuss relations for the bicentric 17-gon can be grouped into two parity classes: one corresponding to odd rotation numbers ($k = 1,3,5,7$) and the other to even rotation numbers ($k = 2,4,6,8$). Each class satisfies a distinct analytical form of the Fuss' relation, which is common to all members of that class. In the following theorem, we present the proof that covers both cases, demonstrating the validity of the relations for odd and even rotation numbers.

Theorem 5 *For a bicentric 17-gon with circumcircle of radius R, incircle of radius r, and distance d between their centers, the corresponding Fuss' relations satisfy:*

$$F_{17}^{(1)}(R,r,d) = F_{17}^{(3)}(R,r,d) = F_{17}^{(5)}(R,r,d) = F_{17}^{(7)}(R,r,d) = 0,$$

for odd rotation numbers $k = 1,3,5,7$, and

$$F_{17}^{(2)}(R,r,d) = F_{17}^{(4)}(R,r,d) = F_{17}^{(6)}(R,r,d) = F_{17}^{(8)}(R,r,d) = 0,$$

for even rotation numbers $k = 2,4,6,8$. The explicit analytical forms of these relations are given in Appendix A as Eq. (A.3) for the odd rotation numbers ($k = 1,3,5,7$) and Eq. (A.4) for the even rotation numbers ($k = 2,4,6,8$).

Proof. For the odd rotation numbers $k = 1,3,5,7$, the proof proceeds analogously to the case $k = 1$ discussed for the 13-gon and 15-gon in [3]. The first tangent t_1 is drawn at the point $P(r+d,0)$ on the incircle C, and the subsequent tangents determine the vertices A_i recursively using system (2). The closure condition is imposed by equating the abscissas of the vertices obtained from A_1 and $A_{(n+1)/2}$, ensuring that $A_i^{(1)} \equiv A_i^{(n+1)/2}$. Since all considered rotation numbers are odd, the geometric symmetry and analytic form of the procedure remain identical, leading to the family of relations listed above, which coincide according to Conjecture 1. □

Bicentric 19-gon. For the bicentric 19-gon, the admissible rotation indices are $k \in \{1,2,3,4,5,6,7,8,9\}$. According to Theorem 2. and Conjecture 1., all Fuss' relations for the bicentric 19-gon can be grouped into two parity classes: one corresponding to odd rotation numbers ($k = 1,3,5,7,9$) and the other to even rotation numbers ($k = 2,4,6,8$). Each class satisfies a distinct analytical form of the Fuss relation, which is common to all members of that class. In the following theorem, we present the proof that covers both cases, demonstrating the validity of the relations for odd and even rotation numbers.

Theorem 6 *For a bicentric 19-gon with circumcircle of radius R, incircle of radius r, and distance d between their centers, the corresponding Fuss' relations satisfy:*

$$\begin{aligned} F_{19}^{(1)}(R,r,d) &= F_{19}^{(3)}(R,r,d) = F_{19}^{(5)}(R,r,d) \\ &= F_{19}^{(7)}(R,r,d) = F_{19}^{(9)}(R,r,d) = 0, \end{aligned}$$

for odd rotation numbers $k = 1,3,5,7,9$, and

$$\begin{aligned} F_{19}^{(2)}(R,r,d) &= F_{19}^{(4)}(R,r,d) = F_{19}^{(6)}(R,r,d) \\ &= F_{19}^{(8)}(R,r,d) = 0, \end{aligned}$$

for even rotation numbers $k = 2,4,6,8$. The explicit analytical forms of these relations are given in Appendix A as Eq. (A.5) for the odd rotation numbers ($k = 1,3,5,7,9$) and Eq. (A.6) for the even rotation numbers ($k = 2,4,6,8$).

Proof. For even rotation numbers, the proof follows the same analytic–geometric principle as in Theorem 3. The initial tangent is drawn at the point $P(d-r,0)$ on the incircle C, corresponding to the even-k configuration. Each subsequent vertex is determined using the tangent condition (2), while the closure condition is established by equating the abscissas of the vertices obtained from opposite sides of the symmetric configuration (for example, $A_3^{(1)}$ and $A_3^{(9)}$ for $n = 17$). The analytical elimination of the coordinates yields polynomial relations in (R,r,d), producing the functions $F_{17}^{(2)}(R,r,d) = 0$, $F_{17}^{(4)}(R,r,d) = 0$, $F_{17}^{(6)}(R,r,d) = 0$, $F_{17}^{(8)}(R,r,d) = 0$, and analogously $F_{19}^{(2)}(R,r,d) = 0$, $F_{19}^{(4)}(R,r,d) = 0$,

$F_{19}^{(6)}(R,r,d) = 0$, $F_{19}^{(8)}(R,r,d) = 0$. For $k = 2$, the construction reduces exactly to the case described in Theorem 3., while for higher even k the algebraic form remains analogous but of higher order. □

Discussion. The results obtained for $n = 15$, $n = 17$, and $n = 19$ confirm the general validity of the analytical method described in Section 3. All relations exhibit the expected symmetry with respect to the parity of the rotation number and reduce to simpler forms for specific (n,k) pairs according to Radić's theorem 2. These findings, together with the detailed derivation for the 13-gon, complete the analytical description of Fuss' relations for bicentric polygons with an odd number of sides up to $n = 19$.

The cases $n = 13$ with $k = 2,4,6$ and $n = 15$ with $k = 2$ had not been reported previously in the literature. The reason lies primarily in the rapidly increasing algebraic complexity of the closure condition $F_n^{(k)}(R,r,d) = 0$ as both n and k increase, leading to polynomial equations of extremely high degree. The resulting polynomials reach very high algebraic degrees, which makes symbolic derivations increasingly intractable without computer algebra assistance. Earlier studies, such as [6]–[7], [9], were therefore limited to lower-degree cases due to these computational constraints. The present work extends those results by deriving explicit analytical expressions for the previously unresolved configurations.

Graphical representations of the bicentric 15-gon ($k = 2,4$), the bicentric 17-gon ($k = 1$–8), and the bicentric 19-gon ($k = 1$–9) are provided in Appendix A.3. These figures illustrate the analytically derived bicentric configurations and visually confirm the polygonal closure predicted by the corresponding Fuss' relations. The numerical values of the incircle radii, computed for $R = 1$ and $d = 0.1$, are listed in Appendix A.2, providing quantitative verification of the analytical results.

5 Conclusion

New analytical forms of the Fuss' relations $F_n^{(k)}(R,r,d) = 0$ have been derived for bicentric polygons with an odd number of sides and higher rotation numbers. Building upon Poncelet's theorem and Radić's theoretical framework, the proposed method allows the derivation of closed-form relations for previously unknown cases of the 13-gon, 15-gon, 17-gon, and 19-gon.

The proofs demonstrate how the analytic–geometric construction, combined with algebraic elimination, naturally yields the closure condition $\rho(R,r,d)\,F_n^{(k)}(R,r,d) = 0$, from which the analytical expressions follow directly. One detailed proof (Theorem 4.1) was presented in full detail, while subsequent theorems were obtained analogously by applying the same geometric principle for different rotation numbers.

Numerical and graphical verifications confirmed the validity of all derived relations, illustrating complete consistency between analytical derivation and computational results. The unified approach developed here provides a clear, extensible framework for deriving Fuss' relations of higher order and may serve as a basis for future generalizations to other classes of bicentric and Poncelet-type polygons.

Beyond its theoretical interest, the presented framework has potential applications in computational geometry and design. The explicit analytical forms of Fuss' relations can be implemented in symbolic computation software to automatically generate bicentric configurations satisfying Poncelet's closure condition. Moreover, such relations may find use in computer-aided design of circular mechanisms, in the geometric modeling of conic envelopes, and in the study of discrete dynamical systems arising from Poncelet-type polygons. These aspects provide a promising direction for future interdisciplinary research.

Acknowledgments. This work is supported by Croatian Science Foundation under the project HRZZ-IP-2024-05-3882. The author thanks Prof. Zoran Kaliman, PhD, for his valuable suggestions, which greatly improved this manuscript.

References

[1] DÖRRIE, H., *100 Great Problems of Elementary Mathematics*. Dover Publications, New York, 1965.

[2] DRAGOVIĆ, V., RADNOVIĆ, M., *Poncelet Porisms and Beyond: Integrable Billiards, Hyperelliptic Jacobians and Pencils of Quadrics*. *Frontiers in Mathematics*, Birkhäuser, Basel, 2011, https://doi.org/10.1007/978-3-0348-0015-0

[3] ORLIĆ BACHLER, M., KALIMAN, Z., Fuss' relation for bicentric tridecagon and bicentric pentadecagon. *Math. Pannon.* **1**(1) (2024), 162–170, https://doi.org/10.1556/314.2024.00015

[4] ORLIĆ, M., KALIMAN, Z., Analytical derivation of Fuss' relations for bicentric hendecagon and dodecagon. *Acta Phys. Polon A* **128** (2015), 201–206, https://doi.org/10.12693/APhysPolA.128.B-82

[5] ORLIĆ, M., KALIMAN, Z. Mathematica in analytical derivation of Fuss' relation. In: *Proceedings of Aplimat 2007*, Bratislava, 2007, 457–462.

[6] RADIĆ, M., An improved method for establishing Fuss' relations for bicentric n-gons where $n \geq 4$ is an even integer. *Rad Hrvat. Akad. Znan. Umjet. Mat. Znan.* **519** (= 18) (2014), 145–170.

[7] RADIĆ, M., Certain relations between triangles and bicentric hexagons. *Rad Hrvat. Akad. Znan. Umjet. Mat. Znan.* **503** (= 16) (2009), 21–40.

[8] RADIĆ, M., Functions of triples of positive real numbers and their use in the study of bicentric polygons. *Beitr. Algebra Geom.* **54** (2013), 709–736, https://doi.org/10.1007/s13366-012-0131-5

[9] RADIĆ, M., ZATEZALO, A., About some kinds of bicentric polygons and concerning relations. *Math. Maced.* **4**(1) (2006), 47–73.

[10] ROITMAN, P., GARCIA, R., REZNIK, D. , New invariants of Poncelet-Jacobi bicentric polygons. *Arnold Math. J.* **7**(4) (2021), 619–637, https://doi.org/10.1007/s40598-021-00188-6

Mandi Orlić Bachler
orcid.org/0000-0002-9011-1892
e-mail: mandi.orlic@tvz.hr

University of Applied Sciences
Av. V. Holjevca 15, Zagreb, Croatia

APENDIX A. Fuss' relations, numerical and graphical results

A.1. Analytical forms of Fuss' relations

In all Fuss' relations presented below, the substitution $p = \frac{R+d}{r}$, $q = \frac{R-d}{r}$ is used. The following analytical expressions correspond to the bicentric polygons derived in Section 4.

$$
\begin{aligned}
F_{13}^{(2)}(R,r,d) =& (q-1)^{12}(q+1)^9 p^{21} - (q-1)^6 q(q+1)^{10}\left(3q^4+10q^2+3\right)p^{20} - 2(q-1)^6 q^2(q+1)^9\left(3q^4-4q^3+10q^2\right.\\
&\left.-4q+3\right)p^{19} + 2(q-1)^6 q^3(q+1)^4\left(13q^8+36q^7+124q^6+156q^5+238q^4+156q^3+124q^2+36q+13\right)p^{18}\\
&+(q-1)^6 q^4(q+1)^5\left(9q^6+66q^5+71q^4+92q^3+71q^2+66q+9\right)p^{17} - (q-1)^6 q^5(q+1)^4\left(99q^6+118q^5+493q^4\right.\\
&\left.+308q^3+493q^2+118q+99\right)p^{16} + 8(q-1)^2 q^6(q+1)^5\left(3q^8-8q^7+34q^6-32q^5+38q^4-32q^3+34q^2-8q+3\right)p^{15}\\
&+8(q-1)^2 q^7(q+1)^4\left(27q^8-84q^7+166q^6-252q^5+318q^4-252q^3+166q^2-84q+27\right)p^{14} - 2(q-1)^2 q^8(q+1)^5\left(63q^6\right.\\
&\left.-34q^5+169q^4-76q^3+169q^2-34q+63\right)p^{13} - 2(q-1)^2 q^9(q+1)^4\left(147q^6-370q^5+709q^4-684q^3+709q^2\right.\\
&\left.-370q+147\right)p^{12} + 4(q-1)^2 q^{10}\left(63q^9+255q^8+536q^7+776q^6+930q^5+930q^4+776q^3+536q^2+255q+63\right)p^{11}\\
&+4q^{11}\left(q^2-1\right)^2\left(63q^6+38q^5+61q^4+188q^3+61q^2+38q+63\right)p^{10} - 2(q-1)^2 q^{12}\left(147q^7+449q^6+867q^5+1097q^4\right.\\
&\left.+1097q^3+867q^2+449q+147\right)p^9 - 2q^{13}\left(q^2-1\right)^2\left(63q^4+120q^3+74q^2+120q+63\right)p^8 + 8q^{14}\left(27q^7+q^6+5q^5-33q^4\right.\\
&\left.-33q^3+5q^2+q+27\right)p^7 + 8q^{15}(q+1)^2\left(3q^4+4q^3-16q^2+4q+3\right)p^6 + q^{16}\left(-99q^5+57q^4+26q^3+26q^2+57q-99\right)p^5\\
&+q^{17}(q+1)^2\left(9q^2+2q+9\right)p^4 + 2q^{18}\left(13q^3-5q^2-5q+13\right)p^3 - 6q^{19}(q+1)^2 p^2 - 3q^{20}(q+1)p + q^{21} = 0\,.
\end{aligned}
\tag{A.1}
$$

$$
\begin{aligned}
F_{15}^{(2)}(R,r,d) =& (q-1)^{10}(q+1)^{14}p^{24} + 4(q-1)^8 q(q+1)^7\left(q^8-q^7+14q^6+q^5+34q^4+q^3+14q^2-q+1\right)p^{23}\\
&-4q^2\left(q^2-1\right)^6\left(q^{10}-8q^9-3q^8-64q^7+2q^6-112q^5+2q^4-64q^3-3q^2-8q+1\right)p^{22} - 4(q-1)^6 q^3(q+1)^5\\
&\left(9q^{10}+8q^9+37q^8+64q^7-46q^6+112q^5-46q^4+64q^3+37q^2+8q+9\right)p^{21} - 2(q-1)^6 q^4(q+1)^4\left(7q^{10}\right.\\
&\left.+116q^9+323q^8+608q^7+1078q^6+856q^5+1078q^4+608q^3+323q^2+116q+7\right)p^{20} + 4(q-1)^6 q^5(q+1)^3\\
&\left(35q^{10}+121q^9+211q^8+340q^7+458q^6+230q^5+458q^4+340q^3+211q^2+121q+35\right)p^{19}\\
&+4(q-1)^6 q^6(q+1)^4\left(35q^8+132q^7+444q^6+412q^5+898q^4+412q^3+444q^2+132q+35\right)p^{18}\\
&-4(q-1)^6 q^7(q+1)^3\left(75q^8+212q^7+444q^6+332q^5+818q^4+332q^3+444q^2+212q+75\right)p^{17}
\end{aligned}
\tag{A.2}
$$

$$
\begin{aligned}
&-(q-1)^4q^8(q+1)^2\left(465q^{10}+474q^9+1773q^8-168q^7-1726q^6-612q^5-1726q^4-168q^3+1773q^2\right.\\
&\left.+474q+465\right)p^{16}+8(q-1)^2q^9(q+1)^3\left(45q^{10}-147q^9+309q^8-876q^7+1534q^6-1858q^5+1534q^4\right.\\
&\left.-876q^3+309q^2-147q+45\right)p^{15}+8q^{10}\left(q^2-1\right)^2\left(111q^{10}-196q^9-163q^9-255q^8-726q^7-110q^6\right.\\
&\left.-110q^5-726q^4+243q^8-288q^7+30q^6+328q^5+30q^4-288q^3+243q^2-196q+111\right)p^{14}\\
&-8(q-1)^2q^{11}\left(21q^{11}-175q^{10}-255q^3-163q^2-175q+21\right)p^{13}-4q^{12}\left(q^2-1\right)^2\left(273q^8-434q^7\right.\\
&\left.+504q^6-142q^5+302q^4-142q^3+504q^2-434q+273\right)p^{12}-8(q-1)^2q^{13}\left(21q^9+238q^8+383q^7\right.\\
&\left.+237q^6+625q^5+625q^4+237q^3+383q^2+238q+21\right)p^{11}+8q^{14}\left(q^2-1\right)^2\left(111q^6-102q^5+177q^4\right.\\
&\left.-4q^3+177q^2-102q+111\right)p^{10}+8(q-1)^2q^{15}\left(45q^7+147q^6+345q^5+247q^4+247q^3+345q^2+147q\right.\\
&\left.+45\right)p^9-q^{16}\left(q^2-1\right)^2\left(465q^4-52q^3+630q^2-52q+465\right)p^8-4(q-1)^2q^{17}\left(75q^5+88q^4+253q^3\right.\\
&\left.+253q^2+88q+75\right)p^7+4q^{18}\left(q^2-1\right)^2\left(35q^2+16q+35\right)p^6+4(q-1)^2q^{19}\left(35q^3+19q^2+19q+35\right)p^5\\
&-2q^{20}(q+1)^2\left(7q^2-16q+7\right)p^4-4q^{21}\left(9q^3-8q^2-8q+9\right)p^3-4q^{22}(q+1)^2p^2+4q^{23}(q+1)p+q^{24}=0\,.
\end{aligned}
$$

$$
\begin{aligned}
F_{17}^{(1)}(R,r,d)=&(q-1)^{16}(q+1)^{20}p^{36}+4(q-1)^{17}q(q+1)^{12}\left(q^6+7q^4+7q^2+1\right)p^{35}-2(q-1)^{16}q^2(q+1)^{12}\\
&\left(5q^6+10q^5+35q^4+28q^3+35q^2+10q+5\right)p^{34}-4(q-1)^9q^3(q+1)^{12}\left(15q^{12}-60q^{11}+294q^{10}-588q^9\right.\\
&\left.+1377q^8-1656q^7+2260q^6-1656q^5+1377q^4-588q^3+294q^2-60q+15\right)p^{33}+(q-1)^{10}q^4(q+1)^{12}\left(25q^{10}\right.\\
&\left.-274q^9+517q^8-1176q^7+1506q^6-2220q^5+1506q^4-1176q^3+517q^2-274q+25\right)p^{32}+32(q-1)^9q^5(q+1)^{12}\\
&\left(13q^{10}-26q^9+149q^8-178q^7+438q^6-312q^5+438q^4-178q^3+149q^2-26q+13\right)p^{31}+16(q-1)^{10}q^6(q+1)^6\\
&\left(9q^{14}+42q^{13}+234q^{12}+410q^{11}+892q^{10}+1214q^9+1937q^8+1788q^7+1937q^6+1214q^5+892q^4+410q^3+234q^2\right.\\
&\left.+42q+9\right)p^{30}-32(q-1)^9q^7(q+1)^6\left(55q^{14}+250q^{13}+820q^{12}+2074q^{11}+4234q^{10}+6542q^9+8843q^8+9660q^7\right.\\
&\left.+8843q^6+6542q^5+4234q^4+2074q^3+820q^2+250q+55\right)p^{29}-4(q-1)^{10}q^8(q+1)^6\left(355q^{12}+480q^{11}+3066q^{10}\right.\\
&\left.+3376q^9+9725q^8+8176q^7+15180q^6+8176q^5+9725q^4+3376q^3+3066q^2+480q+355\right)p^{28}\\
&+16(q-1)^9q^9(q+1)^6\left(315q^{12}+1294q^{11}+4118q^{10}+8258q^9+15389q^8+19696q^7+22948q^6+19696q^5+15389q^4\right.\\
&\left.+8258q^3+4118q^2+1294q+315\right)p^{27}+8(q-1)^4q^{10}(q+1)^6\left(749q^{16}-3476q^{15}+10942q^{14}-25756q^{13}+51400q^{12}\right.\\
&\left.-84404q^{11}+125282q^{10}-154652q^9+168022q^8-154652q^7+125282q^6-84404q^5+51400q^4-25756q^3+10942q^2\right.\\
&\left.-3476q+749\right)p^{26}-16(q-1)^5q^{11}(q+1)^6\left(637q^{14}-586q^{13}+2257q^{12}-6544q^{11}+8415q^{10}-15142q^9+18387q^8\right.\\
&\left.-15872q^7+18387q^6-15142q^5+8415q^4-6544q^3+2257q^2-586q+637\right)p^{25}-4(q-1)^4q^{12}(q+1)^6\left(4095q^{14}\right.\\
&\left.-15830q^{13}+50625q^{12}-103812q^{11}+201091q^{10}-285930q^9+388285q^8-403320q^7+388285q^6-285930q^5\right.\\
&\left.+201091q^4-103812q^3+50625q^2-15830q+4095\right)p^{24}+32(q-1)^5q^{13}(q+1)^6\left(455q^{12}-1020q^{11}+2206q^{10}\right.\\
&\left.-5862q^9+7453q^8-9822q^7+11388q^6-9822q^5+7453q^4-5862q^3+2206q^2-1020q+455\right)p^{23}\\
&+16(q-1)^4q^{14}(q+1)^6\left(2015q^{12}-5812q^{11}+19561q^{10}-32800q^9+62365q^8-71980q^7+89910q^6-71980q^5\right.\\
&\left.+62365q^4-32800q^3+19561q^2-5812q+2015\right)p^{22}-32(q-1)^5q^{15}(q+1)^2\left(429q^{14}+110q^{13}-1298q^{12}\right.\\
&\left.-3398q^{11}-7160q^{10}-6470q^9-3235q^8-2500q^7-3235q^6-6470q^5-7160q^4-3398q^3-1298q^2+110q\right.\\
&\left.+429\right)p^{21}-2(q-1)^4q^{16}(q+1)^2\left(23881q^{14}+47718q^{13}+126203q^{12}+283116q^{11}+412761q^{10}+633018q^9\right.\\
&\left.+786787q^8+763368q^7+786787q^6+633018q^5+412761q^4+283116q^3+126203q^2+47718q+23881\right)p^{20}\\
&+8(q-1)^5q^{17}(q+1)^2\left(715q^{12}-1870q^{11}-11110q^{10}-15406q^9-22747q^8-20356q^7-17172q^6-20356q^5\right.\\
&\left.-22747q^4-15406q^3-11110q^2-1870q+715\right)p^{19}+4(q-1)^4q^{18}(q+1)^2\left(13585q^{12}+35200q^{11}+80542q^{10}\right.\\
&\left.+163952q^9+235663q^8+293392q^7+340868q^6+293392q^5+235663q^4+163952q^3+80542q^2+35200q\right.\\
&\left.+13585\right)p^{18}+8(q-1)^5q^{19}(q+1)^2\left(715q^{10}+2134q^9+10483q^8+10464q^7+14658q^6+12564q^5+14658q^4\right.
\end{aligned}
\tag{A.3}
$$

$$
\begin{aligned}
&+10464q^3+10483q^2+2134q+715\big)p^{17}-2(q-1)^4q^{20}(q+1)^2\left(23881q^{10}+66594q^9+141933q^8+241640q^7\right.\\
&\left.+335562q^6+337644q^5+335562q^4+241640q^3+141933q^2+66594q+23881\right)p^{16}\\
&-32q^{21}\left(429q^{15}-891q^{14}+1089q^{13}-1521q^{12}-57q^{11}+2541q^{10}-1567q^9-235q^8+235q^7+1567q^6\right.\\
&\left.-2541q^5+57q^4+1521q^3-1089q^2+891q-429\right)p^{15}+16q^{22}\left(q^2-1\right)^2\left(2015q^{10}+1130q^9+2360q^8\right.\\
&\left.-2282q^7+889q^6-8288q^5+889q^4-2282q^3+2360q^2+1130q+2015\right)p^{14}+16(q-1)^4q^{14}(q+1)^6\\
&\left(2015q^{12}-5812q^{11}+19561q^{10}-32800q^9+62365q^8-71980q^7+89910q^6-71980q^5+62365q^4-32800q^3\right.\\
&\left.+19561q^2-5812q+2015\right)p^{22}-32(q-1)^5q^{15}(q+1)^2\left(429q^{14}+110q^{13}-1298q^{12}-3398q^{11}-7160q^{10}\right.\\
&\left.-6470q^9-3235q^8-2500q^7-3235q^6-6470q^5-7160q^4-3398q^3-1298q^2+110q+429\right)p^{21}\\
&-2(q-1)^4q^{16}(q+1)^2\left(23881q^{14}+47718q^{13}+126203q^{12}+283116q^{11}+412761q^{10}+633018q^9+786787q^8\right.\\
&\left.+763368q^7+786787q^6+633018q^5+412761q^4+283116q^3+126203q^2+47718q+23881\right)p^{20}+8(q-1)^5q^{17}(q+1)^2\\
&\left(715q^{12}-1870q^{11}-11110q^{10}-15406q^9-22747q^8-20356q^7-17172q^6-20356q^5-22747q^4-15406q^3-11110q^2\right.\\
&\left.-1870q+715\right)p^{19}+4(q-1)^4q^{18}(q+1)^2\left(13585q^{12}+35200q^{11}+80542q^{10}+163952q^9+235663q^8+293392q^7\right.\\
&\left.+340868q^6+293392q^5+235663q^4+163952q^3+80542q^2+35200q+13585\right)p^{18}\\
&+8(q-1)^5q^{19}(q+1)^2\left(715q^{10}+2134q^9+10483q^8+10464q^7+14658q^6+12564q^5+14658q^4+10464q^3+10483q^2\right.\\
&\left.+2134q+715\right)p^{17}-2(q-1)^4q^{20}(q+1)^2\left(23881q^{10}+66594q^9+141933q^8+241640q^7+335562q^6+337644q^5\right.\\
&\left.+335562q^4+241640q^3+141933q^2+66594q+23881\right)p^{16}-32q^{21}\left(429q^{15}-891q^{14}+1089q^{13}-1521q^{12}\right.\\
&\left.-57q^{11}+2541q^{10}-1567q^9-235q^8+235q^7+1567q^6-2541q^5+57q^4+1521q^3-1089q^2+891q-429\right)p^{15}\\
&+16q^{22}\left(q^2-1\right)^2\left(2015q^{10}+1130q^9+2360q^8-2282q^7+889q^6-8288q^5+889q^4-2282q^3+2360q^2+1130q+2015\right)p^{14}\\
&+32q^{23}(q+1)^2\left(455q^{11}-1865q^{10}+4032q^9-6340q^8+8305q^7-9243q^6+9243q^5-8305q^4+6340q^3-4032q^2\right.\\
&\left.+1865q-455\right)p^{13}-4q^{24}\left(q^2-1\right)^2\left(4095q^8-204q^7+4704q^6-10900q^5+4034q^4-10900q^3+4704q^2-204q+4095\right)p^{12}\\
&-16q^{25}(q+1)^2\left(637q^9-2263q^8+4598q^7-6486q^6+7648q^5-7648q^4+6486q^3-4598q^2+2263q-637\right)p^{11}\\
&+8q^{26}\left(q^2-1\right)^2\left(749q^6-698q^5+925q^4-2200q^3+925q^2-698q+749\right)p^{10}+16q^{27}(q+1)^2\left(315q^7-865q^6+1605q^5\right.\\
&\left.-1999q^4+1999q^3-1605q^2+865q-315\right)p^9-4(q-1)^2q^{28}\left(355q^6+30q^5-559q^4-452q^3-559q^2+30q+355\right)p^8\\
&-32q^{29}\left(55q^7+3q^6+7q^5+57q^4-57q^3-7q^2-3q-55\right)p^7+16(q-1)^2q^{30}\left(9q^4-8q^3-41q^2-8q+9\right)p^6\\
&+32q^{31}\left(13q^5+7q^4-3q^3+3q^2-7q-13\right)p^5+5(q-1)^2q^{32}\left(5q^2-2q+5\right)p^4-20q^{33}\left(3q^3+q^2-q-3\right)p^3\\
&-10(q-1)^2q^{34}p^2+4(q-1)q^{35}p+q^{36}=0
\end{aligned}
$$

$$
\begin{aligned}
F_{17}^{(2)}(R,r,d)=&(q-1)^{20}(q+1)^{16}p^{36}-4(q-1)^{12}q(q+1)^{17}\left(q^6+7q^4+7q^2+1\right)p^{35}-2(q-1)^{12}q^2(q+1)^{16}\\
&\left(5q^6-10q^5+35q^4-28q^3+35q^2-10q+5\right)p^{34}+4(q-1)^{12}q^3(q+1)^9\left(15q^{12}+60q^{11}+294q^{10}+588q^9\right.\\
&\left.+1377q^8+1656q^7+2260q^6+1656q^5+1377q^4+588q^3+294q^2+60q+15\right)p^{33}+(q-1)^{12}q^4(q+1)^{10}\\
&\left(25q^{10}+274q^9+517q^8+1176q^7+1506q^6+2220q^5+1506q^4+1176q^3+517q^2+274q+25\right)p^{32}\\
&-32(q-1)^{12}q^5(q+1)^9\left(13q^{10}+26q^9+149q^8+178q^7+438q^6+312q^5+438q^4+178q^3+149q^2+26q\right.\\
&\left.+13\right)p^{31}+16(q-1)^6q^6(q+1)^{10}\left(9q^{14}-42q^{13}+234q^{12}-410q^{11}+892q^{10}-1214q^9+1937q^8-1788q^7\right.\\
&\left.+1937q^6-1214q^5+892q^4-410q^3+234q^2-42q+9\right)p^{30}+32(q-1)^6q^7(q+1)^9\left(55q^{14}-250q^{13}\right.\\
&\left.+820q^{12}-2074q^{11}+4234q^{10}-6542q^9+8843q^8-9660q^7+8843q^6-6542q^5+4234q^4-2074q^3+820q^2\right.\\
&\left.-250q+55\right)p^{29}-4(q-1)^6q^8(q+1)^{10}\left(355q^{12}-480q^{11}+3066q^{10}-3376q^9+9725q^8-8176q^7+15180q^6\right.\\
&\left.-8176q^5+9725q^4-3376q^3+3066q^2-480q+355\right)p^{28}-16(q-1)^6q^9(q+1)^9\left(315q^{12}-1294q^{11}+4118q^{10}\right.
\end{aligned}
\tag{A.4}
$$

$$
\begin{aligned}
&-8258q^9+15389q^8-19696q^7+22948q^6-19696q^5+15389q^4-8258q^3+4118q^2-1294q+315\Big)p^{27}\\
&+8(q-1)^6q^{10}(q+1)^4\Big(749q^{16}+3476q^{15}+10942q^{14}+25756q^{13}+51400q^{12}+84404q^{11}+125282q^{10}\\
&+154652q^9+168022q^8+154652q^7+125282q^6+84404q^5+51400q^4+25756q^3+10942q^2+3476q+749\Big)p^{26}\\
&+16(q-1)^6q^{11}(q+1)^5\left(637q^{14}+586q^{13}+2257q^{12}+6544q^{11}+8415q^{10}+15142q^9+18387q^8+15872q^7\right.\\
&\left.+18387q^6+15142q^5+8415q^4+6544q^3+2257q^2+586q+637\right)p^{25}-4(q-1)^6q^{12}(q+1)^4\left(4095q^{14}\right.\\
&\left.+15830q^{13}+50625q^{12}+103812q^{11}+201091q^{10}+285930q^9+388285q^8+403320q^7+388285q^6\right.\\
&\left.+285930q^5+201091q^4+103812q^3+50625q^2+15830q+4095\right)p^{24}\\
&-32(q-1)^6q^{13}(q+1)^5\Big(455q^{12}+1020q^{11}+2206q^{10}+5862q^9+7453q^8+9822q^7+11388q^6+9822q^5\\
&+7453q^4+5862q^3+2206q^2+1020q+455\Big)p^{23}+16(q-1)^6q^{14}(q+1)^4\left(2015q^{12}+5812q^{11}+19561q^{10}\right.\\
&\left.+32800q^9+62365q^8+71980q^7+89910q^6+71980q^5+62365q^4+32800q^3+19561q^2+5812q+2015\right)p^{22}\\
&+32(q-1)^2q^{15}(q+1)^5\left(429q^{14}-110q^{13}-1298q^{12}+3398q^{11}-7160q^{10}+6470q^9-3235q^8+2500q^7\right.\\
&\left.-3235q^6+6470q^5-7160q^4+3398q^3-1298q^2-110q+429\right)p^{21}-2(q-1)^2q^{16}(q+1)^4\left(23881q^{14}\right.\\
&\left.-47718q^{13}+126203q^{12}-283116q^{11}+412761q^{10}-633018q^9+786787q^8-763368q^7+786787q^6\right.\\
&\left.-633018q^5+412761q^4-283116q^3+126203q^2-47718q+23881\right)p^{20}-8(q-1)^2q^{17}(q+1)^5\left(715q^{12}\right.\\
&\left.+1870q^{11}-11110q^{10}+15406q^9-22747q^8+20356q^7-17172q^6+20356q^5-22747q^4+15406q^3\right.\\
&\left.-11110q^2+1870q+715\right)p^{19}+4(q-1)^2q^{18}(q+1)^4\left(13585q^{12}-35200q^{11}+80542q^{10}-163952q^9\right.\\
&\left.+235663q^8-293392q^7+340868q^6-293392q^5+235663q^4-163952q^3+80542q^2-35200q+13585\right)p^{18}\\
&-8(q-1)^2q^{19}(q+1)^5\Big(715q^{10}-2134q^9+10483q^8-10464q^7+14658q^6-12564q^5+14658q^4-10464q^3\\
&+10483q^2-2134q+715\Big)p^{17}-2(q-1)^2q^{20}(q+1)^4\left(23881q^{10}-66594q^9+141933q^8-241640q^7\right.\\
&\left.+335562q^6-337644q^5+335562q^4-241640q^3+141933q^2-66594q+23881\right)p^{16}\\
&+32(q-1)^2q^{21}\Big(429q^{13}+1749q^{12}+4158q^{11}+8088q^{10}+11961q^9+13293q^8+13058q^7+13058q^6\\
&+13293q^5+11961q^4+8088q^3+4158q^2+1749q+429\Big)p^{15}+16q^{22}\left(q^2-1\right)^2\left(2015q^{10}-1130q^9\right.\\
&\left.+2360q^8+2282q^7+889q^6+8288q^5+889q^4+2282q^3+2360q^2-1130q+2015\right)p^{14}\\
&-32(q-1)^2q^{23}\Big(455q^{11}+1865q^{10}+4032q^9+6340q^8+8305q^7+9243q^6+9243q^5+8305q^4\\
&+6340q^3+4032q^2+1865q+455\Big)p^{13}-4q^{24}\left(q^2-1\right)^2\Big(4095q^8+204q^7+4704q^6+10900q^5\\
&+4034q^4+10900q^3+4704q^2+204q+4095\Big)p^{12}+16(q-1)^2q^{25}\Big(637q^9+2263q^8+4598q^7+6486q^6\\
&+7648q^5+7648q^4+6486q^3+4598q^2+2263q+637\Big)p^{11}+8q^{26}\left(q^2-1\right)^2\Big(749q^6+698q^5+925q^4\\
&+2200q^3+925q^2+698q+749\Big)p^{10}-16(q-1)^2q^{27}\Big(315q^7+865q^6+1605q^5+1999q^4+1999q^3\\
&+1605q^2+865q+315\Big)p^9-4q^{28}(q+1)^2\Big(355q^6-30q^5-559q^4+452q^3-559q^2-30q+355\Big)p^8\\
&+32q^{29}\Big(55q^7-3q^6+7q^5-57q^4-57q^3+7q^2-3q+55\Big)p^7+16q^{30}(q+1)^2\left(9q^4+8q^3\right.\\
&\left.-41q^2+8q+9\right)p^6-32q^{31}\Big(13q^5-7q^4-3q^3-3q^2-7q+13\Big)p^5+5q^{32}(q+1)^2\left(5q^2+2q+5\right)p^4\\
&+20q^{33}\left(3q^3-q^2-q+3\right)p^3-10q^{34}(q+1)^2p^2-4q^{35}(q+1)p+q^{36}=0.
\end{aligned}
$$

$$
\begin{aligned}
F_{19}^{(1)}(R,r,d)=&(q-1)^{25}(q+1)^{20}p^{45}-(q-1)^{16}q(q+1)^{20}\Big(5q^8+60q^6+126q^4+60q^2+5\Big)p^{44}-2(q-1)^{17}q^2(q+1)^{20}\\
&\Big(5q^6-10q^5+35q^4-28q^3+35q^2-10q+5\Big)p^{43}+2(q-1)^{16}q^3(q+1)^{12}\left(45q^{14}+210q^{13}+1143q^{12}+2724q^{11}\right.\\
&\left.+7437q^{10}+11022q^9+17999q^8+17144q^7+17999q^6+11022q^5+7437q^4+2724q^3+1143q^2+210q+45\right)p^{42}\\
&-(q-1)^{17}q^4(q+1)^{12}\Big(5q^{12}-324q^{11}-838q^{10}-2484q^9-3349q^8-6408q^7-5972q^6-6408q^5-3349q^4\\
&-2484q^3-838q^2-324q+5\Big)p^{41}-(q-1)^{16}q^5(q+1)^{12}\left(751q^{12}+1988q^{11}+12142q^{10}+18548q^9+51553q^8\right.
\end{aligned}
\tag{A.5}
$$

$$+50120q^7+82052q^6+50120q^5+51553q^4+18548q^3+12142q^2+1988q+751\Big)p^{40}+4(q-1)^9q^6(q+1)^{12}\left(165q^{18}\right.$$
$$-750q^{17}+3945q^{16}-9320q^{15}+25672q^{14}-45304q^{13}+89152q^{12}-114072q^{11}+159594q^{10}-152628q^9+159594q^8$$
$$-114072q^7+89152q^6-45304q^5+25672q^4-9320q^3+3945q^2-750q+165\Big)p^{39}+4(q-1)^{10}q^7(q+1)^{12}\Big(955q^{16}$$
$$-4120q^{15}+15380q^{14}-44792q^{13}+100556q^{12}-179080q^{11}+282220q^{10}-357736q^9+389618q^8-357736q^7$$
$$+282220q^6-179080q^5+100556q^4-44792q^3+15380q^2-4120q+955\Big)p^{38}-(q-1)^9q^8(q+1)^{12}\Big(5605q^{16}-12720q^{15}$$
$$+79144q^{14}-134992q^{13}+435372q^{12}-552944q^{11}+1155224q^{10}-1068816q^9+1564510q^8-1068816q^7+1155224q^6$$
$$-552944q^5+435372q^4-134992q^3+79144q^2-12720q+5605\Big)p^{37}-(q-1)^{10}q^9(q+1)^{12}\left(13015q^{14}-57594q^{13}\right.$$
$$+197245q^{12}-469636q^{11}+977279q^{10}-1469734q^9+2023725q^8-2150072q^7+2023725q^6-1469734q^5+977279q^4$$
$$-469636q^3+197245q^2-57594q+13015\Big)p^{36}+2(q-1)^9q^{10}(q+1)^6\left(13623q^{20}+58692q^{19}+224578q^{18}+644388q^{17}\right.$$
$$+1537387q^{16}+3161936q^{15}+5726616q^{14}+8736400q^{13}+12079710q^{12}+14399416q^{11}+15362124q^{10}+14399416q^9$$
$$+12079710q^8+8736400q^7+5726616q^6+3161936q^5+1537387q^4+644388q^3+224578q^2+58692q+13623\Big)p^{35}$$
$$+2(q-1)^{10}q^{11}(q+1)^6\Big(15105q^{18}+33250q^{17}+68825q^{16}+227120q^{15}+458932q^{14}+936248q^{13}+1612484q^{12}$$
$$+2079824q^{11}+2366638q^{10}+2622156q^9+2366638q^8+2079824q^7+1612484q^6+936248q^5+458932q^4+227120q^3$$
$$+68825q^2+33250q+15105\Big)p^{34}-(q-1)^9q^{12}(q+1)^6$$
$$(92055q^{18}+383630q^{17}+1452895q^{16}+3794064q^{15}+8841036q^{14}$$
$$+16031112q^{13}+27191804q^{12}+36730864q^{11}+46308290q^{10}+48125652q^9+46308290q^8+36730864q^7+27191804q^6$$
$$+16031112q^5+8841036q^4+3794064q^3+1452895q^2+383630q+92055\Big)p^{33}-(q-1)^{10}q^{13}(q+1)^6\Big(43605q^{16}$$
$$+167220q^{15}+342208q^{14}+1128700q^{13}+2176220q^{12}+3799508q^{11}+5324928q^{10}+6750204q^9+6541086q^8$$
$$+6750204q^7+5324928q^6+3799508q^5+2176220q^4+1128700q^3+342208q^2+167220q+43605\Big)p^{32}$$
$$+16(q-1)^9q^{14}(q+1)^6\Big(14535q^{16}+53048q^{15}+204500q^{14}+460152q^{13}+1051356q^{12}+1636168q^{11}+2599852q^{10}$$
$$+3002376q^9+3472314q^8+3002376q^7+2599852q^6+1636168q^5+1051356q^4+460152q^3+204500q^2+53048q+14535\Big)p^{31}$$
$$+16(q-1)^4q^{15}(q+1)^6\Big(969q^{20}+9664q^{19}-54654q^{18}+152816q^{17}-329771q^{16}+491984q^{15}-652264q^{14}+928624q^{13}$$
$$-1334686q^{12}+1710096q^{11}-1911092q^{10}+1710096q^9-1334686q^8+928624q^7-652264q^6+491984q^5-329771q^4$$
$$+152816q^3-54654q^2+9664q+969\Big)p^{30}-2(q-1)^5q^{16}(q+1)^6\Big(227715q^{18}-235650q^{17}+1366235q^{16}-2686160q^{15}$$
$$+5032460q^{14}-10636024q^{13}+13987228q^{12}-19540144q^{11}+23852538q^{10}-22605324q^9+23852538q^8-19540144q^7$$
$$+13987228q^6-10636024q^5+5032460q^4-2686160q^3+1366235q^2-235650q+227715\Big)p^{29}+2(q-1)^4q^{17}(q+1)^6$$
$$\Big(53295q^{18}-333170q^{17}+1258535q^{16}-2648080q^{15}+5210748q^{14}-8023224q^{13}+12000716q^{12}-15961456q^{11}+20634466q^{10}$$
$$-21500076q^9+20634466q^8-15961456q^7+12000716q^6-8023224q^5+5210748q^4-2648080q^3+1258535q^2-333170q$$
$$+53295\Big)p^{28}+4(q-1)^5q^{18}(q+1)^6\Big(176035q^{16}-304880q^{15}+1143728q^{14}-2592944q^{13}+4381796q^{12}-7836752q^{11}$$
$$+10347280q^{10}-12071952q^9+13810290q^8-12071952q^7+10347280q^6-7836752q^5+4381796q^4-2592944q^3+1143728q^2$$
$$-304880q+176035\Big)p^{27}-4(q-1)^4q^{19}(q+1)^6\Big(85595q^{16}-305012q^{15}+1099080q^{14}-2008892q^{13}+3983924q^{12}$$
$$-5691028q^{11}+8686584q^{10}-9857724q^9+11570274q^8-9857724q^7+8686584q^6-5691028q^5+3983924q^4-2008892q^3$$
$$+1099080q^2-305012q+85595\Big)p^{26}+4(q-1)^5q^{18}(q+1)^6\Big(176035q^{16}-304880q^{15}+1143728q^{14}-2592944q^{13}+4381796q^{12}$$
$$-7836752q^{11}+10347280q^{10}-12071952q^9+13810290q^8-12071952q^7+10347280q^6-7836752q^5+4381796q^4-2592944q^3$$
$$+1143728q^2-304880q+176035\Big)p^{27}-4(q-1)^4q^{19}(q+1)^6\Big(85595q^{16}-305012q^{15}+1099080q^{14}-2008892q^{13}$$
$$+3983924q^{12}-5691028q^{11}+8686584q^{10}-9857724q^9+11570274q^8-9857724q^7+8686584q^6-5691028q^5+3983924q^4$$
$$-2008892q^3+1099080q^2-305012q+85595\Big)p^{26}-2(q-1)^5q^{20}(q+1)^6\left(432497q^{14}-1004458q^{13}+2946827q^{12}\right.$$
$$-6570372q^{11}+10501177q^{10}-15673590q^9+19962699q^8-20001720q^7+19962699q^6-15673590q^5+10501177q^4-6570372q^3$$
$$+2946827q^2-1004458q+432497\Big)p^{25}+2(q-1)^4q^{21}(q+1)^2\Big(314925q^{18}+507650q^{17}+1705925q^{16}+3630000q^{15}$$
$$+5794180q^{14}+9676216q^{13}+12644116q^{12}+17459152q^{11}+21057910q^{10}+20357004q^9+21057910q^8+17459152q^7$$

$$
\begin{aligned}
&+12644116q^6+9676216q^5+5794180q^4+3630000q^3+1705925q^2+507650q+314925\Big)p^{24}+8(q-1)^5q^{22}(q+1)^2\Big(104975q^{16}\\
&+135200q^{15}+206700q^{14}+150960q^{13}-264852q^{12}+53296q^{11}+490644q^{10}+1067520q^9+1730826q^8+1067520q^7\\
&+490644q^6+53296q^5-264852q^4+150960q^3+206700q^2+135200q+104975\Big)p^{23}-8(q-1)^4q^{23}(q+1)^2\Big(104975q^{16}\\
&+240500q^{15}+641004q^{14}+1312380q^{13}+2086220q^{12}+3309396q^{11}+4310420q^{10}+5043900q^9+5682762q^8+5043900q^7\\
&+4310420q^6+3309396q^5+2086220q^4+1312380q^3+641004q^2+240500q+104975\Big)p^{22}-2(q-1)^5q^{24}(q+1)^2\big(314925q^{14}\\
&+372814q^{13}+338975q^{12}+679468q^{11}+320917q^{10}+1684114q^9+3313695q^8+3251688q^7+3313695q^6+1684114q^5+320917q^4\\
&+679468q^3+338975q^2+372814q+314925\big)p^{21}+2(q-1)^4q^{25}(q+1)^2\big(432497q^{14}+1132638q^{13}+2780427q^{12}\\
&+5405644q^{11}+8464185q^{10}+11947394q^9+15022667q^8+15142056q^7+15022667q^6+11947394q^5+8464185q^4\\
&+5405644q^3+2780427q^2+1132638q+432497\big)p^{20}+4(q-1)^5q^{26}(q+1)^2\big(85595q^{12}+127940q^{11}+82070q^{10}+330420q^9\\
&+439669q^8+712072q^7+982836q^6+712072q^5+439669q^4+330420q^3+82070q^2+127940q+85595\Big)p^{19}\\
&-4(q-1)^4q^{27}(q+1)^2\big(176035q^{12}+465360q^{11}+1110750q^{10}+1955664q^9+2999117q^8+3584480q^7\\
&+4196964q^6+3584480q^5+2999117q^4+1955664q^3+1110750q^2+465360q+176035\Big)p^{18}\\
&-2q^{28}(q+1)^2\Big(53295q^{15}-114525q^{14}-130109q^{13}+897919q^{12}-1732589q^{11}+1609255q^{10}-682809q^9\\
&+161411q^8-161411q^7+682809q^6-1609255q^5+1732589q^4-897919q^3+130109q^2+114525q-53295\Big)p^{17}\\
&+2q^{29}\left(q^2-1\right)^2\Big(227715q^{12}+92816q^{11}+441422q^{10}-130352q^9+327981q^8-1085280q^7+253444q^6-1085280q^5\\
&+327981q^4-130352q^3+441422q^2+92816q+227715\big)p^{16}-16q^{30}(q+1)^2\big(969q^{13}-11381q^{12}+42210q^{11}\\
&-82450q^{10}+111859q^9-107151q^8+75852q^7-75852q^6+107151q^5-111859q^4+82450q^3-42210q^2+11381q\\
&-969\big)p^{15}-16q^{31}\left(q^2-1\right)^2\Big(14535q^{10}-450q^9+27455q^8-32640q^7+26298q^6-69692q^5+26298q^4-32640q^3\\
&+27455q^2-450q+14535\big)p^{14}+q^{32}(q+1)^2\Big(43605q^{11}-194675q^{10}+474095q^9-701177q^8+798466q^7-841550q^6\\
&+841550q^5-798466q^4+701177q^3-474095q^2+194675q-43605\Big)p^{13}+q^{33}\left(q^2-1\right)^2\big(92055q^8-54340q^7\\
&+168844q^6-291580q^5+182330q^4-291580q^3+168844q^2-54340q+92055\Big)p^{12}-2q^{34}(q+1)^2\big(15105q^9\\
&-48033q^8+98500q^7-132452q^6+143158q^5-143158q^4+132452q^3-98500q^2+48033q-15105\Big)p^{11}\\
&-2q^{35}\left(q^2-1\right)^2\Big(13623q^6-15782q^5+23569q^4-39460q^3+23569q^2-15782q+13623\Big)p^{10}+q^{36}\big(13015q^9\\
&-4095q^8+5820q^7+10900q^6-11774q^5+11774q^4-10900q^3-5820q^2+4095q-13015\Big)p^9+(q-1)^2q^{37}\Big(5605q^6\\
&+2370q^5-3685q^4-836q^3-3685q^2+2370q+5605\Big)p^8-4q^{38}\Big(955q^7+255q^6+79q^5+651q^4-651q^3-79q^2\\
&-255q-955\big)p^7-4(q-1)^2q^{39}\big(165q^4+76q^3-206q^2+76q+165\big)p^6+q^{40}\Big(751q^5+349q^4-66q^3+66q^2-349q\\
&-751\big)p^5+5(q-1)^2q^{41}\left(q^2+14q+1\right)p^4-10q^{42}\left(9q^3+q^2-q-9\right)p^3+10(q-1)^2q^{43}p^2+5(q-1)q^{44}p-q^{45}=0
\end{aligned}
$$

$$
\begin{aligned}
F_{19}^{(2)}(R,r,d)=&(q-1)^{20}(q+1)^{25}p^{45}+(q-1)^{20}q(q+1)^{16}\Big(5q^8+60q^6+126q^4+60q^2+5\Big)p^{44}\\
&-2(q-1)^{20}q^2(q+1)^{17}\Big(5q^6+10q^5+35q^4+28q^3+35q^2+10q+5\Big)p^{43}-2(q-1)^{12}q^3(q+1)^{16}\big(45q^{14}-210q^{13}\\
&+1143q^{12}-2724q^{11}+7437q^{10}-11022q^9+17999q^8-17144q^7+17999q^6-11022q^5+7437q^4-2724q^3+1143q^2\\
&-210q+45\big)p^{42}-(q-1)^{12}q^4(q+1)^{17}\Big(5q^{12}+324q^{11}-838q^{10}+2484q^9-3349q^8+6408q^7-5972q^6+6408q^5\\
&-3349q^4+2484q^3-838q^2+324q+5\big)p^{41}+(q-1)^{12}q^5(q+1)^{16}\big(751q^{12}-1988q^{11}+12142q^{10}-18548q^9\\
&+51553q^8-50120q^7+82052q^6-50120q^5+51553q^4-18548q^3+12142q^2-1988q+751\Big)p^{40}\\
&+4(q-1)^{12}q^6(q+1)^9\Big(165q^{18}+750q^{17}+3945q^{16}+9320q^{15}+25672q^{14}+45304q^{13}+89152q^{12}+114072q^{11}\\
&+159594q^{10}+152628q^9+159594q^8+114072q^7+89152q^6+45304q^5+25672q^4+9320q^3+3945q^2+750q+165\Big)p^{39}\\
&-4(q-1)^{12}q^7(q+1)^{10}\Big(955q^{16}+4120q^{15}+15380q^{14}+44792q^{13}+100556q^{12}+179080q^{11}+282220q^{10}+357736q^9\\
&+389618q^8+357736q^7+282220q^6+179080q^5+100556q^4+44792q^3+15380q^2+4120q+955\Big)p^{38}\\
&-(q-1)^{12}q^8(q+1)^9\Big(5605q^{16}+12720q^{15}+79144q^{14}+134992q^{13}+435372q^{12}+552944q^{11}+1155224q^{10}+1068816q^9
\end{aligned}
\tag{A.6}
$$

$$+1564510q^8+1068816q^7+1155224q^6+552944q^5+435372q^4+134992q^3+79144q^2+12720q+5605\Big)p^{37}$$
$$+(q-1)^{12}q^9(q+1)^{10}\left(13015q^{14}+57594q^{13}+197245q^{12}+469636q^{11}+977279q^{10}+1469734q^9+2023725q^8+2150072q^7\right.$$
$$\left.+2023725q^6+1469734q^5+977279q^4+469636q^3+197245q^2+57594q+13015\right)p^{36}+2(q-1)^6q^{10}(q+1)^9\left(13623q^{20}\right.$$
$$-58692q^{19}+224578q^{18}-644388q^{17}+1537387q^{16}-3161936q^{15}+5726616q^{14}-8736400q^{13}+12079710q^{12}$$
$$-14399416q^{11}+15362124q^{10}-14399416q^9+12079710q^8-8736400q^7+5726616q^6-3161936q^5+1537387q^4$$
$$\left.-644388q^3+224578q^2-58692q+13623\right)p^{35}-2(q-1)^6q^{11}(q+1)^{10}\left(15105q^{18}-33250q^{17}+68825q^{16}-227120q^{15}\right.$$
$$+458932q^{14}-936248q^{13}+1612484q^{12}-2079824q^{11}+2366638q^{10}-2622156q^9+2366638q^8-2079824q^7+1612484q^6$$
$$\left.-936248q^5+458932q^4-227120q^3+68825q^2-33250q+15105\right)p^{34}-(q-1)^6q^{12}(q+1)^9\left(92055q^{18}-383630q^{17}\right.$$
$$+1452895q^{16}-3794064q^{15}+8841036q^{14}-16031112q^{13}+27191804q^{12}-36730864q^{11}+46308290q^{10}$$
$$-48125652q^9+46308290q^8-36730864q^7+27191804q^6-16031112q^5+8841036q^4-3794064q^3+1452895q^2$$
$$\left.-383630q+92055\right)p^{33}+(q-1)^6q^{13}(q+1)^{10}\left(43605q^{16}-167220q^{15}+342208q^{14}-1128700q^{13}\right.$$
$$+2176220q^{12}-3799508q^{11}+5324928q^{10}-6750204q^9+6541086q^8-6750204q^7+5324928q^6-3799508q^5+2176220q^4$$
$$\left.-1128700q^3+342208q^2-167220q+43605\right)p^{32}+16(q-1)^6q^{14}(q+1)^9\left(14535q^{16}-53048q^{15}+204500q^{14}\right.$$
$$\left.+460152q^{13}+1051356q^{12}-1636168q^{11}+2599852q^{10}-3002376q^9+3472314q^8-3002376q^7+2599852q^6-1636168q^5\right.$$
$$\left.+1051356q^4-460152q^3+204500q^2-53048q+14535\right)p^{31}-16(q-1)^6q^{15}(q+1)^4\left(969q^{20}-9664q^{19}-54654q^{18}-152816q^{17}\right.$$
$$-329771q^{16}-491984q^{15}-652264q^{14}-928624q^{13}-1334686q^{12}-1710096q^{11}-1911092q^{10}-1710096q^9-1334686q^8$$
$$\left.-928624q^7-652264q^6-491984q^5-329771q^4-152816q^3-54654q^2-9664q+969\right)p^{30}$$
$$-2(q-1)^6q^{16}(q+1)^5\left(227715q^{18}+235650q^{17}+1366235q^{16}+2686160q^{15}+5032460q^{14}+10636024q^{13}+13987228q^{12}\right.$$
$$+19540144q^{11}+23852538q^{10}+22605324q^9+23852538q^8+19540144q^7+13987228q^6+10636024q^5+5032460q^4+2686160q^3$$
$$\left.+1366235q^2+235650q+227715\right)p^{29}-2(q-1)^6q^{17}(q+1)^4\left(53295q^{18}+333170q^{17}+1258535q^{16}+2648080q^{15}+5210748q^{14}\right.$$
$$+8023224q^{13}+12000716q^{12}+15961456q^{11}+20634466q^{10}+21500076q^9+20634466q^8+15961456q^7+12000716q^6$$
$$\left.+8023224q^5+5210748q^4+2648080q^3+1258535q^2+333170q+53295\right)p^{28}+4(q-1)^6q^{18}(q+1)^5\left(176035q^{16}\right.$$
$$\left.+304880q^{15}+1143728q^{14}+2592944q^{13}+4381796q^{12}+7836752q^{11}+10347280q^{10}+12071952q^9+13810290q^8\right.$$
$$\left.+12071952q^7+10347280q^6+7836752q^5+4381796q^4+2592944q^3+1143728q^2+304880q+176035\right)p^{27}$$
$$+4(q-1)^6q^{19}(q+1)^4\left(85595q^{16}+305012q^{15}+1099080q^{14}+2008892q^{13}+3983924q^{12}+5691028q^{11}+8686584q^{10}+9857724q^9\right.$$
$$\left.+11570274q^8+9857724q^7+8686584q^6+5691028q^5+3983924q^4+2008892q^3+1099080q^2+305012q+85595\right)p^{26}$$
$$-2(q-1)^6q^{20}(q+1)^5\left(432497q^{14}+1004458q^{13}+2946827q^{12}+6570372q^{11}+10501177q^{10}+15673590q^9+19962699q^8\right.$$
$$\left.+20001720q^7+19962699q^6+15673590q^5+10501177q^4+6570372q^3+2946827q^2+1004458q+432497\right)p^{25}$$
$$-2(q-1)^2q^{21}(q+1)^4\left(314925q^{18}-507650q^{17}+1705925q^{16}-3630000q^{15}+5794180q^{14}-9676216q^{13}+12644116q^{12}\right.$$
$$-17459152q^{11}+21057910q^{10}-20357004q^9+21057910q^8-17459152q^7+12644116q^6-9676216q^5+5794180q^4-3630000q^3$$
$$\left.+1705925q^2-507650q+314925\right)p^{24}+8(q-1)^2q^{22}(q+1)^5\left(104975q^{16}-135200q^{15}+206700q^{14}-150960q^{13}-264852q^{12}\right.$$
$$-53296q^{11}+490644q^{10}-1067520q^9+1730826q^8-1067520q^7+490644q^6-53296q^5-264852q^4-150960q^3+206700q^2$$
$$\left.-135200q+104975\right)p^{23}+8(q-1)^2q^{23}(q+1)^4\left(104975q^{16}-240500q^{15}+641004q^{14}-1312380q^{13}+2086220q^{12}\right.$$
$$-3309396q^{11}+4310420q^{10}-5043900q^9+5682762q^8-5043900q^7+4310420q^6-3309396q^5+2086220q^4-1312380q^3$$
$$\left.+641004q^2-240500q+104975\right)p^{22}-2(q-1)^2q^{24}(q+1)^5\left(314925q^{14}-372814q^{13}+338975q^{12}-679468q^{11}+320917q^{10}\right.$$
$$\left.-1684114q^9+3313695q^8-3251688q^7+3313695q^6-1684114q^5+320917q^4-679468q^3+338975q^2-372814q+314925\right)p^{21}$$
$$-2(q-1)^2q^{25}(q+1)^4\left(432497q^{14}-1132638q^{13}+2780427q^{12}-5405644q^{11}+8464185q^{10}-11947394q^9+15022667q^8\right.$$
$$\left.-15142056q^7+15022667q^6-11947394q^5+8464185q^4-5405644q^3+2780427q^2-1132638q+432497\right)p^{20}$$
$$+4(q-1)^2q^{26}(q+1)^5\left(85595q^{12}-127940q^{11}+82070q^{10}-330420q^9+439669q^8-712072q^7+982836q^6-712072q^5\right.$$
$$\left.+439669q^4-330420q^3+82070q^2-127940q+85595\right)p^{19}+4(q-1)^2q^{27}(q+1)^4\left(176035q^{12}-465360q^{11}+1110750q^{10}\right.$$
$$\left.-1955664q^9+2999117q^8-3584480q^7+4196964q^6-3584480q^5+2999117q^4-1955664q^3+1110750q^2-465360q+176035\right)p^{18}$$

$$
\begin{aligned}
&-2(q-1)^2q^{28}\left(53295q^{15}+114525q^{14}-130109q^{13}-897919q^{12}-1732589q^{11}-1609255q^{10}-682809q^9-161411q^8-161411q^7\right.\\
&\left.-682809q^6-1609255q^5-1732589q^4-897919q^3-130109q^2+114525q+53295\right)p^{17}-2q^{29}\left(q^2-1\right)^2\left(227715q^{12}-92816q^{11}\right.\\
&\left.+441422q^{10}+130352q^9+327981q^8+1085280q^7+253444q^6+1085280q^5+327981q^4+130352q^3+441422q^2-92816q+227715\right)p^{16}\\
&-16(q-1)^2q^{30}\left(969q^{13}+11381q^{12}+42210q^{11}+82450q^{10}+111859q^9+107151q^8+75852q^7+75852q^6+107151q^5+111859q^4\right.\\
&\left.+82450q^3+42210q^2+11381q+969\right)p^{15}+16q^{31}\left(q^2-1\right)^2\left(14535q^{10}+450q^9+27455q^8+32640q^7+26298q^6+69692q^5\right.\\
&\left.+26298q^4+32640q^3+27455q^2+450q+14535\right)p^{14}+(q-1)^2q^{32}\left(43605q^{11}+194675q^{10}+474095q^9+701177q^8+798466q^7\right.\\
&\left.+841550q^6+841550q^5+798466q^4+701177q^3+474095q^2+194675q+43605\right)p^{13}-q^{33}\left(q^2-1\right)^2\left(92055q^8+54340q^7\right.\\
&\left.+168844q^6+291580q^5+182330q^4+291580q^3+168844q^2+54340q+92055\right)p^{12}-2(q-1)^2q^{34}\left(15105q^9+48033q^8+98500q^7\right.\\
&\left.+132452q^6+143158q^5+143158q^4+132452q^3+98500q^2+48033q+15105\right)p^{11}+2q^{35}\left(q^2-1\right)^2\left(13623q^6+15782q^5\right.\\
&\left.+23569q^4+39460q^3+23569q^2+15782q+13623\right)p^{10}+q^{36}\left(13015q^9+4095q^8+5820q^7-10900q^6-11774q^5-11774q^4-10900q^3\right.\\
&\left.+5820q^2+4095q+13015\right)p^9-q^{37}(q+1)^2\left(5605q^6-2370q^5-3685q^4+836q^3-3685q^2-2370q+5605\right)p^8-4q^{38}\left(955q^7-255q^6\right.\\
&\left.+79q^5-651q^4-651q^3+79q^2-255q+955\right)p^7+4q^{39}(q+1)^2\left(165q^4-76q^3-206q^2-76q+165\right)p^6\\
&+q^{40}\left(751q^5-349q^4-66q^3-66q^2-349q+751\right)p^5-5q^{41}(q+1)^2\left(q^2-14q+1\right)p^4-10q^{42}\left(9q^3-q^2-q+9\right)p^3\\
&-10q^{43}(q+1)^2p^2+5q^{44}(q+1)p+q^{45}=0.
\end{aligned}
$$

A.2. Numerical results and verification

All numerical computations were carried out in *Wolfram Mathematica* with 20-digit precision. In this paper, the values are rounded to six significant digits. Unless otherwise stated, parameters were fixed to

$$R=1, \quad d=0.1,$$

and the values of $r_{n,k}$ were obtained as numerical roots of the corresponding Fuss' relations.

n	k	**Fuss' relation**	$r_{n,k}$	**Figure**
13	2	(A.1)	0.856554	Fig. 1
13	4	(A.1)	0.561780	Fig. 2
13	6	(A.1)	0.119618	Fig. 2
15	2	(A.2)	0.876400	Fig. 3
15	4	(A.2)	0.660078	Fig. 3
17	1	(A.3)	0.899948	Fig. 4
17	2	(A.4)	0.887300	Fig. 5
17	3	(A.3)	0.827988	Fig. 4
17	4	(A.4)	0.726898	Fig.5
17	5	(A.3)	0.595549	Fig. 4
17	6	(A.4)	0.441564	Fig. 5
17	7	(A.3)	0.271442	Fig. 4
17	8	(A.4)	0.091569	Fig. 5
19	1	(A.5)	0.899986	Fig. 6
19	2	(A.6)	0.893235	Fig. 7
19	3	(A.5)	0.851932	Fig. 6
19	4	(A.6)	0.773686	Fig. 7
19	5	(A.5)	0.667936	Fig. 6
19	6	(A.6)	0.541099	Fig. 7
19	7	(A.5)	0.398100	Fig. 6
19	8	(A.6)	0.243524	Fig. 7
19	9	(A.5)	0.081955	Fig. 6

Table 1: *Summary of numerically verified values of $r_{n,k}$ for $R=1$ and $d=0.1$.*

A.3. Graphical results

Figures below illustrate the geometric configurations corresponding to the computed values of $r_{n,k}$. All polygons are symmetric with respect to the x-axis and are simultaneously tangent to the incircle C and inscribed in the circumcircle K. Each figure visually confirms the bicentric property of the polygon and the validity of the derived Fuss' relation for the corresponding rotation number k.

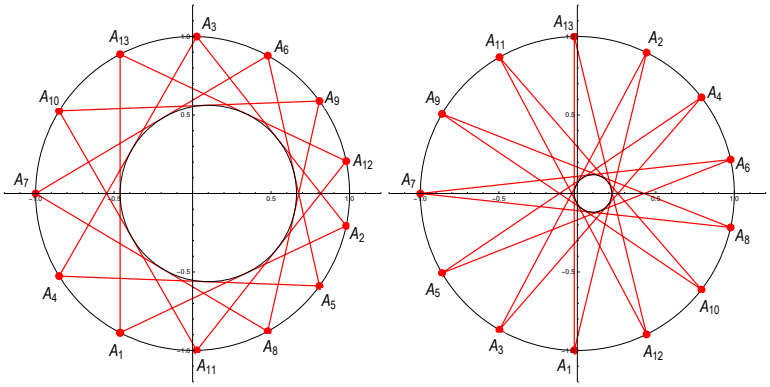

Figure 2: *Symmetrical bicentric 13-gon for* $R = 1$ *and* $d = 0.1$*: (left)* $r_{13,4} = 0.561780$ *(*$k = 4$*); (right)* $r_{13,6} = 0.119618$ *(*$k = 6$*). Each configuration satisfies the corresponding even-class Fuss' relation* $F_{13}^{(k)}(R,r,d) = 0$*.*

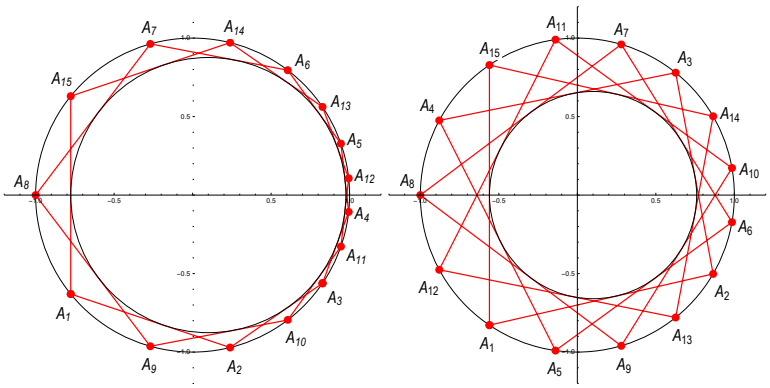

Figure 3: *Symmetrical bicentric 15-gon for* $R = 1$ *and* $d = 0.1$*: (left)* $r_{15,2} = 0.876400$ *(*$k = 2$*); (right)* $r_{15,4} = 0.660078$ *(*$k = 4$*). Each configuration satisfies the corresponding even-class Fuss' relation* $F_{15}^{(k)}(R,r,d) = 0$*.*

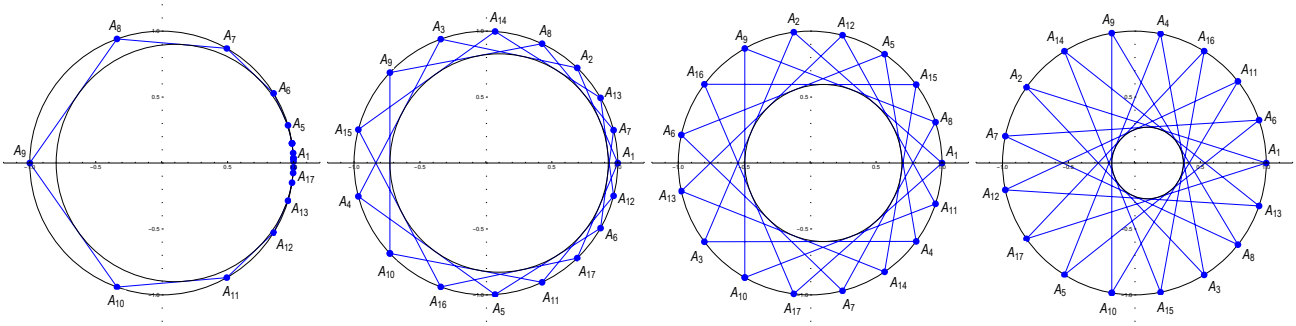

Figure 4: *Symmetrical bicentric 17-gon for* $R = 1$ *and* $d = 0.1$*: (first)* $r_{17,1} = 0.899948$ *(*$k = 1$*); (second)* $r_{17,3} = 0.827988$ *(*$k = 3$*); (third)* $r_{17,5} = 0.595549$ *(*$k = 5$*); (fourth)* $r_{17,7} = 0.271442$ *(*$k = 7$*). Each configuration satisfies the corresponding odd-class Fuss' relation* $F_{17}^{(k)}(R,r,d) = 0$*.*

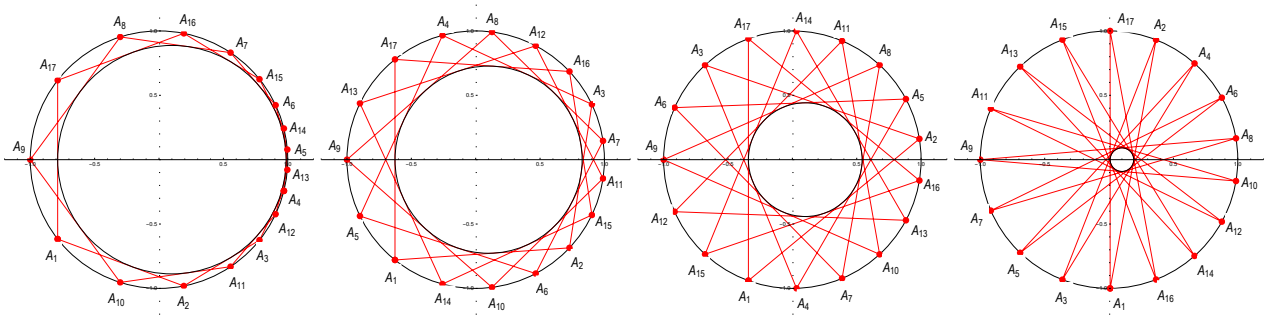

Figure 5: *Symmetrical bicentric 17-gon for* $R = 1$ *and* $d = 0.1$*: (first)* $r_{17,2} = 0.887300$ *(*$k = 2$*); (second)* $r_{17,4} = 0.726898$ *(*$k = 4$*); (third)* $r_{17,6} = 0.441564$ *(*$k = 6$*); (fourth)* $r_{17,8} = 0.0915694$ *(*$k = 8$*). Each configuration satisfies the corresponding even-class Fuss' relation* $F_{17}^{(k)}(R,r,d) = 0$.

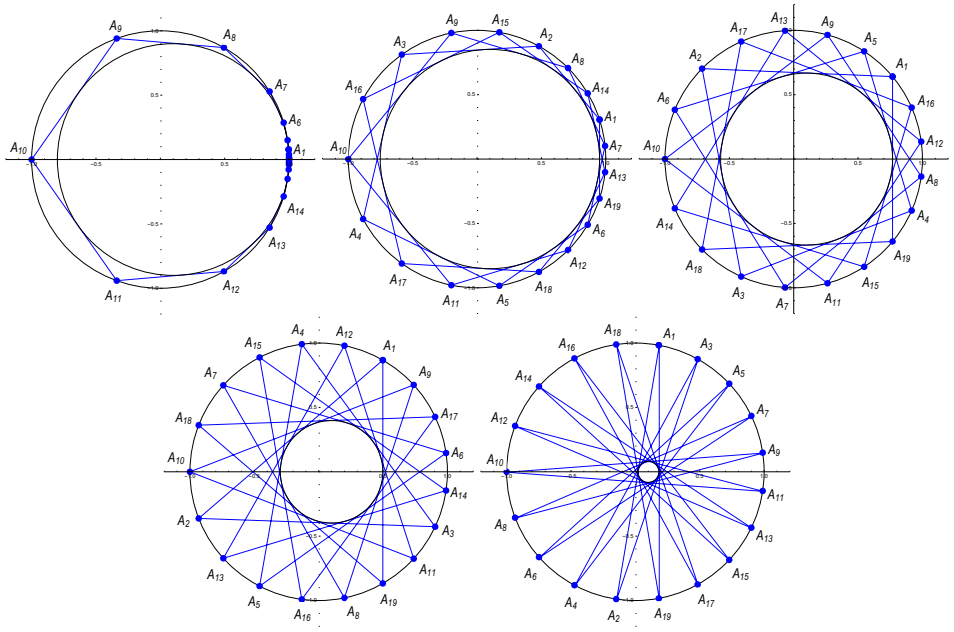

Figure 6: *Symmetrical bicentric 19-gon for* $R = 1$ *and* $d = 0.1$*: (first)* $r_{19,1} = 0.899986$ *(*$k = 1$*); (second)* $r_{19,3} = 0.851932$ *(*$k = 3$*); (third)* $r_{19,5} = 0.667936$ *(*$k = 5$*); (fourth)* $r_{19,7} = 0.398100$ *(*$k = 7$*); (fifth)* $r_{19,9} = 0.0819548$ *(*$k = 9$*). Each configuration satisfies the corresponding odd-class Fuss' relation* $F_{19}^{(k)}(R,r,d) = 0$.

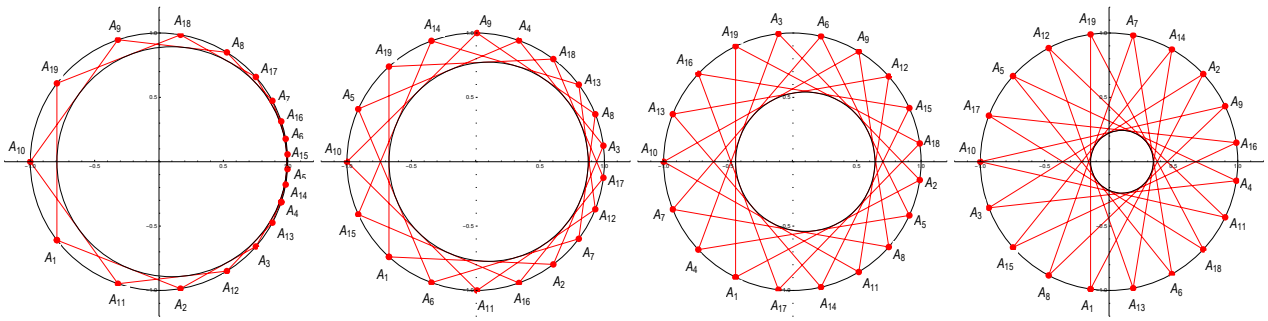

Figure 7: *Symmetrical bicentric 19-gon for* $R = 1$ *and* $d = 0.1$*: (first)* $r_{19,2} = 0.893235$ *(*$k = 2$*); (second)* $r_{19,4} = 0.773686$ *(*$k = 4$*); (third)* $r_{19,6} = 0.541099$ *(*$k = 6$*); (fourth)* $r_{19,8} = 0.243524$ *(*$k = 8$*). Each configuration satisfies the corresponding even-class Fuss' relation* $F_{19}^{(k)}(R,r,d) = 0$.

https://doi.org/10.31896/k.29.4
Original scientific paper
Accepted: 1 November 2025

HIROSHI OKUMURA

A Generalization of the Twin Circles of Archimedes

A Generalization of the Twin Circles of Archimedes

ABSTRACT

We consider the arbelos and generalize Archimedean circles and the twin circles of Archimedes.

Key words: arbelos, Archimedean circle, k-Archimedean circle, twin circles of Archimedes, k-Archimedean twins.

MSC2020: 01A27, 51M04

Poopćenje Arhimedovih kružnica blizanaca

SAŽETAK

U radu proučavamo arbelose i dajemo poopćenje Arhimedovih kružnica i Arhimedovih kružnica blizanaca.

Ključne riječi: arbelos, Arhimedova kružnica, k-Arhimedova kružnica, Arhimedove kružnice blizanci, k-Arhimedovi blizanci

1 Introduction

For a point C on the segment AB such that $|BC| = 2a$, $|CA| = 2b$ and $|AB| = 2c$, let α, β and γ be the semicircles of diameters BC, CA and AB, respectively, constructed on the same side of AB. The area formed by the three semicircles is called an arbelos, and the radical axis of α and β is called the axis. The axis divides the arbelos into two curvilinear triangles with congruent incircles of radius ab/c. It has been believed that the two circles were studied by Archimedes, and they are called the twin circles of Archimedes (see Figure 1). Circles of radius ab/c are called Archimedean circles. In this paper we generalize Archimedean circles and the twin circles of Archimedes.

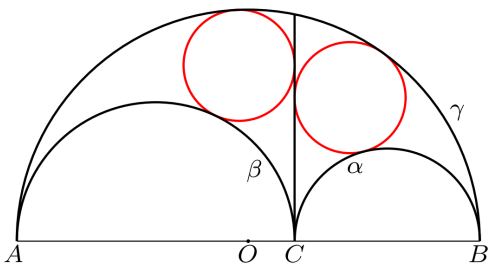

Figure 1.

We use a rectangular coordinate system with origin C such that the farthest point on α from the line AB has coordinates (a,a). The center of γ is denoted by O.

2 k-Archimedean circle

We give a definition of a generalized Archimedean circle.

Definition 1 *Let $w_k = a^2 + kab + b^2$ for a real number k. We say that a circle is k-Archimedean if it has radius*

$$r_k = \frac{abc}{w_k}.$$

The incircle of the arbelos has radius

$$\frac{ab(a+b)}{a^2+ab+b^2} = \frac{abc}{w_1}.$$

Therefore it is 1-Archimedean. The twin circles of Archimedes have radius

$$\frac{ab}{a+b} = \frac{abc}{c^2} = \frac{abc}{w_2}.$$

Therefore they are 2-Archimedean. Hence k-Archimedean circles are generalizations of those circles. 3-Archimedean circles can be found in the following problem in Wasan geometry (see Figure 2):

Problem 1. Three congruent circles of radius r touch the semicircle γ internally so that two of them touch the remaining circle externally and also touches the external common tangent of the semicircles α and β from the side opposite to the point C. Show that the following relation holds:

$$r = \frac{abc}{a^2+3ab+b^2}. \tag{1}$$

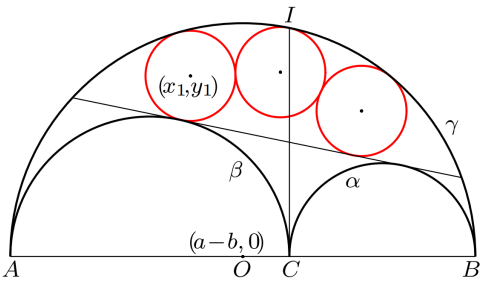

Figure 2.

The problem was proposed by Taguchi in 1817 [3]. Wasan is the Japanese mathematics developed in Edo period. For a brief introduction of Wasan geometry, see [1]. Definition 1 has been made inspired by this problem. It is obvious that r_k is a monotonically decreasing function of k.

3 k-Archimedean twins

In this section we generalize the twin circles of Archimedes. We regard that if t is a perpendicular to AB, then it is represented by the equation $x = t$ with the same symbol t.

Theorem 1 *For a circle δ_a (resp. δ_b) of radius r touching β (resp. α) externally, and γ internally, let t_a (resp. t_b) be the perpendicular to AB touching δ_a (resp. δ_b) from the same side as A (resp. B). Then the circles δ_a and δ_b are k-Archimedean if and only if*

$$t_b - t_a = 2kr. \tag{2}$$

Proof. Let (x_a, y_a) (resp. (x_b, y_b)) be the coordinates of the center of δ_a (resp. δ_b). We have

$$(x_a+b)^2+y_a^2 = (b+r)^2 \text{ and } (x_a-(a-b))^2+y_a^2 = (c-r)^2.$$

Solving the equations for x_a and y_a, we have

$$(x_a, y_a) = \left(r-2b\left(1-\frac{r}{a}\right), \frac{2\sqrt{bc(a-r)r}}{a}\right). \tag{3}$$

Similarly, we have

$$(x_b, y_b) = \left(-r+2a\left(1-\frac{r}{b}\right), \frac{2\sqrt{ac(b-r)r}}{b}\right). \tag{4}$$

Therefore we have

$$t_a = -2b\left(1-\frac{r}{a}\right), \quad t_b = 2a\left(1-\frac{r}{b}\right).$$

Hence we have

$$\begin{aligned}\frac{t_b-t_a}{2r}-k &= \frac{a+b}{r}-\left(\frac{a}{b}+\frac{b}{a}\right)-k \\ &= \frac{c}{r}-\frac{a^2+abk+b^2}{ab} = c\left(\frac{1}{r}-\frac{1}{r_k}\right).\end{aligned}$$

Therefore (2) and $r = r_k$ are equivalent. □

We call the two congruent circles δ_a and δ_b in the theorem *the k-Archimedean twins*, which are generalizations of the twin circles of Archimedes. We have the next corollary (see Figure 3).

Corollary 1 *If k is a positive integer in the event of Theorem 1, there are congruent circles $\delta_a = \delta_1$, δ_2, δ_3, $\cdots$, $\delta_k = \delta_b$ and perpendiculars $t_a = t_0$, t_1, t_2, $\cdots$, $t_k = t_b$ to AB such that $t_i - t_{i-1} = 2r$ for $i = 1, 2, \cdots, k$ and t_{i-1} touches the circles δ_{i-1} and δ_i for $i = 2, 3, \cdots, k$.*

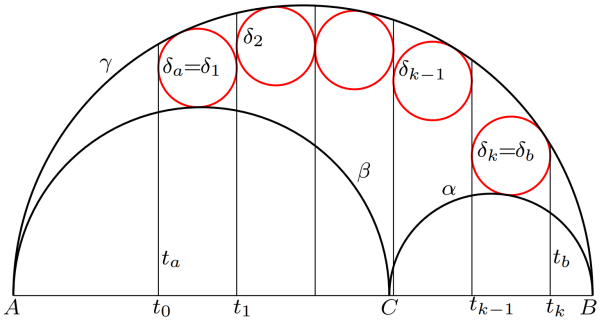

Figure 3: $k = 5$.

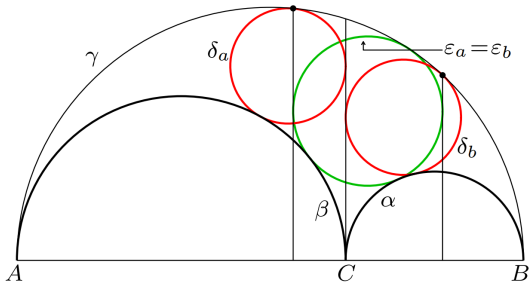

Figure 4: 1-*Archimedean twins and* 2-*Archimedean twins.*

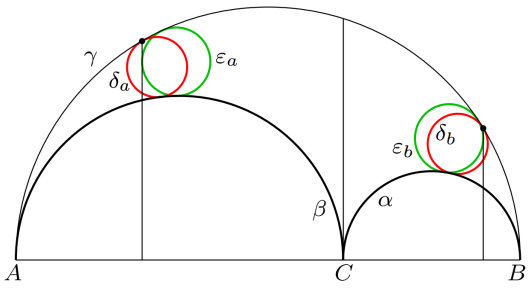

Figure 5: *k-Archimedean twins and $k-1$-Archimedean twins ($k=6$).*

The next theorem shows that $k-1$-Archimedean twins are obtained from k-Archimedean twins, and conversely (see Figures 4 and 5, where 1-Archimedean twins in Figure 4 are overlapping).

Theorem 2 *Let δ_a and ε_a (resp. δ_b and ε_b) be the circles touching β (resp. α) externally, γ internally such that the perpendicular to AB touching ε_a (resp. ε_b) from the same side as A (resp. B) passes through the point of tangency of δ_a (resp. δ_b) and γ. The following statements hold.*
(i) *δ_a (resp. δ_b) is k-Archimedean if and only if ε_a (resp. ε_b) is $k-1$-Archimedean.*
(ii) *δ_a and δ_b are k-Archimedean twins if and only if ε_a and ε_b are $k-1$-Archimedean twins.*

Proof. Let r and x_a be the radius of δ_a and the x-coordinate of its center, respectively. Then

$$x_a = r - 2b\left(1-\frac{r}{a}\right) \tag{5}$$

by (3). Let e be the radius of ε_a. The perpendicular to AB touching ε_a from the same side as A is represented by the equation $x=-2b(1-e/a)$. The point of tangency of γ and δ_a is the external center of similitude of the two circles. Hence it has x-coordinate $(-r(a-b)+cx_a)/(c-r)$. Therefore we have

$$-2b\left(1-\frac{e}{a}\right) = \frac{-r(a-b)+cx_a}{c-r}.$$

Substituting (5) in this equation and solving the resulting equation for $1/e$, we have

$$\frac{1}{e} = \frac{1}{r} - \frac{1}{c}.$$

While we have

$$\frac{1}{c} + \frac{1}{r_{k-1}} = \frac{1}{r_k}.$$

Eliminating $1/c$ from the last two equations, we have

$$\frac{1}{e} - \frac{1}{r_{k-1}} = \frac{1}{r} - \frac{1}{r_k}.$$

Therefore δ_a is k-Archimedean if and only if ε_a is $k-1$-Archimedean. The rest of (i) is proved similarly. The part (ii) is obvious. □

4 Maximal k-Archimedean twins

We consider the maximal k-Archimedean twins. We denote the configuration consisting of an arbelos and k-Archimedean twins δ_a and δ_b with their tangents t_a and t_b by $\mathcal{T}_k$. For $\mathcal{T}_k$, the centers of δ_a and δ_b have x-coordinates t_a+r_k and t_b-r_k, respectively. By Theorem 1 we have the followings: If $k=1$ then $t_a+r_k=t_b-r_k$. If $k<1$ then $t_b-r_k<t_a+r_k$, and if $1<k$ then $t_a+r_k<t_b-r_k$ (see Figures 6 and 7).

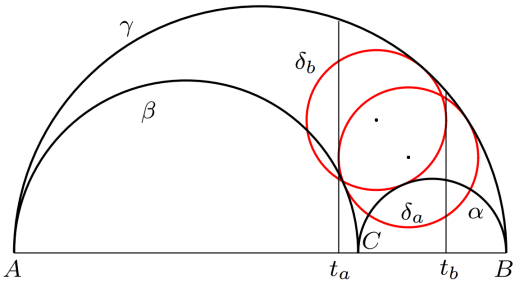

Figure 6: $k<1$, $t_b-r_k<t_a+r_k$.

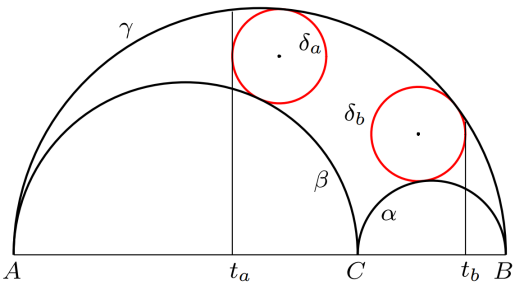

Figure 7: $1<k$, $t_a+r_k<t_b-r_k$.

Assume $a\le b$ for $\mathcal{T}_k$. Then the circles δ_a and δ_b are maximal if δ_a and α overlap (see Figure 9). Solving the equation $r_k=a$ for k in this case, we have

$$k = 1-\frac{a}{b}. \tag{6}$$

Therefore *the k-Archimedean twins exist if and only if $1-a/b\le k$ and the maximal k-Archimedean twins are obtained if* (6) *holds*. Notice that $1-a/b\ge 1-b/a$ in this event. Therefore we can say that *k-Archimedean twins exist if and only if $k\ge\max(1-a/b,1-b/a)$*. A similar result can also be obtained in the case $a>b$. Therefore we have the following theorem.

Theorem 3 *k-Archimedean twins exist if and only if*

$$k \geq \max\left(1-\frac{a}{b}, 1-\frac{b}{a}\right).$$

The maximal k-Archimedean twins are obtained if and only if

$$k = \max\left(1-\frac{a}{b}, 1-\frac{b}{a}\right).$$

Assume $a \leq b$ and $k = 1-a/b$ for $\mathcal{T}_k$. Then we have $r_k = a$ and

$$\begin{aligned}(x_b, y_b) &= \left(-r_k + 2a\left(1-\frac{r_k}{b}\right), \frac{2\sqrt{ac(b-r_k)r_k}}{b}\right) \\ &= \left(a - \frac{2a^2}{b}, \frac{2a\sqrt{b^2-a^2}}{b}\right)\end{aligned}$$

by (4). While solving the equations $x^2+y^2 = 4a^2$ and $(x-(-b))^2+y^2 = b^2$, we get that the semicircles of center C passing through the point B meets β in the point of coordinates

$$\left(-\frac{2a^2}{b}, \frac{2a\sqrt{b^2-a^2}}{b}\right).$$

Therefore this point is one of the endpoints of the diameter of δ_b parallel to AB (see Figure 8). Since $\delta_a = \alpha$, the axis and t_a overlap. Especially if $a = b$, then $\max(1-a/b, 1-b/a) = 0$. Therefore the configuration $\mathcal{T}_0$ exists, where δ_a and δ_b are the maximal 0-Archimedean twins and overlap with α and β, respectively, and t_a and t_b overlap with the axis (see Figure 9).

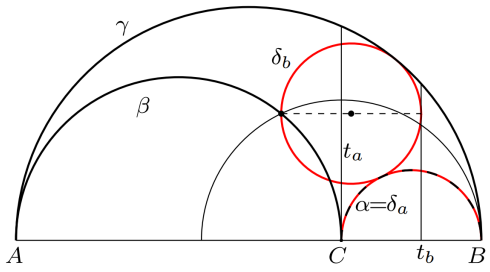

Figure 8: $\mathcal{T}_k$ $(a < b, k = 1-a/b)$.

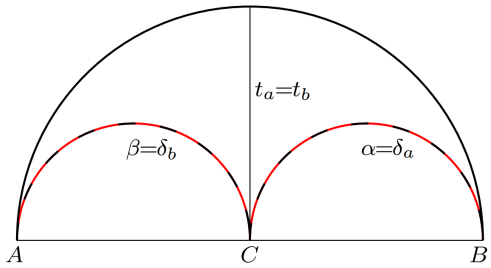

Figure 9: $\mathcal{T}_0$ $(a = b)$.

References

[1] Okumura, H., Wasan geometry. In: Sriraman, B. ed., *Handbook of the Mathematics of the Arts and Sciences*, Springer, Cham, 2020, 1–52, https://doi.org/10.1007/978-3-319-70658-0_122-1

[2] Okumura, H., Watanabe, M., The twin circles of Archimedes in a skewed arbelos, *Forum Geom* **4** (2004), 229–251.

[3] Saitama Prefectural library ed., The sangaku in Saitama, 1969, Saitama Prefectural Library.

Hiroshi Okumura
orcid.org/0000-0003-4332-0189
e-mail: hokmr@yandex.com

Takahanadai Maebashi Gunma 371-0123, Japan

Appendix: Proof of Problem 1

We give a proof of Problem 1, since it was proposed with no solution (see Figure 2). Let δ_i $(i = 1,2,3)$ be the three congruent circles, where δ_1 and δ_3 touch δ_2 externally. Let (x_i, y_i) be the coordinates of the center of the circle δ_i. The point of intersection of γ and the axis is denoted by I. Let t be the external common tangent of α and β. The line t has an equation ([2]):

$$t(x,y) = (a-b)x - 2\sqrt{ab}y + 2ab = 0.$$

While the point I has coordinates $(0, 2\sqrt{ab})$, because γ is represented by an equation $(x-2a)(x+2b)+y^2 = 0$. Hence the line IO is perpendicular to t. Therefore I coincides with the midpoint of the arc of γ cut by t, i.e., the circle δ_2 touches γ at I. Hence we have $x_2^2 + (y_2 - 2\sqrt{ab})^2 = r^2$ and $(x_2-(a-b))^2 + y_2^2 = (c-r)^2$. Solving the two equations for x_2 and y_2, we have

$$x_2 = \frac{(a-b)r}{c}, \quad y_2 = \frac{2\sqrt{ab}(c-r)}{c}. \tag{7}$$

If the perpendicular from the center of δ_1 to AB meet t in a point of coordinates (x_1, y'), then $t(x_1, y') = 0$, while there is a real number $z > 0$ such that $y_1 = y' + z$. Then $t(x_1, y_1) = t(x_1, y'+z) = t(x_1, y') - 2\sqrt{ab}z = -2\sqrt{ab}z < 0$. Hence we get $t(x_1, y_1) < 0$. Therefore we have $t(x_1, y_1)/c = -r$. We also have $(x_2 - x_1)^2 + (y_2 - y_1)^2 = (2r)^2$ and $(x_1 - (a-b))^2 + y_1^2 = (c-r)^2$. Eliminating x_1 and y_1 from the three equations with (7) and solving the resulting equation for r, we get (1).

https://doi.org/10.31896/k.29.5
Original scientific paper
Accepted: 5 November 2025

CHRISTIAN CLEMENZ
BORIS ODEHNAL

Limits of Triangle Centers

Limits of Triangle Centers

ABSTRACT

The construction of a triangle center always produces central triangles which again allow for the construction of the respective center. Doing this infinitely many times may in some cases lead to a known triangle center, but in the vast majority, a new center will show up. The symbolic computational approach is limited in many cases due to the complexity of the computations. In order to overcome these difficulties, we shall start with numerical approaches towards several centers' limits. This gives rise to some conjectures which later allow for an exact determination of the limit of a triangle center.

Key words: triangle center, iterated construction, numerical simulation, limit

MSC2020: 51N20, 51Nxx, 68U05

Granične vrijednosti središta trokuta

SAŽETAK

Konstrukcija središta trokuta uvijek stvara središnje trokute koji ponovno omogućavaju konstrukciju odgovarajućeg središta. Ponavljanje ovog postupka beskonačno mnogo puta može u pojedinim slučajevima dovesti do poznatog središta trokuta, ali u velikoj većini slučajeva pojavit će se novo središte. Simbolički računski pristup je ograničen u mnogim slučajevima zbog složenosti izračuna. Kako bismo prevladali te teškoće, započet ćemo s numeričkim pristupima prema graničnim vrijednostima nekoliko središta. To dovodi do nekih pretpostavki koje kasnije omogućavaju točno određivanje granične vrijednosti središta trokuta.

Ključne riječi: središte trokuta, iterativne konstrukcije, numeričke simulacije, granična vrijednost

1 Introduction

1.1 Related and prior work

In classical and elementary geometry, usually constructions terminate after a finite number of steps. However, some constructions may invite us to repeat them not only once and we may ask ourselves what will happen if we repeat them infinitely many times. Since the constructions that we want to repeat infinitely many times follow the same recipe in each step, the thus produced geometric objects are determined by means of some algorithm. Under certain circumstances, we can expect that such infinitely many times repeated constructions will in the end lead to a useful result, *i.e.*, they produce a limit. Moreover, since the recipe does not change, we may discover a certain simple generation and construction of the limit. These could be, for example, a chain of similar figures (cf. [13]), a geometric sequence, perspectivities, and more as we shall see later. Many constructions in and around the triangle can be performed by means of linear or rational operations, many involve square roots (circle intersections from the constructive point of view), and some cannot be accessed by means of the classical tools (*e.g.*, Morley triangles and their centers).

The only algebraic approach towards iterated triangle center constructions can be found in [1]. There, the degree $d(f)$ of a triangle center $Z = f : \zeta(f) : \zeta^2(f)$ is defined with the help of Z's generating trilinear center function f. This degree either remains unchanged or changes to $d(-2)^{-k}$ for the respective center in the k-th step of the iteration. Unfortunately, the thus defined degree has no deeper geometric meaning and depends on the trilinear center function, *i.e.*, it yields different degrees for different but equivalent representations of the same center. As we shall see, the asymptotic behaviour of linear operators is sometimes crucial in understanding the limiting process of a triangle construction. In [3], this is done for simplices and discloses relations to matrix theory. [6] does not provide limits of triangle centers, but deals with the limit shape of central triangles in some

cases. An intricate but nevertheless interesting approach using bivariate Fourier series for the representation of the limit of a point and iterated pedal triangles is given in [4].

1.2 Aims and contributions of the present note

The repeated center construction in a given triangle can be performed numerically in an easy way. We shall describe the implementation of our numerical simulations in Sec. 2. They allow for a flexible access to the limits of various centers under different assumptions of reference triangles. Among others, we can use the *standard reference triangle* with side lengths $a = 6$, $b = 9$, and $c = 13$ which allows us to compare resulting limits with C. KIMBERLING's *search table* in the Encyclopedia of Triangle Centers (cf. [7]). We will not give an exhaustive treatment of center limits. Just a few well-known and low indexed centers shall be studied. The numerical computations provide us with ideas how to construct the centers that emerge in the limit. In Sec. 3, we shall give exact proofs of what can be conjectured from the numerical experiments.

2 Numerical approach

2.1 Implementation details

In order to visually explore the behaviour of different center constructions, we developed an interactive program using the open source game engine Godot[1] which offers a flexible framework for scripting and displaying 2D graphics that is compatible with many different programming languages. We chose C# because of its easy access to external libraries and overall speed of development. Our program allows for the repeated numerical determination of the first eleven triangle centers listed in C. KIMBERLING's encyclopedia [7]. However, it can be extended to all those centers that have a geometric generation.

The repreated construction of a triangle center needs a new reference triangle in each step. In many cases, it is necessary to use the Cevian or the pedal triangle. Depending on the definition and construction of the center under consideration, a base triangle different from the latter two is chosen. We shall discuss this in more detail in Sec. 3. In our interactive program one can either choose the pedal triangle $\Delta_p(X_i)$ or the Cevian triangle $\Delta_C(X_i)$ related to the triangle center X_i as the starting triangle for the next step in the iteration. The reference triangle shall not be changed during the iteration. The Spieker point X_{10} is the only exception that uses its own construction method, which will be explained in Sec. 2.4.7.

[1] Godot Game Engine – https://godotengine.org

2.2 Precision

As with any numerical approach, calculations need to be of a certain precision to guarantee the robustness of and the confidence in the results. What kind of target precision is needed depends on multiple factors.

The first precision requirement stems from the values in C. KIMBERLING's search table. In their 6–9–13 triangle search table, a precision of twenty decimals is used. Typically, double precision floating point numbers are stored using 64 bits and can cover a very large range of numbers, in C# for example this range is $\sim 10^{-324}$ to 10^{308}. However, their maximum precision is only around 15–17 digits [11] and are, therefore, insufficient for our purpose. Additionally, C# provides the *decimal* numeric type that is recommended for higher precision, especially for values $-1 < x < 1$. This type can store up to 28–29 digits to the right of the decimal point. In theory, these values should be precise enough to store results that can be compared with search table values.

However, the second requirement is defined by the precision needed by the used mathematical operations. As values are expected to shrink rapidly, an even higher precision is needed to guarantee that operations still result in values that are robust according to the first requirement. After only very few iterations of repeated triangle construction, some *decimal* type results may already be indistinguishable from zero. Particularly, any construction that involves vector normalization or normal projection suffers greatly from low precision. In such cases, very small vector norms can lead to divisions by zero induced by rounding errors and prohibit any further iteration.

One way of tackling this problem is the use of decimal numbers with arbitrary precision. These are not included in most programming languages by default and may need to be imported from an external library. The *Extended Numerics* package for C# by ADAM WHITE [15] is such a library that includes an arbitrary *BigDecimal* type. It stores exponent and mantissa separately as integers and calculates in base 10 rather than using the usual binary format for floating point numbers. One particular feature of *BigDecimal* allows us to truncate the result of any operation to an arbitrary decimal point while still using the full potential range of decimals for the calculation itself. This offers the deliberate choice to reduce the precision in order to improve computation speed by introducing a certain degree of rounding errors without the risk of running out of precision during an operation. Unfortunately, this feature does not entirely prevent the numerical problems but rather delay them if further iterations are needed. As a default, we limit the precision to around 25–50 digits to keep the program we developed interactive. For our numerical results in Section 2.4.9, we opted for a higher precision.

2.3 First numerical results

Along with the visuals, we looked at a variety of different properties that could give further insight into the behaviour of the repeated construction. For the resulting triangles, we calculated the ratio of the side lengths and interior angles that can reveal whether there are any systematic changes in their overall shape, such as regularization or other obvious patterns. For the resulting centers, we create a curve that connects subsequent centers and calculate the distance of and angle between subsequent segments, respectively. These two properties give hints at the tendency to converge and if the centers are collinear. Putting all these values together may give insights on how to tackle these constructions algebraically. Additionally, we will also describe any intermediary centers that are contained in the search table if they are found during the construction, as these could also be valuable information.
Note that we primarily focused on the behaviour of the 6-9-13 triangle. Any findings we described below refer to this triangle unless stated otherwise. When looking up search values in KIMBERLING's search table, we assume a tolerance of 10^{-7}, meaning these values are likely to describe the same center if their absolute difference is smaller than this tolerance. We do so because numerical errors on either side may hide the fact that it may be the same center. This threshold was chosen empirically, as we found that differences are either noticeably larger than that or almost zero. A much smaller tolerance may be applicable, especially if we increase precision and iteration count.
A list of our calculated search values can be found in Table 1 at the end of this section.

2.3.1 Incenter X_1

Repeatedly constructing the incenter quickly leads to a regularization of the resulting triangles for both pedal and Cevian triangle construction (cf. Thm. 1). While both constructions seem to converge, neither of the two points determined numerically is contained in the search table. Only the incenter of the intouch triangle, *i.e.*, the incenter of the intouch triangle known as X_{177} (cf. [7, 8]) appears in the search table.

2.3.2 Centroid X_2

In the case of the centroid X_2, the medial triangle Δ_m of Δ equals the Cevian triangle $\Delta_C(X_2)$. Consequently, the second centroid is that of Δ_m which equals X_2. Hence, repeating the centroid construction with the Cevian triangle returns the centroid X_2 of Δ in the limit.
The pedal triangle construction on the other hand exhibits a different behaviour. It quickly regularizes the triangles after around four iterations, while the distance between each new centroid is indistinguishable from zero as early as seven iterations, finalizing the convergence. The point the centroids converge towards is not contained in the search table. On the second iteration the created center is X_{373}.

2.4 Circumcenter X_3

Repeating the circumcenter construction using the Cevian triangles as the reference triangles, we observe an overall chaotic behaviour. The triangle center X_{23719} is the circumcenter of Δ_m and appears as the circumcenter in the second step of the iteration (cf. Fig. 1).

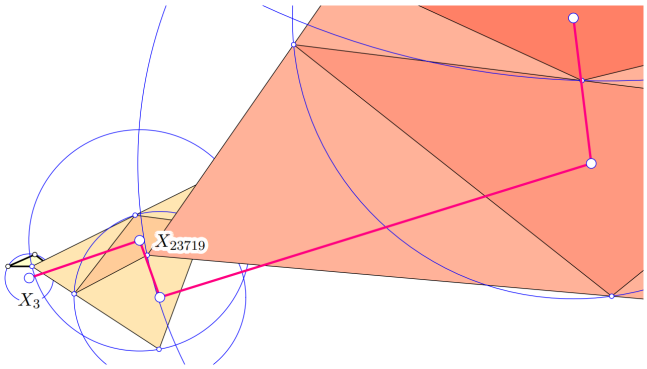

Figure 1: *The chaotic path of the circumcenter of its predecessor's Cevian triangle: Only two points in the sequence are known.*

In contrast, the pedal triangle construction exhibits a very obvious convergence towards the centroid X_2. Now, all intermediate points are collinear centers located on the Euler line. The first five centers after following the circumcenter can be found in the search table and are in order of their construction $X_5, X_{140}, X_{3628}, X_{16239}, X_{61877}$. They lie on the Euler line as well as all subsequent centers do, see Thm. 2.

2.4.1 Orthocenter X_4

In this particular case, we have $\Delta_C(X_4) = \Delta_p(X_4) = \Delta_o$. Let now $\Delta_o = A'B'C'$ such that $A' \in [B,C]$ (cyclic). Further, $\sphericalangle AA'C = \sphericalangle BB'C = \frac{\pi}{2}$. If α, β, γ denote the interior angles of Δ, then $\sphericalangle A'AC = \sphericalangle B'BC = \frac{\pi}{2} - \gamma$, since A, C', A', C and B, C', B', C are concyclic. Thus, $\sphericalangle A'C'B' = \sphericalangle A'AC + \sphericalangle B'BC = \pi - \gamma$ (cyclic). From that, we can deduce that the interior angles of the k-th orthic triangle are equal to

$$\alpha(k) = (-1)^{k+1}\pi + (-2)^k\alpha \qquad \mod 2\pi \quad \text{(cyclic)}.$$

This means that the orthic triangles rotate with exponential speed. Besides, it is by no means guaranteed that the orthic triangle at some level stays within the interior of its predecessor. The same holds true for the orthocenter.
A very special result is due to NEUBERG (see [2]): The third pedal triangle of a fixed point with respect to a given triangle Δ is similar to Δ. Unfortunately, NEUBERG's result

deals with a fixed point whose pedal triangles are studied. Here, and in the following, the point whose pedals or Cevians are used changes from step to step.
Clearly, the orthocenter reaches a limit in the case of an equilateral triangle Δ. We shall not discuss right and isosceles triangles here.
The second step of the iteration, yields X_{52} as the orthocenter of the orthic triangle which fits with the results in [7, 8].

2.4.2 Nine-point center X_5

Constructing this center repeatedly exhibits very chaotic behaviour for both construction types of reference triangles. While the construction based on $\Delta_C(X_5)$ does not seem to have any obvious patterns, the construction based on the pedal triangle appears to regularize the reference triangles. This happens much slower compared to other center constructions that do so. The second nine-point center found using pedal triangles equals X_{13365} which is referred to as *Point Beid 48* in [7].

2.4.3 Symmedian point X_6

The Symmedian point has a very interesting behaviour. While the Cevian triangle construction only leads to a regularization, the pedal triangle construction has a more unique behaviour. Its center points move on a zig-zag curve with a constant interior angle of 129.4365 degrees finally converging towards the center X_{1285}. Notably, on the second step of the iteration the created center can be recognized as X_{18907} in the search table.

2.4.4 Gergonne point X_7

The Gergonne point exhibits a regularization when using the Cevian triangles and seems to converge towards a point not contained in the search table.
The pedal triangle construction however looks a lot more interesting as it seems to have some underlying pattern which can be seen in Figure 2. The constructed centers seem to be almost collinear visually, but on further inspection the angle between iterations is around 178.1–178.3 degrees. The resulting triangles visually seem to alternate between two different shapes, one of them being similar to the starting triangle. However, numerically there is always an additional small deviation from those shapes after each iteration.

2.4.5 Nagel point X_8

When using Cevian triangles, the construction of the Nagel point stops after only three iterations because the resulting triangles rapidly collapse to a line and calculations become unstable. Even on a precision higher than the limit of the interactive program, further iterations do not make sense.
The same is true for the pedal triangles, however, the construction is possible for a few more iterations. If not for the numerical instability, this type of construction would seem to converge as the centers seem to follow a zig-zag curve with each additional line of the curve slowly getting shorter and angles between them getting smaller which can be seen in Figure 3.

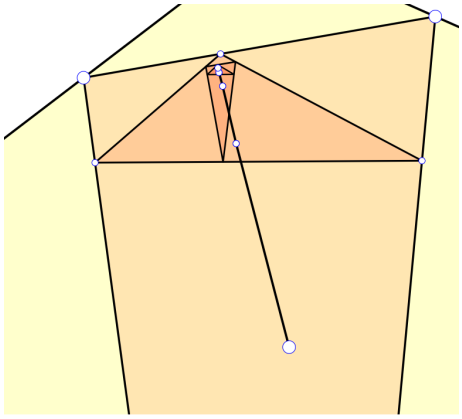

Figure 2: *The trail of the Gergonne point X_7: Only four steps of the iteration are to show that the second and fourth pedal triangle are almost similar to Δ.*

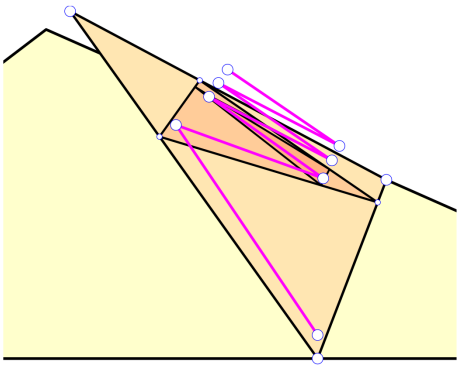

Figure 3: *The oscillating path of the Nagel point X_8: The corridor of "even" and "odd" points is slowly getting narrower.*

2.4.6 Mittenpunkt X_9

Similar to the Nagel point, the construction of the Mittenpunkt using Cevian triangles stops after only three steps. Both share a similar construction using excircles and the problem of triangles collapsing. Using pedal triangles instead leads to a quick triangle regularization and the centers seem to converge towards a point not found in the search table.

2.4.7 Spieker center X_{10}

As briefly mentioned above, we treat the repeated construction of the Spieker center differently. This is because the

construction of this center naturally already leads to a triangle that is suitable for repeated use. As the Spieker point being the incenter of a triangle's medial triangle, it is convenient to use the intouch triangle of the medial triangle for repeated construction of the Spieker center. This subsequently regularizes the used triangles and the center seems to converge on a zig-zag curve towards a point not contained in the search table. The center found on the second iteration has the same search value as X_{58689}.

2.4.8 Feuerbach point X_{11}

Finally, we come to the Feuerbach point, where the Cevian construction also leads to a collapse of the triangles but with a higher numerical stability due to different operations used for construction. The center seems to converge towards a point not found in the search table before eventually also becoming unstable. The repeated pedal triangle construction results in an interesting pattern of periodically alternating between similar triangle shapes but again with numerical deviations after each iteration.

2.4.9 Search value results

As our final numerical results, we list the search value found for each center and construction type in Table 1. We used 40 iterations of repeated center construction paired with a precision of 80 digits. For better readability, we truncated values in Table 1 after 20 digits right of the decimal point. Only X_3 and X_6 lead to already known triangle centers in KIMBERLING's seach table using repeated construction from pedal triangles and are X_2 and X_{1285}, respectively.

3 Analytical framework and first results

3.1 Proper choice of coordinates

When dealing with results from Euclidean geometry, computations are preferably done in Cartesian coordinates. Therefore, we impose the frame of reference such that the vertices of the triangle $\Delta = ABC$ are given by

$$A = (0,0),\ \ B = (c,0),\ \ C = (u,v), \tag{1}$$

where u and v are subject to

$$\begin{aligned} &u^2+v^2 = b^2,\ \ (u-c)^2+v^2 = a^2 \quad \Longleftrightarrow \\ &u = \frac{1}{2c}(-a^2+b^2+c^2),\ \ v = \frac{2F}{c} \end{aligned} \tag{2}$$

and $a = \overline{BC}$, $b = \overline{CA}$, $c = \overline{AB}$ are the side lengths of the base triangle Δ and F equals Δ's area.
This setting allows an immediate switch to (exact or homogeneous) trilinear coordinates. The y-coordinate y_P of each point (center) is the third trilinear coordinate of this particular point P, since it is the oriented distance of P to the line $[A,B]$ (the x-axis). In any case, y_P will be a function in a, b, c and, cyclically replacing them according to $a \to b$, $b \to c$, $c \to a$, turns y_P into the first trilinear coordinate function of P, *i.e.*, it becomes the trilinear distance to $[B,C]$, and so, we obtain the generating center function. This allows for a comparison with the Encyclopedia of Triangle Centers [7]. For example, the coordinates of Δ's incenter X_1 in the present coordinate system are

$$X_1 = \left(\frac{1}{2}(-a+b+c), \frac{2F}{a+b+c}\right). \tag{3}$$

	Cevian triangle	Pedal triangle
X_1	1.95770029904487735665	0.80433539504925636000
X_2	2.62936879248871824114	1.76867523171775377550
X_3	-3891699654776.25808763607293483169	2.62936879248116398887
X_4	-1.02844023546083472296	-1.028440235460834722964
X_5	0.76566640603164320837	1.32186957169792197941
X_6	1.09217049764661208244	0.10296691685647652550
X_7	0.80433539504925636000	0.15823641292070149571
X_8	2.53702599581424750311	1.56932209282972051791
X_9	3.12652311458376376898	2.15889133044926341090
X_{11}	2.57245781384282079537	2.17029063766605551907

	Intouch triangle of medial triangle
X_{10}	3.19337592231807969123

Table 1: *Search values per center and construction type. X_{10} uses its own special construction method. X_3 changes value after each iteration and does not seem to converge. For X_4 Cevian and pedal construction result in the same triangles. X_8, X_9, and X_{11} terminate after only a handful of iterations. The search values for X_3 and X_6 using pedal triangles are contained in* KIMBERLING's *search table and are X_2 and X_{1285}, respectively.*

Its second coordinate equals $\frac{2F}{a+b+c}$ and a cyclic shift of a, b, c does not alter it. Further, we can cut out all factors which are cyclically symmetric in a, b, c (here, they are F and $a+b+c$) and we obtain the trilinear center function of X_1 which equals 1 (cf. [7, 8]). For centers with a more intricate trilinear representation, we evaluate at the triangle with $a=6$, $b=9$, $c=13$ and compare with the respective search table on [7].

When we aim at a repeated construction of triangle centers, we have to determine a new reference triangle in each step. There are two simple but in some sense natural choices:
1. the pedal triangle $\Delta_p(X)$ of a point X whose vertices are the orthogonal projections of X onto the sides of a triangle Δ and
2. the Cevian triangle $\Delta_C(X)$ of a point X whose vertices are the projections of X from the vertices of a triangle to the opposite sides.

They will serve as the reference triangles in most of the cases we shall treat here. We shall not mix the triangles of reference from step to step, since this may cause a chaotic behaviour and no convergence will be observed.

The construction of a pedal triangle will fail for all centers X_i of Δ on the circumcircle, since these pedals lie on their respective Simson line. The Cevian triangle and the pedal triangle coincide if the chosen center equals the orthocenter X_4.

We are not restricted to the pedal triangle or the Cevian triangle. In some cases, we may choose another central triangle that may be related closer to the center that is repeatedly constructed.

3.2 Algebraic results

3.2.1 Centroid

It is not worth mentioning that the centroid X_2 is stable if we repeat the construction of the centroid always using the Cevian triangle. The Cevian triangle is the medial triangle of its predecessor in each step and all medial and medial of medial triangles are perspective to each other and the centroid X_2 serves as the perspector, while the line at infinity takes the role of the perspectrix.

In Fig. 4, the centroid X_2^{i+1} is constructed as the centroid of the pedal triangle of its predecessor. Although the polygon $X_2X_2^1X_2^2\ldots$ shows a spiraloid behaviour there is no simple generation that can easily be detected. Simulations show that the sequence of centroids converges and the search value equals $1.768675231717\ldots$, but there is no known center corresponding to that.

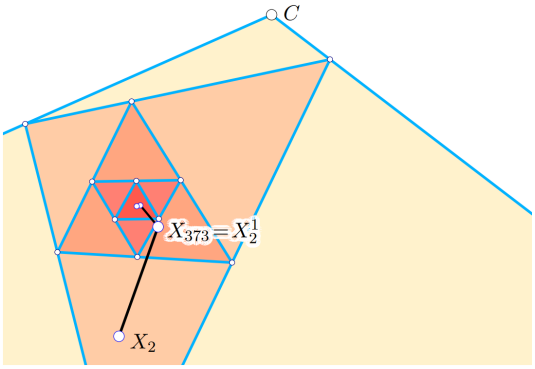

Figure 4: *The limit of $X_2^{i+1}(\Delta_p(X_2^i))$ is not yet known and the growth rules of the polygon $X_2X_2^1X_2^2\ldots$ cannot easily be read off from the figure.*

3.2.2 Incenter

The incenter of Δ is a rather nasty chum. Although it is given by $1:1:1$ in terms of homogeneous trilinear coordinates (cf. [7, 8]), for X_1 has equal (oriented) distances to Δ's sides, its Cartesian representation (3) involves square roots (since the triangles area F does). Repeating the construction of the incenter using the intouch triangle $\Delta_i=\Delta_p(X_1)$ (triangle of contact points of the incircle with the side lines of Δ) doubles the problems. Again angles have to be halved, or equivalently, unit vectors between points whose coordinates already involve square roots have to determined. The "next" incenter is that of Δ_i and is labelled X_{177} (and called the 1st *Mid-Arc Point*) in KIMBERLING's encyclopedia with the trilinear center function

$$\sqrt{bc}\sqrt{a-b+c}\sqrt{a+b-c}(\sqrt{b}\sqrt{a-b+c}+\sqrt{c}\sqrt{a+b-c})$$

(compare the equivalent trigonometric expression in [7, 8]).

As a matter of fact, X_1 always lies in the interior of Δ. Moreover it also lies in the interior of its pedal triangle $\Delta_p(X_1)=\Delta_i$, the intouch triangle (contact points of the incircle and the side lines of Δ). It also lies in the interior of its Cevian triangle $\Delta_C(X_1)$ which we shall investigate later. If we repeat the incenter construction with either Δ_i or $\Delta_C(X_1)$, we find a triangle center in the interior of the next intouch or Cevian triangle. It is clear that all these central triangles are getting smaller in each step, lie always in the interior of the preceding triangles, and it is near to assume that both Δ_i and $\Delta_C(X_1)$, and X_1 converge to a point after infinitely many construction steps. Unfortunately, the algebraic complexity even of $X_1(\Delta_i)=X_{177}$ and also of $X_1(\Delta_i(X_{177}))$ make clear that an algebraic approach towards X_1^∞ is hopeless.

Nonetheless, we can show that the intouch triangle reaches a special shape in the limit:

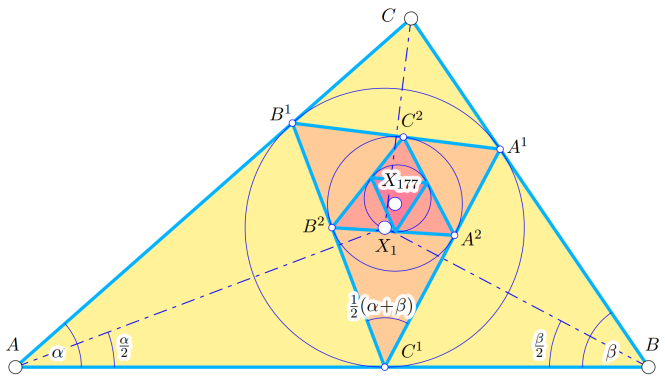

Figure 5: *The repeated construction of the intouch triangle regularizes the triangle. A limit of the incenter that is obtained as the last intouch triangle can only be found numerically.*

Theorem 1 *The repeated intouch triangle construction yields an equilateral triangle after infinitely many steps.*

Proof. We read Fig. 5 and find that $\overline{AC^1} = \overline{AB^1}$, and thus, C^1AB^1 is isosceles. Hence, $\sphericalangle AC^1B^1 = \sphericalangle AB^1C^1 = \frac{1}{2}(\pi-\alpha)$. Further, $\sphericalangle BC^1A^1 = \frac{1}{2}(\pi-\beta)$, and thus, $\gamma' := \sphericalangle A^1C^1B^1 = \frac{1}{2}(\alpha+\beta)$ and the same holds true for the other interior angles of Δ_i (with cyclic replacements of all involved objects and values). So, the interior angles of Δ and Δ_i are related by the linear mapping

$$\begin{pmatrix} \alpha' \\ \beta' \\ \gamma' \end{pmatrix} = \frac{1}{2}\begin{pmatrix} 0 & 1 & 1 \\ 1 & 0 & 1 \\ 1 & 1 & 0 \end{pmatrix}\begin{pmatrix} \alpha \\ \beta \\ \gamma \end{pmatrix}.$$

The symmetric coordinate matrix of this linear mapping can be diagonalized by $\mathbf{T}^{-1}\mathbf{L}\mathbf{T} = \mathbf{D}$, where $\mathbf{D} = \operatorname{diag}(1, -\frac{1}{2}, -\frac{1}{2})$ and the transformation matrix $\mathbf{T}$ equals

$$\begin{pmatrix} \frac{1}{3} & -\frac{1}{3} & -1 \\ \frac{1}{3} & -\frac{1}{3} & 0 \\ \frac{1}{3} & \frac{2}{3} & 1 \end{pmatrix}.$$

We can apply the linear mapping infinitely many times: $\mathbf{L}^\infty = (\mathbf{T}\mathbf{D}\mathbf{T}^{-1})^\infty = \mathbf{T}\mathbf{D}^\infty\mathbf{T}^{-1} = \mathbf{T}\operatorname{diag}(1,0,0)\mathbf{T}^{-1} = \frac{1}{3}\mathbf{U}$ where $\mathbf{U}$ is the 3×3 matrix all of whose entries are equal to 1. This means $\alpha^{(\infty)} = \frac{1}{3}(\alpha+\beta+\gamma) = \frac{\pi}{3}$ (and cyclic) which proves the theorem. □

3.2.3 Circumcenter

Some facts from the elementary geometry of the triangle along with the numerical simulation indicate the following:

Theorem 2 *The circumcenter X_3 of Δ converges towards the centroid X_2 of the base triangle Δ, provided that the pedal triangle of X_3 serves as the reference triangle in each construction step.*

Proof. The pedal triangle of X_3 equals the medial triangle Δ_m of Δ. The circumcenter of Δ_m is the nine-point center X_5 of Δ and both lie on the Euler line. Hence, the circumcenter of the pedal triangle of X_5 in Δ_m is the point X_{140} which is just called the *midpoint of X_3 and X_5* in C. KIMBERLING's Encyclopedia [7].

Consequently, X_{140} is also located on the Euler line and all further circumcenters of the respective pedal triangles gather there. Moreover, the circumcenters jump forth and back always halving the previous segment (see Fig. 6).

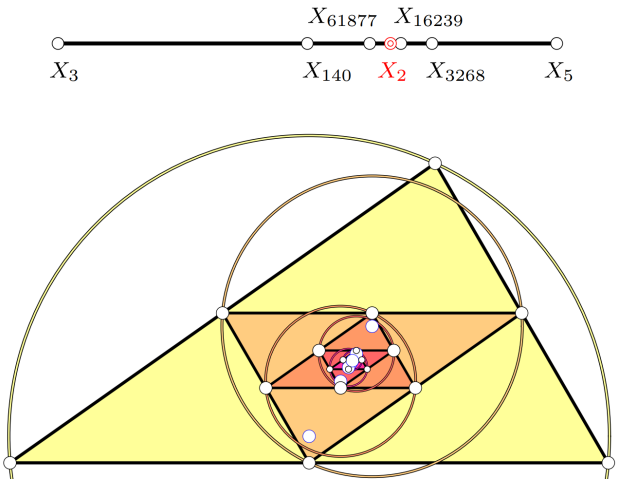

Figure 6: *The centroid is the circumcenter limit (above). Some on the initial pedal (medial) triangles with their circumcircles occuring in the limit procedure (below) share the Euler line (indicated by blue circles).*

We obtain the following sequence

$$\begin{aligned} X_3^0 &= X_3, \\ X_3^1 &= X_5, \\ X_3^2 &= \tfrac{1}{2}(X_3^1 + X_3^0) = X_{140}, \\ X_3^3 &= \tfrac{1}{4}(X_3^2 + X_3^1) = X_{3268}, \\ X_3^4 &= \tfrac{1}{8}(X_3^3 + X_3^2) = X_{16239}, \\ X_3^5 &= \tfrac{1}{16}(X_3^4 + X_3^3) = X_{61877}, \\ &\vdots \end{aligned}$$

and, expressing these affine combinations as sums of X_3^1 and X_3^0, we find

$$X_3^k = \frac{1}{2^{k-2}}\left(\jmath(k-1)X_3^{k-1} + \jmath(k)X_3^{k-2}\right),$$

where $\mathcal{J}(k) = \frac{1}{3}(2^k - (-1)^k)$ is the k-th Jacobsthal number (cf. [14]), which approaches $\frac{1}{3}2^k$ for increasing k. Now, we can find the limit point X_3^∞ as

$$\begin{aligned}&\lim_{k\to\infty} X_3^k = \\ &= \tfrac{1}{3}\lim_{k\to\infty} \tfrac{1}{2^{k-1}}\left((2^{k-1} - (-1)^{k-1}X_3^1 + (2^k - (-1)^k)X_3^0\right) = \\ &= \tfrac{2}{3}X_5 + \tfrac{1}{3}X_3 = X_2\end{aligned}$$

which completes the proof. □

From the proof of Thm. 2 we can infer:

Theorem 3 *The triangle centers X_5 (nine-point center), X_{140}, X_{3268}, X_{16239}, X_{61877}, ... in this sequence converge towards the centroid X_2 of the base triangle Δ, provided that the pedal triangle and the circumcenter construction are combined in each step.*

The numerical simulation described in Sec. 2 indicates the following:

Theorem 4 *The Symmedian point X_6 converges towards the 1st Lemoine dilation center X_{1285}, provided the pedal triangle serves as the reference triangle in each step.*

Proof. In order to verify the result, we compute some instances of the Symmedian point and show that it traverses a zig-zag polygon which consists of infinitely many similar copies that terminate in X_{1285}. The first Symmedian point X_6 is that of Δ with coordinates

$$X_6 = \frac{1}{2\tau}\left(c(-a^2+3b^2+c^2), 4cF\right),$$

where $\tau := a^2+b^2+c^2$ and its pedal triangle has the vertices (in that particular order, *i.e.*, the first vertex on $[B,C]$)

$$\begin{gathered}\tfrac{1}{4c\tau}\left(c^4+8b^2c^2-b^4-(a^2-b^2)^2, 4F(a^2-b^2+3c^2)\right),\\ \tfrac{1}{4c\tau}\left((a^2-b^2-c^2)(a^2-b^2-3c^2), 4F(-a^2+b^2+3c^2)\right),\\ \tfrac{1}{2\tau}\left(c(a^2-3b^2-c^2), 0\right).\end{gathered}$$

The next Symmedian points are

$$X_6^1 = \frac{1}{4c\tau^2}\begin{pmatrix} a^6 - a^4(3b^2+4c^2) + a^2(b^2+c^2)(3b^2+c^2) - b^6 + 8b^4c^2 + 7b^2c^4 + 2c^6 \\ -4(a^4 - a^2(2b^2+c^2) + b^4 - b^2c^2 - 4c^4)F \end{pmatrix},$$

$$X_6^2 = \frac{1}{8c\tau^3}\begin{pmatrix} a^8 - a^6(2b^2-c^2) - a^4(19b^2+17c^2)c^2 + \dots \\ -4F\left(a^6 - a^4(b^2-4c^2) - a^2(b^2+8c^2)b^2 + \dots\right) \end{pmatrix},$$

$$X_6^3 = \frac{1}{16c\tau^4}\begin{pmatrix} -a^{10} + a^8(13b^2+16c^2) - 2a^6(17b^4+32b^2c^2+25c^4) + \dots \\ 4F\left(a^8 - (12b^2+13c^2) + a^4(22b^4+13b^2c^2+13c^4) + \dots\right) \end{pmatrix},$$

$$X_6^4 = \frac{1}{32c\tau^5}\begin{pmatrix} a^{12} + 3a^{10}(4b^2+c^2) - a^8(27b^4+17b^2c^2+10c^4) + \dots \\ -4F\left(a^{10} + a^8(13b^2+6c^2) - 2a^6(7b^4-24b^2c^2-21c^4) + \dots\right) \end{pmatrix}.$$

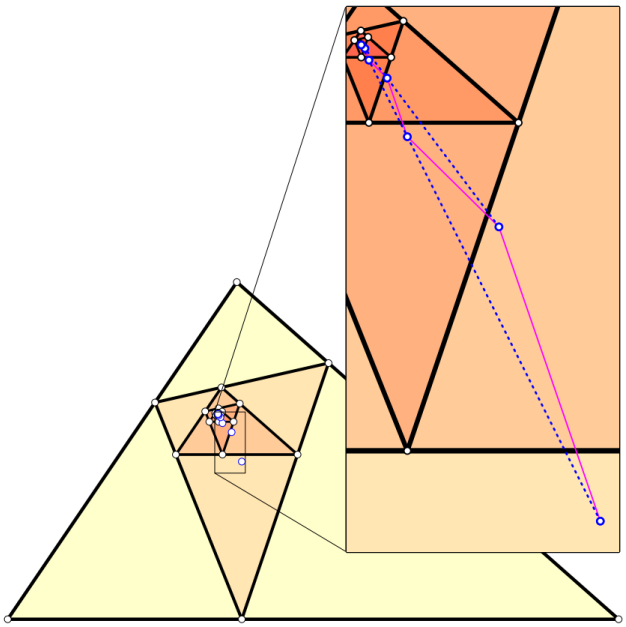

Figure 7: *The zig-zag path of the Symmedian points dithers to X_{1285}. The dotted lines joining the "even" and "odd" points intersect in the similarity center X_{1285}.*

Now, we are able to verify that the polygons $P_{012} = X_6X_6^1X_6^2$ and $P_{234} = X_6^2X_6^3X_6^4$ are similar. The scaling factor of the similarity $P_{012} \to P_{234}$ equals

$$f = \frac{12F^2}{\tau^2} = \frac{3}{4}\left(1 - \frac{2}{\tau^2}\left(a^4+b^4+c^4\right)\right) < 1.$$

The involved pedal triangles are also similar, and thus, we can be sure that the construction of any further part of the X_6^i polygon consists of pieces similar to the initial part. Instead of adding a geometric sequence of vectors, we note that the points $X_6, X_6^2, X_6^4, \dots$ and the points $X_6^1, X_6^3, X_6^5, \dots$ are collinear. Therefore, we intersect the lines passing through the "odd" and "even" points in order to obtain the limit

point

$$L = [X_6, X_6^2] \cap [X_6^1, X_6^3] =$$
$$= \frac{1}{2c}\begin{pmatrix} \star \\ \dfrac{-4F(a^2-b^2-3c^2)(a^2-b^2+3c^2)}{7a^4+2a^2b^2+2a^2c^2+7b^4+2b^2c^2+7c^4} \end{pmatrix}.$$

Cyclically shifting a, b, c in the second coordinate function and cutting out cyclic symmetric factors (F and the quartic polnomial in the denominator) yields the generating trilinear center function

$$bc(3a^2-b^2+c^2)(3a^2+b^2-c^2)$$

and the search value 0.1029669168564765255 together with the trilinear representation given at [7] identifies this point as X_{1285}. □

References

[1] AGAOKA, Y., Degree of a Triangle Center and a Generalization of the Euler Line. *Beitr. Algebra Geom.* **51**(1) (2010), 63–89.

[2] CASEY, J., *A Sequel to the First Six Books of the Elements of Euclid*. Hodges, Figgis & co., Dublin, 1886.

[3] CHANG, G.Z., DAVIS, P.J., Iterative processes in elementary geometry. *Am. Math. Mon.* **90**(7) (1983), 421–431, https://doi.org/10.1080/00029890.1983.11971250

[4] DIXMIER, J., KAHANE, J.-P., NICOLAS, J.-L., Un exemple de non-dérivabilit'e en géométrie du triangle. *Enseign. Math.* (2) **53**(3–4) (2007), 369–428.

[5] HALBEISEN, L., HUNGERBÜHLER, N., The exponential pencil of conics. *Beitr. Algebra Geom.* **59** (2018), 549–571, https://doi.org/10.1007/s13366-017-0375-1

[6] ISMAILESCU, D., JACOBS, J., On sequences of nested triangles. *Period. Math. Hung.* **53** (2006) (1–2), 169–184, https://doi.org/10.1007/s10998-006-0030-3

[7] KIMBERLING, C., *Encyclopedia of Triangle Centers. Available at:* https://faculty.evansville.edu/ck6/encyclopedia

[8] KIMBERLING, C., Triangle Centers and Central Triangles. (*Congressus Numerantium Vol. 129*) Utilitas Mathematica Publishing, Winnipeg, 1998.

[9] KINGSTON, J.G., SYNGE, J.L., The sequence of pedal triangles. *Am. Math. Mon.* **95**(7) (1988), 609–620, https://doi.org/10.1080/00029890.1988.11972056

[10] Lax, P.D., The ergodic character of sequences of pedal triangles. *Am. Math. Mon.* **97**(5) (1990), 377–381, https://doi.org/10.1080/00029890.1990.11995610

[11] MICROSOFT, *Floating-point numeric types - C# reference.* Available at: https://learn.microsoft.com/en-us/dotnet/csharp/language-reference/builtin-types/floating-point-numeric-types

[12] ODEHNAL, B., Poristic loci of triangle centers. *J. Geom. Graph.* **15**(1) (2011), 45–67.

[13] ODEHNAL, B., Two Convergent Triangle Tunnels. *KoG* **22** (2018), 3–11, https://doi.org/10.31896/k.22.1

[14] SLOANE, N.J.A.. *The On-Line Encyclopedia of Integer Sequences (OEIS).* Available at: https://oeis.org

[15] WHITE, A., *BigDecimal: An arbitrary-precision decimal (base 10) floating-point number class*. Available at: https://github.com/AdamWhiteHat/BigDecimal

Christian Clemenz
e-mail: christian.clemenz@uni-ak.ac.at
University of Applied Arts Vienna
Oskar-Kokoschka-Platz 2, A-1010 Vienna, Austria

Boris Odehnal
orcid.org/0000-0002-7265-5132
e-mail: boris.odehnal@uni-ak.ac.at
University of Applied Arts Vienna
Oskar-Kokoschka-Platz 2, A-1010 Vienna, Austria

https://doi.org/10.31896/k.29.6
Original scientific paper
Accepted: 10 November 2025

GEORG GLAESER

Geometric Construction of a Family of Keplerian Ellipses

A Geometric Construction of a Family of Keplerian Ellipses

ABSTRACT

We investigate a one-parameter family of Keplerian ellipses in a plane sharing a fixed focus F_1 and passing through a prescribed point P with identical instantaneous speed. By means of a purely geometric construction – the reflection of the ray F_1P in the tangent at P – the second focus F_2 is located on a circle f_2, yielding simple loci for the centers M and the secondary vertices C, D (both circles) and for the principal vertices A, B (conchoids of a circle). The family admits an envelope, itself an ellipse whose semiaxes are obtained in closed form. The configuration provides a direct geometric interpretation of the vis-viva relation: All members share the same semimajor axis a, and thus, the same orbital period. When rotated about the axis F_1P, the envelope ellipses form a family of confocal ellipsoids of revolution, thus connecting the planar Kepler construction with the classical geometry of quadrics.

Key words: Keplerian ellipses, envelope ellipse, conchoid, limaçon, vis-viva relation, energy equation

MSC2020: 70F15, 51A05, 51N20, 37J35

Geometrijska konstrukcija familije Keplerovih elipsa

SAŽETAK

Istražujemo jednoparametarsku familiju Keplerovih elipsa u ravnini koje imaju isto žarište F_1 i prolaze kroz danu točku P jednakom trenutnom brzinom. Pomoću čisto geometrijske konstrukcije – refleksija zrake F_1P na tangenti u točki P – drugo žarište F_2 leži na kružnici f_2, dobivaju se geometrijska mjesta središta M i sporednih tjemena C, D (dvije kružnice) i glavnih tjemena A, B (konhoide kružnice). Familija elipsi ima envelopu, također elipsu, čije su poluosi dobivene u zatvorenoj formi. Ova konfiguracija pruža izravno geometrijsko tumačenje vis-viva relacije: Svi članovi dijele istu veliku glavnu poluos a, pa onda i isti orbitni period. Kada rotiraju oko osi F_1P, elipse envelope tvore familiju konfokalnih rotacijskih elipsoida, čime se ravninska Keplerova konstrukcija povezuje s klasičnom geometrijom kvadrika.

Ključne riječi: Keplerove elipse, elipsa envelopa, konhoida, puž, vis-viva relacija, jednadžba energije

1 Motivation

This paper addresses certain physical relationships within the framework of Keplerian ellipses – not only from a physical but, above all, from a geometrical point of view – and arrives at several remarkable results. More specifically, it focuses on applying the vis-viva equation (energy equation of the Kepler orbit) to spatial objects, an approach that makes it possible to describe and analyse elliptical orbits in three-dimensional space in a fully consistent way (Fig. 1).

2 State of the Art and Related Work

The idea to organize Kepler orbits into families determined by position and speed goes back at least to Laporte [8], who studied the one-parameter family of ellipses obtained from a fixed point with equal initial speed and varying direction. Butikov provided an accessible modern account of such families and their qualitative geometry [2], and later discussed envelopes in the context of ballistic and elliptic trajectories [3]. Very recently, Heckman [7] revisited the family of Kepler ellipses through a fixed point from a geometric Hamiltonian viewpoint: He showed, in particular,

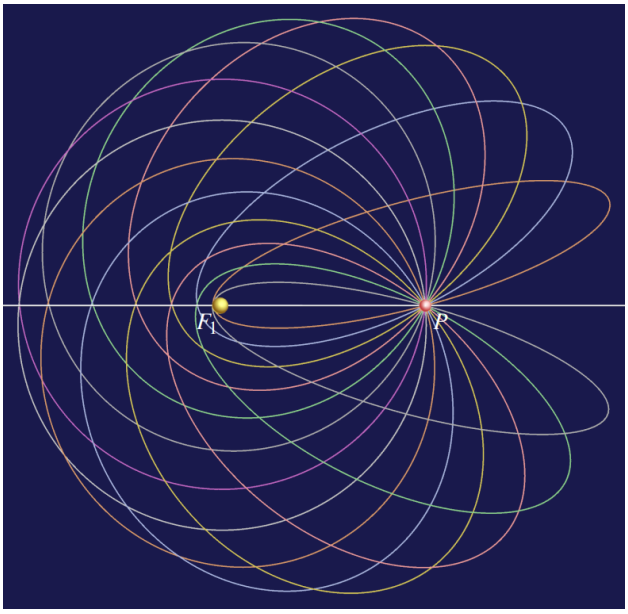

Figure 1: *Family of Keplerian ellipses corresponding to the same initial orbital speed* v*, but with different directions of the velocity vector* $\vec{v}$*. Each ellipse passes through the fixed point P and has the same focus* F_1.

that the locus of second foci is a circle of radius $2a - r$ centered at the passing point P, that all members share the same period, and he described a bounding ellipse for the swept region.

To the best of our knowledge, a *purely geometric* construction of the common *envelope ellipse* for the constant-speed family – based on reflecting the ray F_1P in the tangent at P and exploiting the collinearity of P, F_2 and the contact point – together with explicit *loci* for the centers (m), secondary vertices (C, D), and the conchoid loci for the major vertices (A, B), as well as the extremal configuration with maximal b and the cusped limaçon case $a = d$, does not appear explicitly in the literature cited above. The present paper provides such a unified geometric treatment and closed formulas for the envelope's semiaxes.

3 Introduction

Kepler's discovery that the planets move in ellipses rather than circles marks one of the most elegant links between geometry and physics. The corresponding vis-viva relation,

$$\mathrm{v}^2 = \mu\left(\frac{2}{r} - \frac{1}{a}\right),$$

connects the instantaneous distance r and speed v of a body in a central fields of gravitation with the global parameter a, the semimajor axis of its elliptical orbit.

We consider here, in purely geometric terms, the *family of all Keplerian ellipses* that share a fixed focus F_1 and pass through a given point P with identical speed. While the tangent direction in P varies, the energy and semimajor axis remain constant, forming a one-parameter family of ellipses. The central question is the determination of their *envelope*.

It is a matter of fact that the ray F_1P, when reflected in the tangent at P, passes through the second focus F_2 of the corresponding ellipse. The line PF_2 then meets the envelope in the point of contact, proving the collinearity of F_1, F_2, and the contact point and showing that all ellipses share a single bounding ellipse.

We further describe the loci of the centers, foci, and vertices of the family – circles and conchoids – and identify the limiting cases of maximal minor axis and vanishing eccentricity. The construction provides a concise geometric interpretation of the vis-viva relation and unites classical conic geometry with orbital dynamics.

4 The Vis-Viva Equation

The vis–viva relation (1) remains the cornerstone of orbital mechanics and is discussed in detail in modern treatments such as Murray and Dermott [9], Roy [11], Danby [4], and Vallado [12].

It states that

$$\mathrm{v}^2 = \mu\left(\frac{2}{\mathrm{r}} - \frac{1}{a}\right), \tag{1}$$

where

- v is the instantaneous orbital velocity of the moving body,
- r its current distance from the focus F_1 (the central mass),
- a the semimajor axis of the corresponding Kepler ellipse,
- $\mu = \mathrm{G}M$ the *gravitational parameter*,

and

$$\mathrm{G} = 6.67430 \times 10^{-11}\,\mathrm{m}^3\,\mathrm{kg}^{-1}\,\mathrm{s}^{-2}$$

denotes the universal gravitational constant, M the mass of the central attracting body.

Equation (1) expresses the conservation of total mechanical energy along a Keplerian orbit. The first term, $\frac{1}{2}\mathrm{v}^2$, represents the specific kinetic energy, whereas μ/r denotes the negative potential term. The relation applies equally to elliptical, parabolic, and hyperbolic trajectories, and reduces to the circular case when $\mathrm{r} = a$, yielding $\mathrm{v} = \sqrt{\mu/\mathrm{r}}$.

In the form of Eq. (1), one essentially determines the orbital speed v from the given semimajor axis a and the instantaneous distance r. It is noteworthy that the equation contains *no information* about the direction of the velocity vector $\vec{v}$; it merely provides its magnitude $\mathrm{v} = \|\vec{v}\|$.

Conversely, if the instantaneous orbital velocity v and the current distance r are known, the semimajor axis a of the corresponding Keplerian ellipse can be derived directly from Eq. (1):

$$\boxed{\frac{1}{a} = \frac{2}{\mathrm{r}} - \frac{\mathrm{v}^2}{\mu} \quad \Longleftrightarrow \quad a = \frac{1}{\dfrac{2}{\mathrm{r}} - \dfrac{\mathrm{v}^2}{\mu}}\,.} \tag{2}$$

This inverse form is widely used in orbital mechanics to compute the semimajor axis from position–velocity data at any given point of the trajectory.

From a *geometrical* point of view, Eq. (2) expresses that the orbital energy –, and thus the size of the ellipse – is completely determined by the *instantaneous* position and speed of the moving body. In the plane of motion, the direction of the velocity vector $\vec{v}$ is tangent to the ellipse at the current point, while its magnitude defines, through Eq. (1), the scale of the entire orbit. Consequently, the value of a derived from a single observation (r, v) uniquely determines the corresponding ellipse, up to the spatial orientation of its major axis.

A particularly important limiting case of Eq. (1) occurs when the semimajor axis a tends to infinity, corresponding to a *parabolic escape trajectory*. In this limit, the total mechanical energy approaches zero, and the orbital speed becomes the *escape velocity*

$$\boxed{\mathrm{v}_e = \sqrt{\frac{2\mu}{\mathrm{r}}}}\,. \tag{3}$$

Any higher velocity results in a hyperbolic orbit and permanent escape from the gravitational field of the central body. Conversely, for $\mathrm{v} < \mathrm{v}_e$ the motion remains bound, and Eq. (2) yields a finite semimajor axis a.

From a purely geometrical standpoint, the escape velocity marks the limiting case in which the semimajor axis a of the Kepler ellipse tends to infinity. As $a \to \infty$, the ellipse gradually opens, its curvature at the current point decreases, and the second focus recedes to infinity. The ellipse thus transforms smoothly into a *parabola* whose focus coincides with the central mass F_1 and whose directrix lies at an infinite distance.

In this limiting configuration, the moving body possesses just enough kinetic energy to reach infinity with zero residual speed – precisely the condition $\mathrm{v} = \mathrm{v}_e = \sqrt{2\mu/\mathrm{r}}$. Hence, the parabolic orbit forms the natural boundary between bound and unbound motion, connecting the family of Keplerian ellipses continuously to the branch of hyperbolic trajectories.

Remark 1 (Bound-Unbound Criterion) *In order to ensure that the curve κ_ψ represents a* closed Keplerian ellipse*, the orbital velocity* v *in the given point P must not exceed the* parabolic escape velocity. *Quantitatively, this means that the instantaneous velocity* v *may at most exceed the circular velocity* $\mathrm{v}_{\mathrm{circ}}$ *by a factor of* $\sqrt{2}$*:*

$$\mathrm{v} \le \sqrt{2}\,\mathrm{v}_{\mathrm{circ}} \quad \textit{with} \quad \mathrm{v}_{\mathrm{circ}} = \sqrt{\frac{\mu}{r}}.$$

If $\mathrm{v} = \sqrt{2}\,\mathrm{v}_{\mathrm{circ}}$*, the resulting orbit becomes parabolic* ($a \to \infty$)*; for* $\mathrm{v} > \sqrt{2}\,\mathrm{v}_{\mathrm{circ}}$*, it turns into a hyperbola. This* $\sqrt{2}$*-limit provides a simple geometric criterion for distinguishing bounded (elliptic) from unbounded (parabolic or hyperbolic) trajectories, and it holds universally for all central gravitational fields for all central gravitational fields (see [1, pp. 66–68]).*

In the present paper, however, we shall restrict our attention exclusively to *elliptical orbits*, leaving the parabolic and hyperbolic cases aside.

Remark 2 (Constant Period and Spatial Interpretation) *Since the semimajor axis a is identical for all members of the considered family of Keplerian ellipses, the orbital period T is the same for all of them as well, according to Kepler's third law,*

$$T = 2\pi\sqrt{\frac{a^3}{\mu}}.$$

Thus, all particles moving on these ellipses complete their revolution in equal time, even though their orbital shapes and instantaneous velocities differ.

Because the construction depends only on the line through F_1 and P, the same argument applies to any plane containing this line. Hence the family may be regarded as a three-dimensional system of identical orbits distributed over all planes passing through F_1P. In this sense, the model admits a natural spatial interpretation: Each ellipse represents the projection of an orbit lying in a different orbital plane but governed by the same gravitational parameter μ and the same total energy.

The time-evolution of the corresponding particles can be visualized by the accompanying sequence of frames shown in Fig. 2, and in the supplementary video available online ([5]).

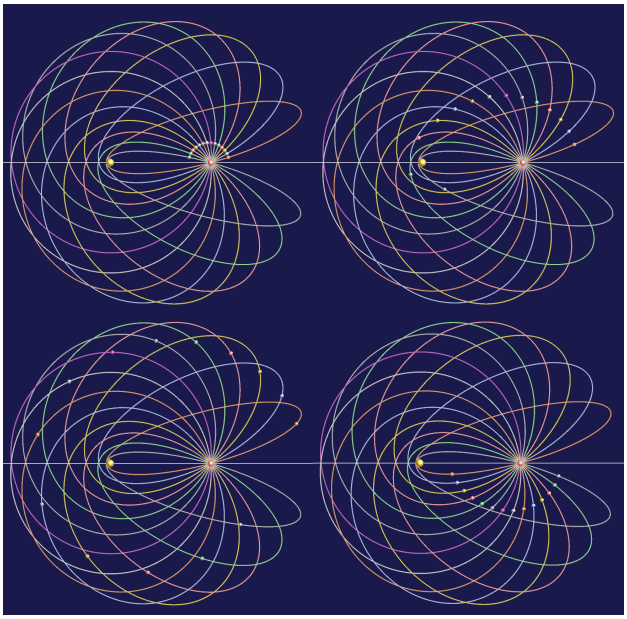

Figure 2: *Sequence of frames illustrating the motion of several particles along the family of Keplerian ellipses with identical semimajor axis a and focus F_1. Each ellipse corresponds to a different orientation of the tangent at P, but all orbits share the same period T and gravitational parameter μ, as illustrated in the supplementary video [5].*

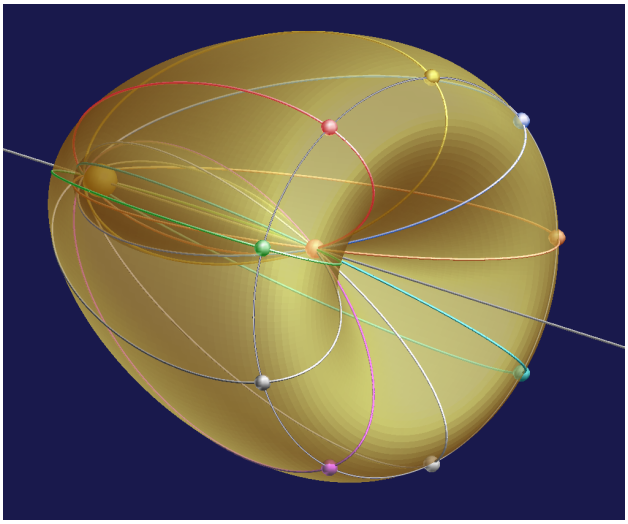

Figure 3: *Isoenergetic family of Keplerian trajectories launched with identical speed from the same point along all directions of a conical field of initial velocities. All orbits share the same semimajor axis a but differ in eccentricity and orientation. They return to the common starting point simultaneously after one complete revolution.*

Launching from the same point with identical speed along all directions of a cone of revolution whose axis is the orbital tangent yields an isoenergetic family of Keplerian ellipses with the same semimajor axis a but generally different eccentricities. All trajectories of this family have identical orbital periods, since the revolution time depends solely on the semimajor axis according to Kepler's third law. Consequently, although the eccentricities and spatial orientations of the orbits differ, all projectiles return to their common starting point simultaneously after one full revolution. The resulting configuration is illustrated in Fig. 3.

The time-evolution of this isoenergetic family is illustrated in Fig. 2, where all trajectories start simultaneously from the same point and return to it after one full revolution. An animated version of this figure, showing the continuous propagation of the orbits and the simultaneous rendezvous of the projectiles, is available as supplementary material online.

5 Geometric Construction

Having examined the physical foundation of Keplerian motion, we now turn to a purely *geometrical interpretation* of the same family of ellipses. Instead of deriving the orbital parameters from forces and energies, we shall describe the entire configuration in terms of *fixed points, distances, and loci*. This approach reveals several remarkable geometric properties – in particular, the existence of an *envelope ellipse* that is tangent to all Keplerian ellipses of a given family. For a comprehensive geometric treatment of conic sections and their focal properties, see [6].

6 Geometrical Construction

Let us begin with the question of how to construct an ellipse when one focus F_1, the total major axis length $2a$, and a point P at a fixed distance $d = |F_1P|$ are given, together with the tangent t at P, which forms an angle ψ with the reference axis $\overline{F_1P}$. The solution is remarkably simple.

Since an ellipse is the locus of all points whose distances to two fixed foci sum to the constant $2a$, and since the tangent at any point bisects the angle between the focal radii, we proceed as follows (Fig. 4):

Construction. Define a fixed counterpoint G on the ray F_1P such that $|F_1G| = 2a$. Reflect G about the tangent t through P; the reflection point is F_2,

$$F_2 = \mathrm{Ref}_t(G).$$

As the tangent direction ψ varies, G remains fixed while its mirror image F_2 moves along a circle f centered at P with

radius

$|PF_2| = 2a - d$.

This circle represents the *locus of all possible second foci* of the family of ellipses κ_ψ. The tangent t bisects the focal angle,

$\angle GPF_2 = 2\psi \Rightarrow \angle F_1PF_2 = \pi - 2\psi$.

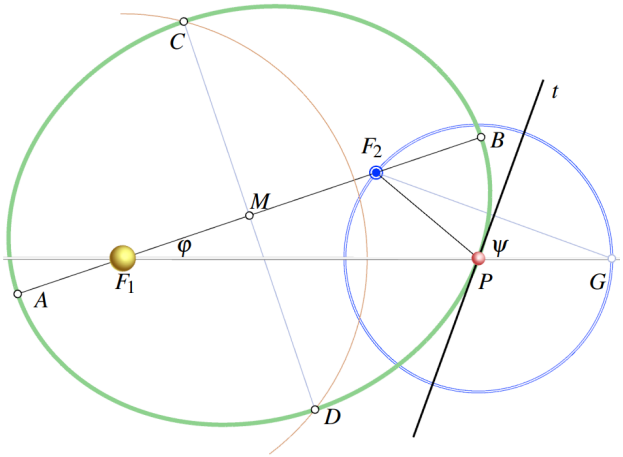

Figure 4: *Geometric construction of the ellipse κ_ψ from the given focus F_1, the tangent t at the point P with $|F_1P| = d$, and the total major axis $2a$. Reflect the line F_1P about t and mark on the reflected ray from P the segment of length $2a - d$ to obtain the second focus F_2. Equivalently, F_2 is the mirror image of the fixed point G on F_1P satisfying $|F_1G| = 2a$. The tangent t bisects the angle $\angle F_1PF_2 = \pi - 2\psi$. The construction fixes the center M, the vertices A, B, and the semiaxes $a, b(\psi)$.*

7 Three Circular Loci

Fix a focus F_1, a point P with $|F_1P| = d$, and a common semimajor axis a. For the one-parameter family $\{\kappa_\psi\}$ of Kepler ellipses through P we have:

1. **Locus of the second focus.** Evaluating the focal sum at $X = P$ gives $|PF_2| = 2a - d$. Hence the second focus F_2 runs on the circle

   f_2 : center P, radius $2a - d$.

2. **Locus of the ellipse centers.** Since the center M is the midpoint of F_1F_2, and F_2 moves on the circle around P, the midpoint $M = \frac{1}{2}(F_1 + F_2)$ describes a circle with half the radius and centered at the midpoint of F_1P. Writing Q for the midpoint of F_1P,

   m : center Q, radius $a - \frac{d}{2}$.

3. **Locus of the secondary vertices.** At the secondary vertices C, D the distances to the foci are equal by symmetry, and $|F_1C| + |F_2C| = 2a$ yields $|F_1C| = |F_2C| = a$ (likewise for D). Hence

   c : center F_1, radius a,

   i.e., all secondary vertices lie on the circle of radius a about F_1.

Figure 5 illustrates the configuration: The focus-locus f_2 (centered at P), the center-locus m (centered at the midpoint Q of F_1P), and the circle c carrying all secondary vertices C, D (centered at F_1).

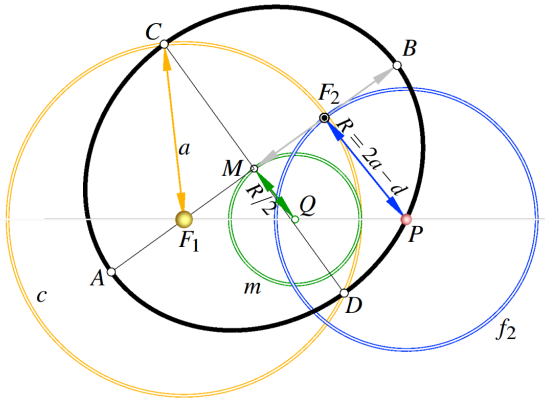

Figure 5: *Three circular loci for the family $\{\kappa_\psi\}$: The second focus F_2 moves on f_2 (center P, radius $2a - d$); the ellipse center M moves on m (center Q, the midpoint of F_1P, radius $a - \frac{d}{2}$); and the secondary vertices C, D lie on the circle c (center F_1, radius a).*

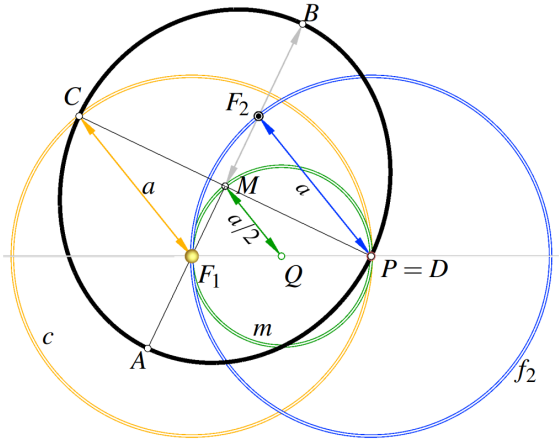

Figure 6: *Special case $a = d$: The focus locus f_2 (center P, radius a), the center locus m (center Q, radius $a/2$), and the circle c of minor vertices (center F_1, radius a).*

Remark 3 (Special case $a = d$) *In the special case $a = d$ the three circular loci simplify as follows: The second focus runs on f_2 with radius $|PF_2| = 2a - d = a$ (center P), the ellipse centers M run on m with radius $a - \frac{d}{2} = \frac{a}{2}$ (center Q, the midpoint of F_1P), and the minor vertices C, D lie on the circle c of radius a about F_1 (unchanged). The configuration is illustrated in Fig. 6.*
A particularly remarkable feature of this configuration is that the lower vertices *D of all ellipses coincide with the fixed point P.*

8 Focal distance and eccentricity

The midpoint M of the focal segment F_1F_2 is the center of κ_ψ, and satisfies

$$|F_1M| = |MF_2| = c_\psi,$$

which defines the *linear eccentricity*

$$c_\psi = \tfrac{1}{2}\sqrt{d^2 + (2a-d)^2 - 2d(2a-d)\cos(2\psi)}\,.$$

The corresponding (dimensionless) eccentricity is

$$e_\psi = \frac{c_\psi}{a}.$$

Equation of the ellipse. The ellipse κ_ψ has the polar equation (with origin at F_1, polar angle α measured from $\overline{F_1P}$):

$$r(\alpha) = \frac{a(1-e_\psi^2)}{1 + e_\psi\cos(\alpha - \varphi)},$$

where φ denotes the orientation of the major axis relative to $\overline{F_1P}$.

Remark 4 (Velocity Ratios at Pericenter and Apocenter) *For every Keplerian ellipse κ_ψ with semimajor axis a and eccentricity e_ψ, the instantaneous orbital velocity follows from the vis-viva relation*

$$\mathrm{v}^2 = \mu\left(\frac{2}{r} - \frac{1}{a}\right).$$

At the circular radius $r = a$ one obtains

$$\mathrm{v}_{\mathrm{circ}} = \sqrt{\frac{\mu}{a}}.$$

At pericenter and apocenter, where

$$r_{\mathrm{peri}} = a(1-e_\psi), \qquad r_{\mathrm{apo}} = a(1+e_\psi),$$

the corresponding velocities are

$$\mathrm{v}_{\mathrm{peri}} = \sqrt{\frac{\mu}{a}}\sqrt{\frac{1+e_\psi}{1-e_\psi}}, \qquad \mathrm{v}_{\mathrm{apo}} = \sqrt{\frac{\mu}{a}}\sqrt{\frac{1-e_\psi}{1+e_\psi}}.$$

Hence the ratios relative to the circular velocity are

$$\boxed{\frac{\mathrm{v}_{\mathrm{peri}}}{\mathrm{v}_{\mathrm{circ}}} = \sqrt{\frac{1+e_\psi}{1-e_\psi}}, \qquad \frac{\mathrm{v}_{\mathrm{apo}}}{\mathrm{v}_{\mathrm{circ}}} = \sqrt{\frac{1-e_\psi}{1+e_\psi}}.}$$

The pericentric velocity therefore exceeds the circular value, while the apocentric velocity falls below it. At the parabolic limit $e_\psi \to 1$ the pericentric velocity approaches $\sqrt{2}\,\mathrm{v}_{\mathrm{circ}}$, corresponding to the escape condition ([1, §2.5]).

Remark 5 (Special case $a = d$) *If the semimajor axis equals the focal distance to the given point, $a = d$, then the major axis of κ_ψ is aligned with the reflected ray through P, and the axis angle equals the tangent angle:*

$$\varphi = \psi.$$

In this case the eccentricity reduces to

$$e_\psi = \frac{c_\psi}{a} = \left|\sin\psi\right|,$$

and the vis–viva relations yield the pericentric and apocentric velocities, relative to the circular speed $\mathrm{v}_{\mathrm{circ}} = \sqrt{\mu/a}$:

$$\boxed{\frac{\mathrm{v}_{\mathrm{peri}}}{\mathrm{v}_{\mathrm{circ}}} = \sqrt{\frac{1+|\sin\psi|}{1-|\sin\psi|}}, \qquad \frac{\mathrm{v}_{\mathrm{apo}}}{\mathrm{v}_{\mathrm{circ}}} = \sqrt{\frac{1-|\sin\psi|}{1+|\sin\psi|}}}$$

(for ψ taken modulo π). At $\psi = 0$ one has $\mathrm{v}_{\mathrm{peri}} = \mathrm{v}_{\mathrm{apo}} = \mathrm{v}_{\mathrm{circ}}$ (circular case), while as $|\psi| \to \pi/2$ the apocentric velocity tends to 0 and $\mathrm{v}_{\mathrm{peri}} \to \sqrt{2}\,\mathrm{v}_{\mathrm{circ}}$ (parabolic limit).

Proof (vis–viva only). *From $\mathrm{v}^2 = \mu(2/r - 1/a)$, with $r_{\mathrm{peri,apo}} = a(1 \mp e_\psi)$ and $e_\psi = |\sin\psi|$, one obtains directly $\mathrm{v}_{\mathrm{peri}} = \mathrm{v}_{\mathrm{circ}}\sqrt{(1+e_\psi)/(1-e_\psi)}$ and $\mathrm{v}_{\mathrm{apo}} = \mathrm{v}_{\mathrm{circ}}\sqrt{(1-e_\psi)/(1+e_\psi)}$.*

Semiminor axis. From $b^2 = a^2 - c_\psi^2$ follows

$$b^2(\psi) = d\left(a - \frac{d}{2}\right) + \frac{d(2a-d)}{2}\cos(2\psi),$$

and thus,

$$b(\psi) = \cos\psi\sqrt{d(2a-d)}.$$

Hence the semiminor axis attains its maximum for $\psi = 0$, when the tangent is parallel to $\overline{F_1P}$:

$$b_{\max} = \sqrt{d(2a-d)}.$$

This value equals the geometric mean of the focal distances $d = |F_1P|$ and $(2a-d) = |PF_2|$. For $\psi = \frac{\pi}{2}$, the points F_1, P, and F_2 become collinear, the focal separation is maximal ($c_\psi = a$), and the ellipse degenerates into a line segment.

Summary. The family κ_ψ is completely determined by the parameters (a, d, ψ). The quantities φ, e_ψ, c_ψ, and $b(\psi)$ follow from the above relations. The fixed point G serves as a convenient geometric reference: All members of the family arise as mirror images of G with respect to their respective tangents $t(\psi)$.

9 The Envelope of the Family of Keplerian Ellipses

Let κ_ψ be one of the Kepler ellipses of the family. We mark on it a point H as the second intersection of the ellipse with the guiding ray PF_2. For this point, the sum of the focal distances is constant. Since

$$\begin{aligned} |F_1H| + |PH| &= \big\{\, |F_1H| + |F_2H| \,\big\} + |F_2P| \\ &= \big\{\, 2a \,\big\} + (2a - d) = 4a - d, \end{aligned}$$

the point H lies on an auxiliary ellipse h with foci F_1 and P and semimajor axis $2a - \frac{d}{2}$. At H, the tangents to κ_ψ and h coincide, because in both cases the tangent is the angle bisector of the same pair of guiding rays. Consequently, h touches every member of the family κ_ψ, and therefore, constitutes the *envelope* of all Keplerian ellipses of this type.

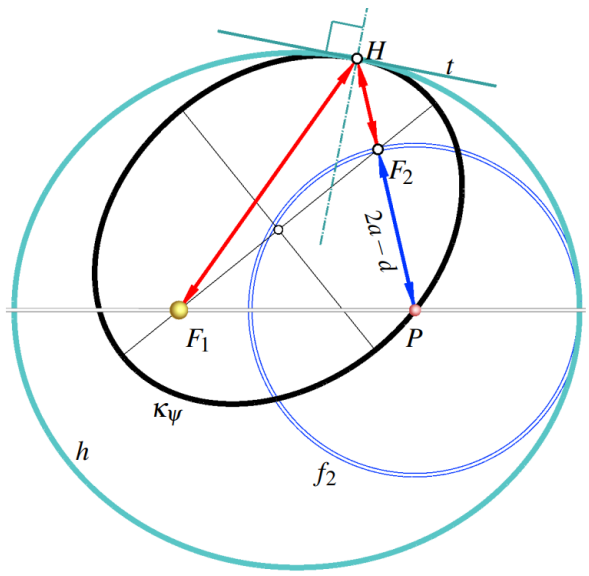

Figure 7: *Geometric proof of the envelope. For each tangent t through P, the reflection of the ray SP determines the second focus F_2. The intersection of the line PF_2 with the family's outer boundary defines the point H, which lies on the envelope ellipse h. The points P, F_2, and H are collinear.*

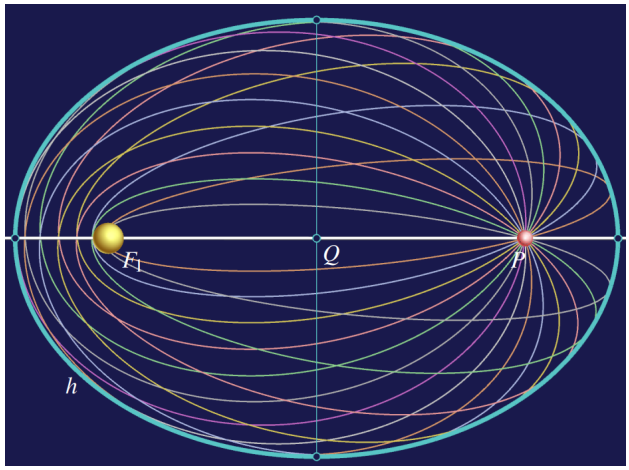

Figure 8: *The complete family of Kepler ellipses with fixed focus F_1 and identical speed at P. Each ellipse touches the envelope h (cyan curve). The envelope itself is an ellipse with semimajor axis $a_h = 2a - d$ and semiminor axis $b_h = \sqrt{(2a-d)d}$.*

The overall configuration is illustrated schematically in Fig. 7, showing the family of ellipses for different orientations of the tangent at P and their envelope h.

Moreover, the reflection of the point of contact H in the common tangent t always lies on the principal axis F_1P, at a distance of $4a - d$ from F_1.

Remark 6 (On intersections within the family) *Two distinct members κ_ψ and $\kappa_{\psi'}$ of the constant-speed family pass through P but have different tangents there (for $\psi \neq \psi'$), hence the intersection at P is transveral. By Bézout's theorem, two conics intersect with total multiplicity 4 in the complex projective plane; the remaining intersection multiplicities are accounted for by two common (complex) tangents through the fixed focus F_1 in the dual picture. Thus, neighbouring members typically meet only at P in the real plane.*

Spatial version. For each admissible tangential velocity at P, the corresponding Kepler ellipse κ_ψ is tangent to the envelope ellipse h with foci F_1 and P and semimajor axis $a_h = 2a - \frac{d}{2}$. If the entire configuration is rotated about the axis F_1P, the envelope h generates an *egg-shaped ellipsoid of revolution* whose focal points are F_1 and P.

As the velocity in P varies, the semimajor axis a changes according to the vis-viva relation $a = \frac{\mu r}{2\mu - r v^2}$, so that a ranges from 0 (for $v \to \infty$) up to $d\sqrt{2}$ at the parabolic limit. Hence all Keplerian ellipses passing through the fixed point P with any sub-parabolic velocity form a continuous one-parameter

family of *confocal egg-shaped ellipsoids of revolution* – as discussed in [10] – each touching its corresponding planar Kepler ellipse along the generator defined by the common tangent at P.

Remark 7 (The complete picture, a spatial arrangement of Keplerian ellipses) *Through the fixed point P there pass infinitely many tangents t, each characterized by its spatial orientation (two degrees of freedom) and by the magnitude of the velocity vector (one additional degree of freedom). Hence, the set of all Kepler ellipses passing through P forms a three-dimensional continuum: For every direction and speed in P there exists exactly one Keplerian orbit of the family.*

However, among these infinitely many ellipses, all those that differ only by a rigid motion (translation or rotation) are congruent. Thus, within this three-dimensional continuum, there exists a one-dimensional subfamily of congruent ellipses, leaving only a two-dimensional manifold of distinct shapes. Equivalently, if the semiaxes a and b are taken as parameters, the space of all geometrically different ellipses is two-dimensional, corresponding to the degrees of freedom of shape and eccentricity.

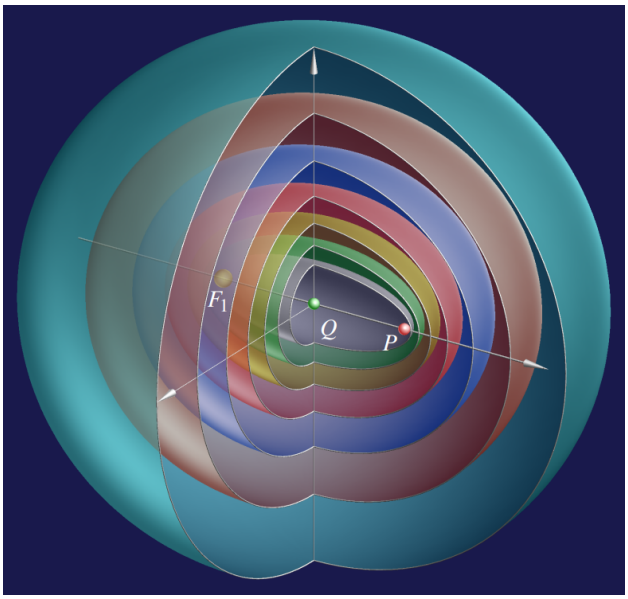

Figure 9: *Rotation of the envelope ellipse h about the axis F_1P generates an egg-shaped ellipsoid of revolution. The fixed points F_1 and P serve as common foci of all such ellipsoids, each corresponding to a Kepler ellipse κ_ψ of equal velocity in P. The colored layers illustrate the associated system of* confocal quadrics *sharing the same focal points F_1 and P. Each planar Kepler ellipse arises as a section through F_1, P, and its corresponding focus F_2.*

10 Loci of the Principal Vertices A and B

We return zu the planar version. Let m be the circle of ellipse centers with center C (the midpoint of F_1P) and radius $r_0 = a - \frac{d}{2}$. With F_1 as pole, let φ denote the polar direction. The ray from F_1 at angle φ meets m at distance

$$s(\varphi) = \tfrac{d}{2}\cos\varphi + \sqrt{r_0^2 - (\tfrac{d}{2}\sin\varphi)^2}\,.$$

The principal vertices are obtained by shifting $\pm a$ along this ray:

$$\boxed{r_A(\varphi) = s(\varphi) + a, \qquad r_B(\varphi) = |\,s(\varphi) - a\,|}\,.$$

Hence both loci are *conchoids of the circle m with pole F_1*.

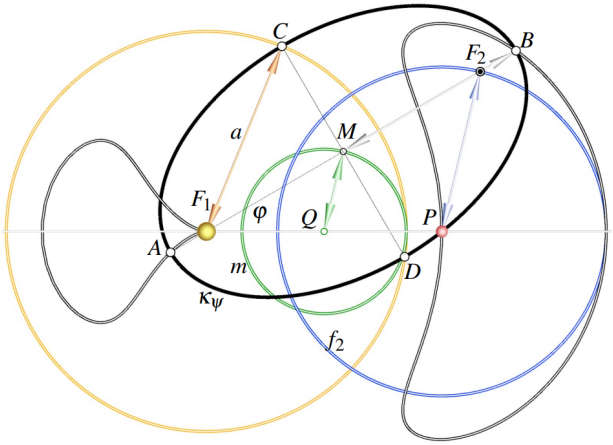

Figure 10: *General case: The loci of A (outer branch) and B (inner branch) are conchoids of the center circle m with pole F_1.*

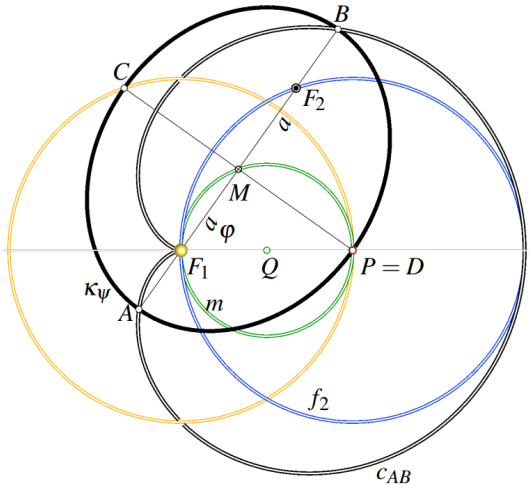

Figure 11: *Special case $a = d$: The conchoids degenerate into a cusped Pascal snail c_{AB}.*

Remark 8 (Identity of the two Pascal snails) *For the special case $a = d$, the loci of the two main vertices A and B of the ellipses κ_φ are given in polar coordinates by*

$$r_A(\varphi) = a(1+\cos\varphi), \qquad r_B(\varphi) = a(1-\cos\varphi).$$

Although these equations look different, they describe the same cusped Pascal snail *(a cardioid–type limaçon), merely rotated by π:*

$$r_B(\varphi+\pi) = a(1+\cos\varphi) = r_A(\varphi).$$

Hence the two vertex loci coincide geometrically, each covering the same curve twice with opposite orientation. The cusp corresponds to $\varphi = 0$, where A and B coincide at P, and the maximal distance $r = 2a$ occurs at $\varphi = \pi$.

The loci of the two main vertices A and B of all ellipses κ_φ (for the case $a = d$) form a single cusped Pascal snail *given in polar coordinates by $r = a(1+\cos\varphi)$. The cusp corresponds to $\varphi = 0$, where A and B coincide at P, and the maximal distance $r = 2a$ occurs at $\varphi = \pi$.*

In order to visualize the variation of the orbital velocity along this curve, we now plot the apocentric speed v_{apo} of the corresponding ellipses κ_φ above the cardioid. If the velocity is plotted with opposite sign for $-\frac{\pi}{2} < \varphi < +\frac{\pi}{2}$, the surface becomes continuous and differentiable at the parabolic limits. This orientation change reflects the natural reversal of motion along the cardioid when the orbit passes through its side point.

For a continuous, orientation preserving plot we use the signed apocentric speed

$$v^{\text{or}}_{\text{apo}}(\varphi) = s(\varphi)\, v_{\text{circ}} \sqrt{\frac{1-|\sin\varphi|}{1+|\sin\varphi|}}, \qquad s(\varphi) = -\operatorname{sgn}(\cos\varphi),$$

so that the sign flips at $\varphi = \pm\frac{\pi}{2}$.

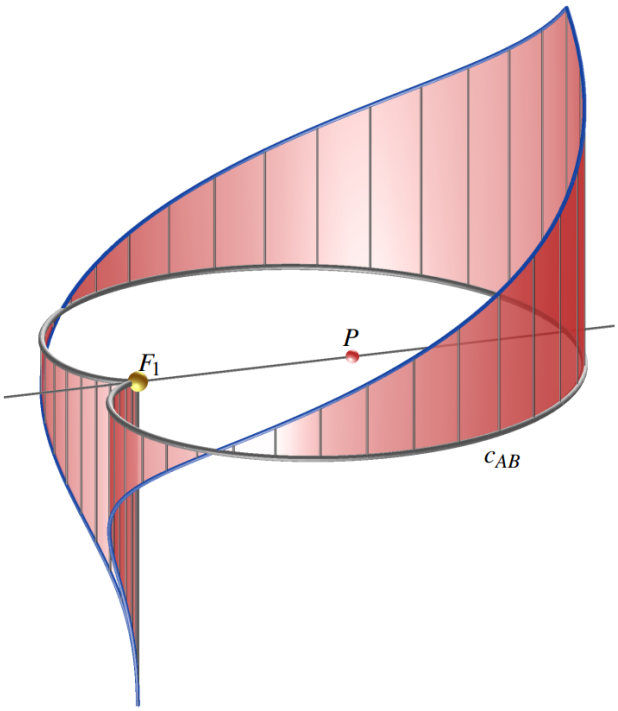

Figure 12: *Signed apocentric velocity over the cardioid $r = a(1+\cos\varphi)$. The black curve is the locus of apocentric vertices B (case $a = d$). The red ribbon shows $v^{\text{or}}_{\text{apo}}(\varphi)$, with the sign chosen via $s(\varphi) = -\operatorname{sgn}(\cos\varphi)$, yielding a smooth continuation through the parabolic limit $v_{\text{apo}} = 0$ at $\varphi = \pm\frac{\pi}{2}$.*

Conclusions and Future Work

The geometric constructions discussed above reveal a remarkable coherence between the analytic and envelope representations of the Kepler family. Starting from a purely planar setting, the reflection-based construction provides an intuitive bridge between the focal geometry of conic sections and their dynamical interpretation.

We have presented a purely geometric treatment of a remarkable family of Keplerian ellipses passing through a fixed point P with identical speed. By reflecting the ray F_1P in the tangent at P we located the second focus F_2 and established a simple proof that all such ellipses share a common bounding ellipse as their envelope. The semiaxes of this envelope can be expressed in closed form in terms of a and d.

In addition, we derived the loci of the centers, foci, and vertices of the entire family. The centers and minor vertices describe circles, whereas the principal vertices trace conchoids of the center circle, merging into a cusped Pascal snail in the special case $a = d$. These constructions demonstrate that classical geometry naturally reproduces the relations known from orbital mechanics.

From a physical point of view, the constant-speed family represents all possible bound orbits of equal total energy starting from P. Each member corresponds to a distinct initial direction, yet all share the same period according to Kepler's third law. The envelope thus provides a geometric visualization of the energy boundary in a central field.

A three-dimensional interpretation arises when the envelope ellipse h is rotated about the axis F_1P, generating an *egg-shaped ellipsoid of revolution*. The entire family of Kepler ellipses can therefore be embedded into a system of *confocal quadrics* sharing the same foci F_1 and P, providing a spatial counterpart to the planar focal construction (cf. Fig. 9).

Future work may extend this approach to inclined orbital planes and precessing ellipses, or explore analogous envelope constructions for hyperbolic and parabolic trajectories. The presented geometric framework also lends itself to educational and visual applications linking classical geometry with dynamical systems.

Beyond the purely geometric framework presented here, the same configuration may also be viewed in a dynamical context. Considering, for instance, the Jupiter system with a massless satellite (a "null moon" moving in the same orbital plane, the geometry of the present family arises as the limiting case of the barycentric two-body system when the satellite mass tends to zero. In this limit, the fixed focus F_1 represents the planet, and the moving focus F_2 corresponds to the barycentre of the combined system, thus providing a natural physical interpretation of the focal envelope. This observation may open a link between purely geometric envelopes and dynamical orbital models and will be explored in a forthcoming study.

References

[1] BATE, R.R., MUELLER, D.D., WHITE, J.E., *Fundamentals of Astrodynamics*. Dover Publications, New York, 1971.

[2] BUTIKOV, E.I., Families of Keplerian orbits. *Eur. J. Phys.* **24** (2003), 175–183, https://doi.org/10.1088/0143-0807/24/2/358

[3] BUTIKOV, E.I., The envelope of ballistic trajectories and elliptic orbits. *Eur. J. Phys.* **83** (2015), 952–958, https://doi.org/10.1119/1.4928176

[4] DANBY, J.M.A., *Fundamentals of Celestial Mechanics*. 2nd ed. Willmann–Bell, Richmond, VA, 1988.

[5] GLAESER, G., *Kepler Ellipses: Animated Supplementary Video*. University of Applied Arts Vienna, 2025, https://tethys.uni-ak.ac.at/kepler-ellipsen.mp4

[6] GLAESER, G., STACHEL, H., ODEHNAL, B., *The Universe of Conics*. 2nd ed., Springer Spektrum, Heidelberg, 2024, https://doi.org/10.1007/978-3-662-70306-9

[7] HECKMAN, G.J., Exercises on the Kepler ellipses through a fixed point in space, after Otto Laporte. *Indag. Math.* **36**(6) (2025), 1592–1599, https://doi.org/10.1016/j.indag.2025.02.004

[8] LAPORTE, O., On Kepler Ellipses Starting from a Point in Space. *Am. J. Phys* **38** (1970), 837–840, https://doi.org/10.1119/1.1976479

[9] MURRAY, C.D., DERMOTT, S.F., *Solar System Dynamics*. Cambridge University Press, Cambridge, 1999.

[10] ODEHNAL, B., STACHEL, H., GLAESER, G., *The Universe of Quadrics*. Springer-Verlag, Berlin, Heidelberg, 2020, https://doi.org/10.1007/978-3-662-61053-4

[11] ROY, A.E., *Orbital Motion*, 4th ed., Institute of Physics Publishing, Bristol and Philadelphia, 2005.

[12] VALLADO, D.A., *Fundamentals of Astrodynamics and Applications*, 4th ed. Microcosm Press, Hawthorne, CA, 2013.

Georg Glaeser
e-mail: georg.glaeser@uni-ak.ac.at

University of Applied Arts Vienna
Oskar-Kokoschka-Platz 2, A-1010 Vienna, Austria

https://doi.org/10.31896/k.29.8
Professional paper
Accepted: 27 November 2025

IVA KODRNJA

On Remarkable Properties of Number 2025

On Remarkable Properties of Number 2025

ABSTRACT

In this paper we investigate the number 2025 and visualize its regularity. This is a perfect square, but a deeper look reveals much more structure related to counting lattice points in polygons and polyhedra. We will also discuss the frequency of square and regular years and the uniqueness of such a regular year number.

Key words: figure numbers, trigonal numbers, tetrahedral numbers

MSC2020: 05A17, 52C05

O izuzetnim svojstvima broja 2025

SAŽETAK

U ovom članku proučava se broj 2025 i vizualizira njegova regularnost. Ovaj broj je potpuni kvadrat, a dubljim uvidom otkrivamo bogatu strukturu i povezujemo je s prebrojavanjem cjelobrojnih točaka u poligonalnim domenama. Također dajemo osvrt na frekvenciju pojave kvadratnih i regularnih godina te jedinstvenost ovakve regularne godine.

Ključne riječi: poligonalni broj, trigonalni broj, tetredralni broj

1 Introduction

Number 2025 is very special. It is a perfect square, an odd square, a square of triangular number, sum of two, three and four squares, sum of cubes. It is a regular number, a number that has only 3 and 5 as prime divisors since

$$2025 = 81 \cdot 25 = 9^2 \cdot 5^2 = 3^4 \cdot 5^3$$

and finally, it is a product of squares. In Table 1 we give a (noncomplete) list of sequences that contain 2025 in the Online Encyclopedia of Integer Sequences (OEIS [8]).

Regularity of number 2025 can be visualized by polygonal symmetries connected to number sequences mentioned. Number 2025 belongs to the class of figure numbers, polygonal numbers which are used for counting lattice points inside polygons [1, 10].
In Section 2 we give recursions and graphical representations of some number sequences from Table 1. We show that the predecessor 2024 and successor 2026 are also figure numbers; 2024 is a tetrahedral number (3), while $2026 = 2 \cdot 1013$ is successor of a square number and 1013 is a centered square number, sum of consecutive squares $n^2 + (n+1)^2$ with $n = 22$.

Sequence in OEIS	Occurence	Description of sequence	$2025 =$
A000290	$n = 45$	perfect square	45^2
A016754	$n = 22$	odd square (centered octagonal number)	$(2 \cdot 22 + 1)^2$
A000537	$n = 9$	sum of cubes (square of triangular number)	$\left(\frac{9 \cdot 10}{2}\right)^2$
A001481	$n = 626$	sum of two squares	$27^2 + 36^2$
A051037	$n = 109$	5-smooth number (regular number)	$3^4 \cdot 5^2$
A238237	$n = 2$	*torn* number	$(20 + 25)^2$
A350869	$n = 2$	square of sum of all numbers with one digit	$\left(\frac{(10^1-1)\cdot 10^1}{2}\right)^2$

Table 1: *Occurrences of number* 2025 *in OEIS and corresponding formulas*, [8].

n	Prime Factorization	$\varphi(n)$	n	Prime Factorization	$\varphi(n)$
2000	$2^4 \times 5^3$	800	2013	$3 \times 11 \times 61$	1200
2001	$3 \times 23 \times 29$	1232	2014	$2 \times 19 \times 53$	936
2002	$2 \times 7 \times 11 \times 13$	720	2015	$5 \times 13 \times 31$	1440
2003	2003	2002	2016	$2^5 \times 3^2 \times 7$	576
2004	$2^2 \times 3 \times 167$	664	2017	2017	2016
2005	5×401	1600	2018	2×1009	1008
2006	$2 \times 17 \times 59$	928	2019	3×673	1344
2007	$3^2 \times 223$	1332	2020	$2^2 \times 5 \times 101$	800
2008	$2^3 \times 251$	1000	2021	43×47	1932
2009	$7^2 \times 41$	1680	2022	$2 \times 3 \times 337$	672
2010	$2 \times 3 \times 5 \times 67$	528	2023	7×17^2	1632
2011	2011	2010	2024	$2^3 \times 11 \times 23$	880
2012	$2^2 \times 503$	1004	2025	$3^4 \times 5^2$	1080
			2026	2×1013	1012
			2027	2027	2026

Table 2: *Prime factorization and Euler's function* $\varphi(n)$ *for* $2000 \leq n \leq 2027$.

In Section 3 we look at the fact that 2025 is the square of the sum of digits

$$(0+1+2+\cdots+9)^2 = 45^2 = 2025$$

in the decimal representation system, so that it appears in another integer sequence $A238237$ in OEIS [8], sequence of numbers which, when split in two parts of equal length, then added and squared, give the same number,

$$2025 = (20+25)^2. \tag{1}$$

In the last Section 4 we discuss the distribution of integer sequences from the upper part of Table 1 within the natural numbers and show that year 2025 is unique in the following way:

Theorem 1. *Consecutive integers* 2024 *and* 2025 *are the only pair of consecutive integers such that a tetrahedral number is predecessor of an odd square number and they appear with the same index* $n = 22$ *in their respective integer sequences.*

Graphics were made using Geogebra, Rhinoceros 3d with Grasshopper, SAGE [7, 9].

The author would like to thank the referee for many useful suggestions on how to improve the paper.

2 Visualizations of properties of number 2025

2.1 Divisors of 2025

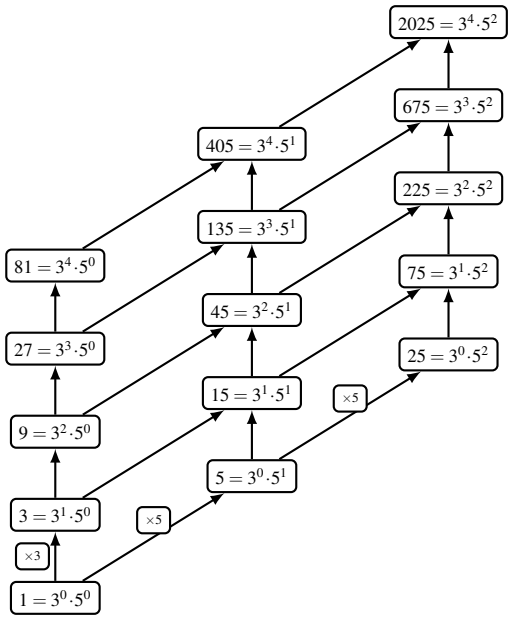

Figure 1: *Hasse diagram of divisors of number 2025.*

Number 2025 has 15 divisors, two of which, 3 and 5, are prime. In Figure 1, we can see the Hasse diagram of divisors of 2025. In Table 2 we see prime factorization and values of Euler function $\varphi(n)$ [3], which represents the number of numbers less than n that are relatively prime to n for $n = 2000, \ldots, 2027$.

Number 2025 is smooth, it has a small set of prime divisors, each of which is itself small. Regular or 5-smooth numbers are numbers with greatest prime divisor less then or equal to 5, so their prime factorization is

$$2^i \cdot 3^j \cdot 5^k, \quad i,j,k \geq 0.$$

As we can see from Table 2, 2025 is the first regular number after 2000 and the next one is $2048 = 2^{11}$, a power of 2. Regular numbers are more frequent within the natural numbers then all other integer sequences from Table 1 which have sparse, polynomial distribution, see (14). Distribution of regular numbers is of order $(\log n)^3$.

2.2 Triangular and tetrahedral numbers

Square root of 2025 is number 45, sum of digits of the decimal system. This number is a triangular number, figure number and first in the class of polygonal numbers counting points in triangular lattices. Triangular numbers also count combinations, T_n is the number of unordered pairs, subsets with two elements, of the set with $n+1$ elements,

$$T_n = \binom{n+1}{2} = \frac{n(n+1)}{2} = 1+2+\cdots+n \tag{2}$$

and can be visualized by counting integer points in a triangular lattice, Fig. 2.

		$k=2$ Triangular	$k=3$ Tetrahedral		
1					
1	1				
1	2	1			
1	3	3	1		
1	4	6	4	1	
1	5	10	10	5	1
1	6	15	20	15	6
1	7	21	35	35	21
1	8	28	56	70	56
1	9	36	84	126	126
1	10	45	120	210	252
1	11	55	165	330	462
		⋮	⋮		
1	24	276	2024	10626	...

Table 3: *Pascal triangle* $P(n,k) = \binom{n}{k}$, $n,k \geq 0$.

They appear in the Pascal triangle, Table 3, as the third diagonal and tetrahedral numbers as the fourth.

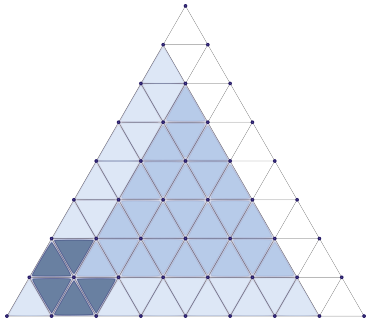

Figure 2: *Triangular lattice with* $T_9 = 45$ *vertices.*

From the triangular lattice in Fig. 2 we can see the recursion of the number of points in the grid, $T_n - T_{n-1} = n$, with the rule of succession is adding a new line with n points as we can see from light blue triangle corresponding to T_8 in Fig. 2. We can also observe hexagons in triangular lattices. The number of hexagons is equal to the number of interior points of the lattice since they are center points of hexagons, so the number of hexagons is the difference of the number of all points and boundary points, $T_n - 3(n-1) = T_{n-3}$.
Sums of first n triangular numbers are tetrahedral numbers (*A*000292 in OEIS), and as the name suggests count points in triangular pyramids, Fig. 3.

$$Te_n = \sum_{k=1}^{n} T_k = \sum_{k=1}^{n} \left(\sum_{i=1}^{k} i \right) = \binom{n+2}{3} = \frac{n(n+1)(n+2)}{6}. \tag{3}$$

Recursion for tetrahedral numbers is $Te_{n+1} = Te_n + T_n$ which can be seen by adding a new horizontal layer to a pyramidal lattice, Fig. 3.

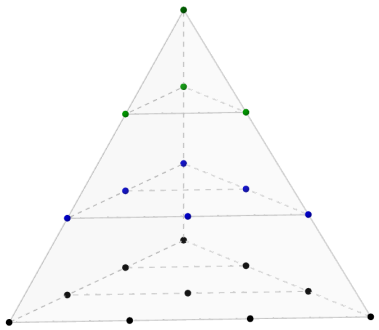

Figure 3: *Tetrahedron with* $Te_4 = 20$ *points.*

2.3 Square numbers

A perfect square is a number of form n^2, $n \in \mathbb{N}$. For square numbers we have the recursive formula

$$(n+1)^2 = n^2 + 2n + 1, \tag{4}$$

which can be seen visually when counting points in $n \times n$ square lattice. We can divide $n \times n$ points of the lattice into $(n-1) \times (n-1)$ square and $2n+1$ points that will make the last row and column, Fig. 4. We see that square numbers are polygonal numbers, used to count points within a polygonal area. We can also interpret them through metrics, so that n^2 is area of a square with side length n.
From the recursive formula (4) we see that we can represent n^2 as sum of the first n odd numbers

$$n^2 = \sum_{k=1}^{n} (2n-1). \tag{5}$$

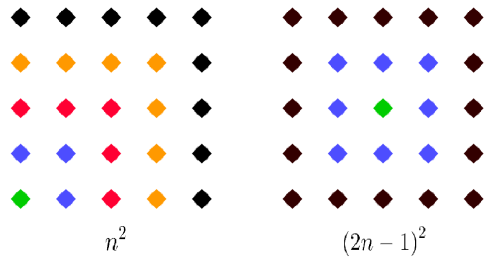

Figure 4: *Recursive generation of square and odd square numbers as Pythagorean gnomons.*

On the other hand, we can divide integer points in a square area into two triangular areas, and the number of integer points satisfy $T_n + T_{n-1} = n^2$. In Fig. 5 we see $2025 = T_{45} + T_{44} = 1035 + 990$ points divided in two triangular parts of the square with side length 45.

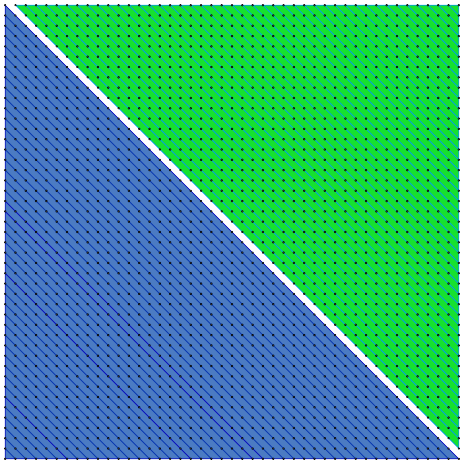

Figure 5: *2025 points in a square grid divided into two triangular areas.*

There is another interesting appearance of triangular numbers. If we look at $n \times n$ square grid, then T_n is number of rectangles found in it. A rectangle is defined by two horizontal and two vertical lines, so number of rectangles is equal to square of number of pairs chosen from set of $n+1$ lines found in the square grid by the product rule.

2.4 Square of triangular number is sum of cubes

Number properties, especially of harmonic whole numbers or 3-smooth numbers were studied from ancient times and the following formula for the sum of first n cubes was a result from the Pythagorean school. Nichomachus' Theorem states

$$1^3 + 2^3 + \cdots + n^3 = (1 + 2 + \cdots + n)^2 \tag{6}$$

and today this is special case of Faulhaber's formula, [6] saying that sum of p-th powers of first n numbers is a rational polynomial in n of degree $p+1$. Coefficients of this polynomial were first found by Jakob Bernoulli while studing these *Sumas potestaum* and they are now called Bernoulli numbers B_n,

$$\sum_{k=1}^{n} k^p = \frac{1}{p+1} \sum_{i=0}^{n} \binom{p+1}{i} B_i n^{p+1-i} \tag{7}$$

For $p = 1$ the sums are triangular numbers, for sum of squares $p = 2$ we have square pyramidal numbers and for $p = 3$, (6) squares of triangular numbers.
One interesting formula for Bernoulli numbers is as follows, [2]

$$B_n = \frac{2n!}{(2\pi)^n} \left(\frac{1}{1^n} + \frac{1}{2^n} + \frac{1}{3^n} + \ldots \right). \tag{8}$$

When we want to visualize eq. (6), we can look at cubes as volumes of solid bodies or as number of points inside cubes. We can do the same for planar formulas we have seen earlier, so n^2 is area of a square of side with length n, or number of integer points in a $(n-1) \times (n-1)$ grid, since division of a side of length n will yield $n+1$ point. We can see in Fig. 5 how union of two triangles in a square will not give the same area. Relationship of the area A of polygonal domain with integer coordinates of vertices and the number of integer points in the interior I and number of points that lie on the boundary B is given by Pick's theorem [1]

$$A = I + \frac{B}{2} - 1. \tag{9}$$

For counting points in polyhedrons there is no simple formula that connects discrete and continuous volume. This is a wast subject of enumerative geometry known as Erhart theory,[1]. In our case we can see this issue. For the cube, volume a cube with one vertex at origin point of side length n will give n^3 and number of integer points is $(n+1)^3$. But if we instead look at the trirectangular tetrahedron inside a cube, that contains one cube corner, then volume is $n^3/6$. Using eq. (6), we have that volume of union of 9 cubes with side lengths from 1 to 9 is 2025, Fig. 6, and the volume od their tetrahedrons is $2025/6 \approx 337.5$. If we look at

integer points in the cubes, there will be 3025 points and in tetrahedrons we have Te_n points so we have total of

$$1+4+10+20+35+56+84+120+165=495$$

points. Ratios of discrete and continuous volumes is $(1+\frac{1}{n})^3$ for cubes and $(1+\frac{6}{n}+\frac{11}{n^2}+\frac{6}{n^3})^3$ for tetrahedrons, so we see that in tetrahedral lattices integer points are denser then in the cubic ones.

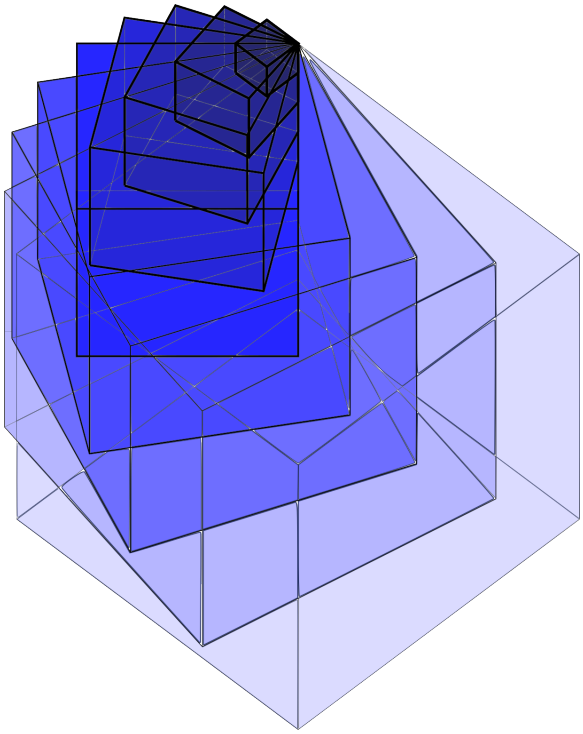

Figure 6: *Nine cubes with sum of volumes equal to 2025.*

2.5 Odd squares

Odd square numbers can be written in the form $(2n+1)^2$ for $n \geq 0$. Then 2025 is an odd square for $n = 22$. These numbers are also called centered octagonal numbers because they count points lying on sides of octagons together with the central point, Fig. 7.

$$(2n+1)^2 = 4n^2+4n+1 = 4n(n+1)+1 = 8\frac{n(n+1)}{2}+1 \tag{10}$$

Here we have the recursion $(2n+1)^2 = (2n-1)^2+8n$ so adding $8n$ new points gives the next odd square, Fig. 4.
For number 2025 we have:

$$2025 = 8\cdot 253+1 = 8(22\cdot 23)+1 = \sum_{k=1}^{22} 8k+1. \tag{11}$$

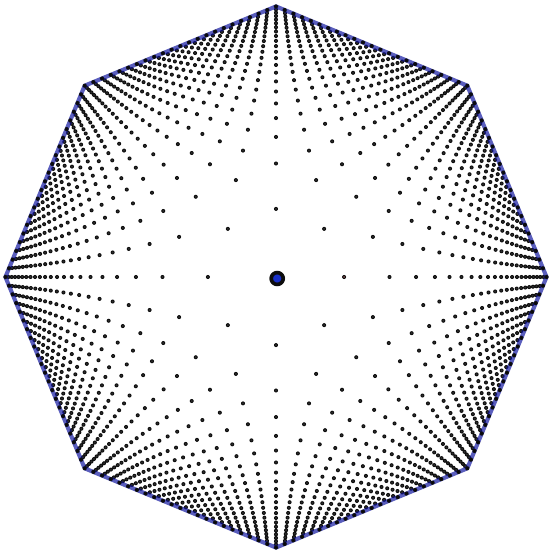

Figure 7: *2025 points in centered octagonal arrangement.*

In Fig. 7 we can see the 2025 points from eq. (11). The points are lying on 22 octagons, where k-th octagon has a side divided into k parts, which together with the central point gives 2025 points. Counting using symmetry, it suffices to count the points strictly inside an angle of $\left[0, \frac{2\pi}{8} = \frac{\pi}{4}\right\rangle$, which would be $1+2+\cdots+22$.
When we remove the central point, the number of remaining points gives a tetrahedral number $2024 = 8\cdot 11\cdot 23$.
Here the symmetry group is the dihedral group D_4 of order 8, since the area inside the angle of $\left[0, \frac{\pi}{4}\right\rangle$ can be rotated four times for the angle $\frac{\pi}{4}$ and then mirrored by the horizontal axes, which is the same symmetry of the Hasse diagram in Fig. 1, having 8 parallelograms or the symmetry of coordinate system in space, where one octant generates the space with four rotations and one reflection.

3 Interesting number digits properties of 2025

Number 45 is the sum of all numbers written with one digit,

$$45 = 0+1+2+3+4+5+6+7+8+9.$$

In general, the sum of all numbers with the number of digits less or equal to n ($A037182$ in OEIS) is

$$a(n) = \frac{10^n\cdot(10^n-1)}{2}. \tag{12}$$

The sum of all number with at most two digits is the sum of all number less then 100 which is $4095 = 99\cdot 100/2$.
Then 2025 is the smallest square of such a number ($A350869$ in OEIS), which has interesting consequences in linking operations on numbers (addition, multiplication) and concatenation of digits to represent numbers.

Namely, 2025 is a *torn* number, (A238237 in OEIS), when we split it in two equal parts, add them and then square we arrive at 2025 again,

$$2025 = 45^2 = (20+25)^2. \tag{13}$$

Another example of a torn number is $3025 = 55^2$, the next square of the triangular number $T_{10} = 55$. These numbers are also called Kaprekar numbers [5]. We have $2025 = 20\cdot 10+2\cdot 10+5 = 2\cdot 10^2+2\cdot 10+5$.
There is another digit property, increase digit square preserving property. Namely $2025 = 45^2$ and increasing each digit by 1 gives $3036 = 56^2$. If we denote the decimal representation of a number $\overline{abcd} = a\cdot 10^3+b\cdot 10^2+c\cdot 10+d$, then $\overline{ab}-\overline{cd} = 5$ for 2025 and 3136. We have

$$n^2 = 100ab+cd = 100ab+ab+5 = 101ab+5$$

so the prime number $101 = 45+56$ gives remainder 5 when dividing n^2.

4 *Square* and other special years

Since we are now in the year 2025, we can ask how frequent square years are, and the answer is given by the distribution of square numbers in natural numbers. Since the difference of two consecutive squares is $2n+1$, it is clear that the gaps increase. Last square year was $44^2 = 1936$, so $2025 = 1936+2\cdot 44+1$ comes 89 years later and for the next one we will wait 91 years. Square years are currently in a *once in a lifetime* frequency and it is decaying. In Table 2 we have prime factorization for year numbers since the last regular year 2000.
We list some sequence elements neighboring 2025 for integer sequences from Table 1:

- perfect squares

  $\ldots 1849, 1936, n = 45 : 2025, 2116, 2290\ldots$

- odd squares (centered octagonal numbers)

  $\ldots 1681, 1849, n = 22 : 2025, 2209, 2401\ldots$

- squares of triangular numbers

  $\ldots 784, 1296, n = 9 : 2025, 3025, 4356\ldots$

- regular numbers

  $\ldots 1944, 2000, n = 109 : 2025, 2048, 2160\ldots$

- *tetrahedral numbers*

  $\ldots 1330, 1540, 1771, n = 22 : \mathit{2024}, 2300, 2600, 2925\ldots$

- *centered square numbers* $4n^2+4n+2$

  $\ldots 1522, 1682, 1850, n = 22 : \mathit{2026}, 2210, 2402, 2602\ldots$

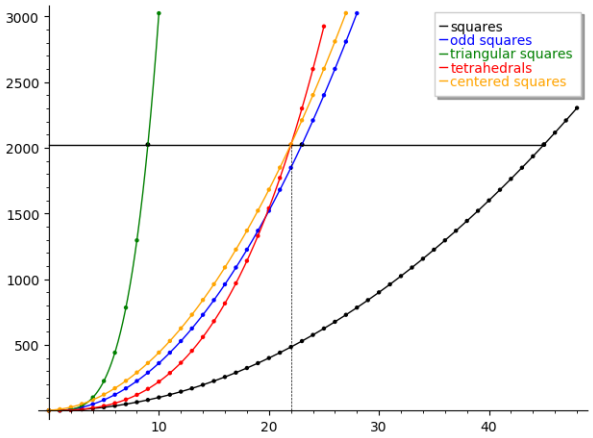

Figure 8: *Graphs of* x^2, $(2x+1)^2$, $\left(\frac{x(x+1)}{2}\right)^2$, $\frac{x(x+1)(x+2)}{6}$ *and* $(2x+1)^2+1$.

The odd squares are subset of squares so they are twice less frequent. The fastest growing sequence are squares of triangular numbers, their distribution is of order n^4.
Distribution of regular numbers within natural numbers differs from other sequences in Table 1; square numbers have polynomial growth while regular numbers are more dense and follow logarithmic growth. Some bounds regarding distribution of regular numbers can be found in [4], here is one explicit bound

$$\frac{1}{k!}\prod_{p\le y}\frac{\log x}{\log p} \ge \Psi(x,y) \ge \frac{1}{k!}\prod_{p\le y}\frac{\log X}{\log p} \tag{14}$$

for $x \ge y \ge 2$ and $x \ge 4$, where $\Psi(x,y)$ is number of integers less of equal to x that are y-smooth and $X = \prod_{p\le y} p$.
Next regular year will be 2048 but all other square or regular years will happen in the next century.
Another interesting question can be posed about consecutive regularity we see in $2024- > 2025- > 2026$, tetrahedral number as predecessor of square of triangular number and its successor 2026 is two times centered square number $C_{4,n} = (2n+1)^2+1$ for $n \ge 1$, (A069894 in OEIS). It is also worth mentioning the Pythagorean triple $(45, 1012, 1013)$ which is representation of 2025 as difference of squares, $2025 = 1013^2 - 1012^2$ and another one $(27, 36, 45)$ which represents 2025 as sum of squares. The perimeter of that triangle with legs 27 and 36 and hypotenuse 45 equals 108 and division into triangle sides will yield ratio of $3:4:5$, so this is a derived triple $9(3,4,5)$. This year we even had 'Pythagorean date' 16.9.'25 that relates to the first triple $(3,4,5)$.

Now we will prove that $(2024, 2025)$ is the only pair of consecutive numbers such that a tetrahedral number followed by an odd square number at the same index in respective sequences. The reason is that 2024 is the last tetrahedral number that is less then an odd square number in the same index.

Proof of Theorem 1 From Fig. 8 we can see that around $n = 22$, which is index of 2025 as odd square, 2024 as tetrahedral and 2026 as twice the centered square number is exactly where twice the centered square number become greater then tetrahedral number of the same index. Intersection of graphs for $\frac{x(x+1)(x+2)}{6}$ and $(2x+1)^2+1$ in Fig. 8 is

$$\alpha + \frac{169}{3\alpha} + 7 \approx 22.023$$

for $\alpha = \left(\frac{1}{9}\sqrt{219129}+426\right)^{\frac{1}{3}}$. For $n = 22$ we have $Te_{22} = 2024$ and $(2\cdot 22+1)^2 = 2025$, so

$$\frac{n(n+1)(n+2)}{6} = (2n+1)^2 - 1$$

has an integer solution. All greater tetrahedral numbers will be greater then odd squares, as we can see in Table 4, the difference of odd squares and tetrahedral numbers is $\frac{k(k+1)(22-k)}{6}$ and is zero for $k = 22$. □

From Table 4 we see two other consecutive pairs of tetrahedral numbers 9 and 2600, with odd square successors 10 and 2601 respectively, where the indices differ. There is another pair of consecutive numbers, tetrahedral $Te_5 = 35$ and even square $(T_3)^2 = 36$ which also have different indices in corresponding sequences.

We end with final remark that year 2025 is numerically a unique moment in history!

k	$(2k+1)^2$	Te_k	$-\frac{k(k+1)(k-22)}{6}$
0	1	0	1
1	**9**	1	8
2	25	4	21
3	49	**10**	39
4	81	20	61
⋮	⋮	⋮	⋮
21	1849	1771	78
22	**2025**	**2024**	1
23	2209	2300	-91
24	2401	**2600**	-199
25	**2601**	2925	-324
26	2809	3276	-467

Table 4: *Odd squares, tetrahedral numbers and their difference.*

Acknowledgments. This work is supported by the Croatian Science Foundation under the project number HRZZ-IP-2022-104615.

References

[1] BECK, M., ROBINS, S., *Computing the Continuous Discretely*. Springer, 2007, https://doi.org/10.1007/978-1-4939-2969-6

[2] *Collected Papers of Srinivasa Ramanujan*. Edited by G. H. Hardy, P. V. Seshu Aigar, and B. M. Wilson, Cambridge Univ. Press, 1927.

[3] DUJELLA, A., *Number Theory*, Školska knjiga, Zagreb, 2021.

[4] GRANVILLE, A., Smooth numbers: Computational Number Theory and Beyond. In: Buhler JP, Stevenhagen P, eds. *Algorithmic Number Theory: Lattices, Number Fields, Curves and Cryptography*, Mathematical Sciences Research Institute Publications. Cambridge University Press, 2008, 267–324, https://doi.org/10.1017/9781139049801.010

[5] *Kaprekar numbers in Wikipedia*, https://en.wikipedia.org/wiki/Kaprekar_number, accessed: 17.11.2025.

[6] KNUTH, D.E., Johann Faulhaber and sums of powers, *Math. Comp.* **61** (1993), 277–294.

[7] *McNeel, R. and others, Rhinoceros 3D, Version 7.0.* Robert McNeel amp; Associates, Seattle, WA., 2010, https://www.rhino3d.com/

[8] OEIS ("The Online Encyclopedia of Integer Sequences"), https://oeis.org/, accessed: 9.11.2025.

[9] *Sage Mathematics Software* (Version 8.8), The Sage Developers, 2019, http://www.sagemath.org.

[10] TEO, B.K., SLOANE, N.J.A. , *Magic Numbers in Polygonal and Polyhedral Clusters*, Inorg. Chem. **24** (1985), 4545–4558, https://doi.org/10.1021/ic00220a025

Iva Kodrnja
orcid.org/0000-0003-3976-4166
e-mail: iva.kodrnja@geof.unizg.hr

University of Zagreb Faculty of Geodesy
Kačićeva 26, 10 000 Zagreb, Croatia

https://doi.org/10.31896/k.29.7
Original scientific paper
Accepted 13 November 2025

BORIS ODEHNAL

Projective Parallelians and Related Porisms

Projective Parallelians and Related Porisms

ABSTRACT

We give a projective generalization of the construction of parallelians and the thus defined conics. To any properly chosen point P and line g in the plane of a triangle $\Delta = ABC$, we construct six points that always lie on a conic $\mathcal{P}$, the parallelian conic $\mathcal{P}$ of the pivot P with respect to Δ. Further, we find the parallelian tangent conic $\mathcal{T}$, the parallelian inconic I, and two further conics $\mathcal{D}$ and $\mathcal{J}$ that are related in a natural way with Δ and P. Any pair out of these conics gives rise to a certain porism and even a chain of porisms by means of polarization. We study the regularity and singularity as well as the relative position of these conics with respect to the line g depending on the choice of P and g. We also give a detailed study of the sets of possible pivot points changing the triangle or hexagon porisms of any pair of conics into such with one-parameter families of quadrangles and pentagons.

Key words: parallelian, parallelian conic, porism, triangle cubic, triangle center, algebraic transformation

MSC2020: 51M15, 51M04, 14E05

Projektivne paralelijane i s njima povezane porizme

SAŽETAK

Dajemo projektivno poopćenje konstrukcije paralelijana i tako definiranih konika. Za bilo koju dobro odabranu točku P i pravac g u ravnini trokuta $\Delta = ABC$ konstruiramo šest točaka koje uvijek leže na jednoj konici $\mathcal{P}$, paralelijanskoj konici $\mathcal{P}$ točke P s obzirom na trokut Δ. Nadalje, nalazimo paralelijansku tangentnu koniku $\mathcal{T}$, paralelijansku upisanu koniku I i dvije daljnje konike $\mathcal{D}$ i $\mathcal{J}$ koje su prirodno povezane s Δ i P. Bilo koji par ovih konika rezultira određenom porizmom, pa čak i lancem porizmi pomoću polarizacije. Proučavamo regularnost i singularnost kao i posebne položaje ovih konika prema pravcu g ovisno o izboru polazne točke P i pravca g. Također, dajemo detaljno istraživanje skupova mogućih polaznih točaka koje mijenjaju trokutaste ili šesterokutne porizme bilo kojeg para konika u porizme s jednoparametarskim familijama četverokuta i peterokuta.

Ključne riječi: paralelijana, paralelijanska konika, porizma, kubika trokuta, središte trokuta, algebarska transformacija

1 Introduction

In the present paper, we shall construct several chains of porisms that are attached to a triangle $\Delta = ABC$, a point P, and a line g in a natural way. The initial steps of the construction can be done in a purely synthetic way and the same holds true for the proofs of the existence of the conics involved. The construction (synthetic or algebraic) are exclusively done in the framework of projective geometry. At a later stage, we have to deploy the analytical approach. This allows us to deduce some algebraic properties of the porisms and some conditions on the choice of the pivot point P.

1.1 Prior and related work

In recent years, porisms were studied mainly within the framework of Euclidean geometry, focusing on invariants [14, 15, 25], traces [6, 9, 11, 16, 21, 23], closure conditions [7, 8], and relations to billards and Poncelet grids [10, 26, 27, 28, 29]. Nevertheless, results concerning the projective nature of porisms are also given in [24, 29]. An excellent overview on the history and various approaches towards the classical forms of porisms can be found in [3, 5].

Occasionally, the article [1] disclosed the relations between Euclidean parallelian conics and the related proisms. As we shall see, all the results from [1] allow an explanation from the superordinate standpoint of projective geometry as is

the case with some results from the Euclidean geometry of the triangle (cf. [20]).

1.2 Contributions of the present paper

In Section 2, we show the existence of the projectivized parallelian conic $\mathcal{P}$ and the parallelian inconic I. This can be done in a purely synthetic way. Further, the first porisms are described and extended to the chains of porisms that are obtained by means of polarization or by tracing the (discrete) exponential pencil of conics spanned by I and $\mathcal{P}$.

Section 3 is to show that the parallelian conic $\mathcal{P}$ is enclosed by two triangles Δ_U and Δ_V whose six vertices lie on a conic $\mathcal{D}$. This gives rise to a triangle porism between $\mathcal{P}$ and $\mathcal{D}$, and consequently, this gives rise to a chain of triangle porisms. Moreover, the six vertices of Δ_U and Δ_V form a hexagon with an inconic $\mathcal{J}$ (provided a certain ordering of points). Thus, we also find a further hexagon porism independent of the hexagon porisms discovered so far.

Section 4 mentions the relations to already existing and Euclidean cases.

Finally, in Section 5, we discuss all possible pairings of projectivized parallelian conics and the thus defined porisms (and chains of porisms). In particular, we derive conditions on the pivot point P such that certain types of porisms can be found in between the chosen pairs of conics. We shall not discuss whether these porisms do really exist between regular conics or not.

2 Projective parallelians

2.1 The first porism

In the projective plane, we choose a triangle $\Delta = ABC$ and called it henceforth the *base triangle*. The union of the three side lines $[A,B]$, $[B,C]$, $[C,A]$ shall be denoted by $\Delta^\star$. Further a point P which is not incident with any line of $\Delta^\star$ is chosen and called the *pivot point*. Then, we assume that $g \notin \Delta^\star$ is a line neither incident with a vertex of Δ nor passing through P.

We shall label the three intersection points of $\Delta^\star$'s lines with g with $C^\star := g \cap [A,B]$ (cyclic). Now, we call the lines $[P,A^\star]$, $[P,B^\star]$, and $[P,C^\star]$ the *g-parallels* of $[B,C]$, $[C,A]$, and $[A,B]$ through P. The projections of P from the points $A^\star$, $B^\star$, $C^\star$ onto the non-incident sides of Δ are defined as

$$\begin{aligned} P_1 &:= [P,C^\star] \cap [B,C], P_2 := [P,C^\star] \cap [C,A], \\ P_3 &:= [P,A^\star] \cap [C,A], P_4 := [P,A^\star] \cap [A,B], \\ P_5 &:= [P,B^\star] \cap [A,B], P_6 := [P,B^\star] \cap [B,C]. \end{aligned} \tag{1}$$

The points $P_1,\ldots,P_6$ are the projectivized versions of the elementary geometric parallelians (cf. [18]), and therefore, we call them the *g-parallelians* of P with respect to Δ.

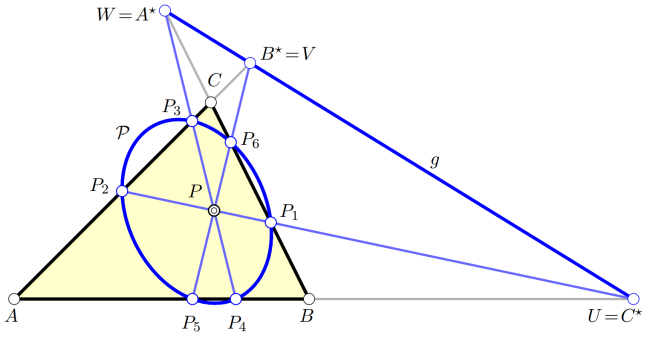

Figure 1: *The conic $\mathcal{P}$ on the six g-parallelians.*

With these preparations, it is rather elementary to show the following:

Theorem 1 *The g-parallelians $P_1,\ldots,P_6$ are located on a single conic $\mathcal{P}$, the* parallelian conic *of P.*

Proof. According to PASCAL's theorem (cf. [12, p. 220]), six points $P_1,\ldots,P_6$ lie on a single conic if, and only if, the three point $U := [P_1,P_2] \cap [P_4,P_5]$, $V := [P_2,P_3] \cap [P_5,P_6]$, $W := [P_3,P_4] \cap [P_6,P_1]$ are collinear. By construction, $U = C^\star$, $V = B^\star$, and $W = A^\star$, which are collinear (located on g). □

Fig. 1 illustrates the contents of Thm. 1.

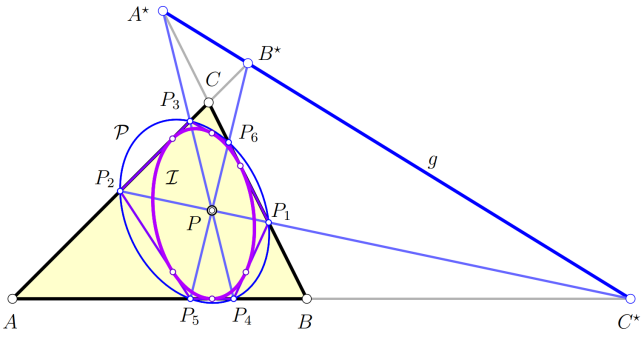

Figure 2: *The inconic I that comes along with $\mathcal{P}$.*

Further, we can confirm the existence of an inscribed conic:

Theorem 2 *The hexagon $H_1 := P_2P_3P_6P_1P_4P_5$ is tangent to a single conic I, the* parallelian inconic *of P.*

Proof. We define $l_1 := [P_2,P_3]$, $l_2 := [P_3,P_6]$, $l_3 := [P_6,P_1]$, $l_4 := [P_1,P_4]$, $l_5 := [P_4,P_5]$, and $l_6 := [P_5,P_2]$, apply BRIANCHON's theorem (see [12, p. 222]), and find $[l_1,l_2] \cap [l_4,l_5] = [A^\star,P]$, $[l_2,l_3] \cap [l_5,l_6] = [C^\star,P]$, $[l_3,l_4] \cap [l_6,l_1] = [B^\star,P]$. The latter three lines are incident with P, *i.e.*, P equals the Brianchon point of the six lines $l_1,\ldots,l_6$. Therefore, $l_1,\ldots,l_6$ are tangents of a single conic. □

The results of Thms. 1 and 2 give rise to a porism:

Theorem 3 *The pair $(\mathcal{P}, I)$ allows for a poristic family of hexagons with vertices on $\mathcal{P}$ and edges tangent to I.*

Proof. The existence of a single hexagon interscribed between $\mathcal{P}$ and I is necessary and sufficient in order to guarantee the existence of a one-parameter family of interscribed hexagons (cf. [3, 5]). □

2.2 The first chain of porisms

For what follows, we shall describe points and lines by homogeneous coordinates. It appears useful to assume that the vertices of Δ are the base points of the projective frame. Hence, $A = 1:0:0$, $B = 0:1:0$, $C = 0:0:1$. The pivot point shall be given by $P = \xi:\eta:\zeta \neq 0:0:0$ (and, since P is not contained in any line of $\Delta^\star$, we have $\xi\eta\zeta \neq 0$). The line g can be represented by its homogeneous equation as $lx+my+nz=0$, or equivalently, by its homogeneous coordinates $l:m:n \neq 0:0:0$ which also satisfy $lmn \neq 0$, since g shall not be incident with any vertex of Δ. Further, we have $l\xi+m\eta+n\zeta \neq 0$, for $P \notin g$.

It is a matter of elementary linear algebra to determine the equations (up to non-zero multiples) of $\mathcal{P}$ and I (cf. [12, p. 254]). So, we find

$$\begin{aligned}&\mathcal{P}:\\ &\sum_{\text{cyclic}} l\eta\zeta(m\eta+n\zeta)x^2-\xi(2\eta\zeta mn+\zeta\xi nl+\xi\eta lm+l^2\xi^2)yz=0,\\ &I:\\ &\sum_{\text{cyclic}} l^2(m\eta+n\zeta)^2x^2-2mn(l\xi+m\eta)(l\xi+n\zeta)yz=0.\end{aligned} \tag{2}$$

Here, in the following, $\sum_{\text{cyclic}} f(l,m,n,\xi,\eta,\zeta,x,y,z)$ means the *cyclic sum* of $f(\ldots)$, *i.e.*,

$$\begin{aligned}\sum_{\text{cyclic}} f(l,m,n,\xi,\eta,\zeta,x,y,z) &:= f(l,m,n,\xi,\eta,\zeta,x,y,z)\\ &+f(m,n,l,\eta,\zeta,\xi,y,z,x)+f(n,l,m,\zeta,\xi,\eta,z,x,y).\end{aligned}$$

The variables in the argument (function) are shifted twice cyclically and the three functions are summed up.

The conics I and $\mathcal{P}$ span a pencil of the third kind. The common pole equals the pivot point P, the common polar line p has the homogeneous coordinates

$$\eta\zeta(m\eta+n\zeta):\zeta\xi(n\zeta+l\xi):\xi\eta(l\xi+m\eta). \tag{3}$$

It is easily verified that the three harmonic conjugates of P with respect to the pairs (P_1,P_2), (P_3,P_4), and (P_5,P_6) are collinear and line up on p. This fact yields a linear construction of p as shown in Fig. 3.

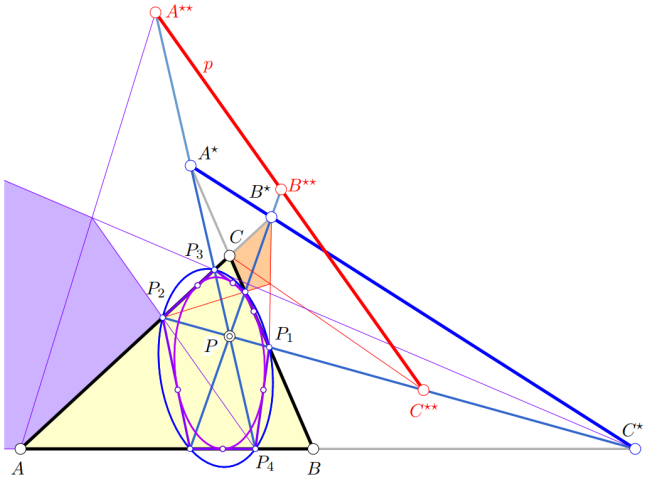

Figure 3: *Linear construction of the common polar p of $\mathcal{P}$ and I: $C^{\star\star}$ is the harmonic conjugate of P with respect to the pair (P_1,P_2) and, in like manner, $A^{\star\star}$ is the harmonic conjugate of P with respect to (P_3,P_4).*

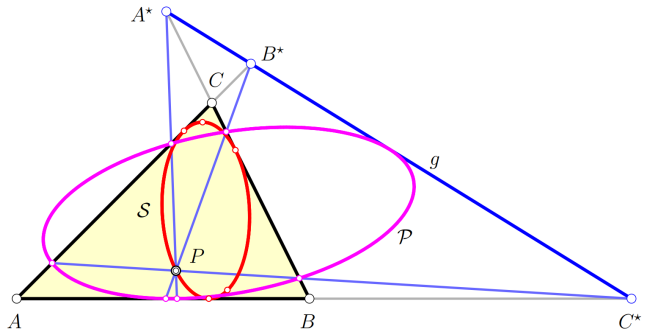

Figure 4: *The conic $\mathcal{P}$ touches g if P is chosen on the inconic $\mathcal{S}$.*

Fig. 4 demonstrates that a properly chosen pivot point P leads to a parallelian conic $\mathcal{P}$ that touches g. The equations (2) of the parallelian conic and the parallelian inconic allow us to state:

Theorem 4
1. The g-parallelian conic $\mathcal{P}$ touches the line g if, and only if, the pivot point P is chosen on the g-Steiner inconic $\mathcal{S}$ of Δ with the equation

$$\mathcal{S}: \sum_{\text{cyclic}} l^2x^2-2mnyz=0. \tag{4}$$

$\mathcal{P}$ is singular if P is chosen on the g-Steiner circumconic

$$\mathcal{S}': \sum_{\text{cyclic}} lmxy=0 \tag{5}$$

and the 'centers' of the singular conics fulfill the g-Steiner Deltoid

$$Q: \sum_{\text{cyclic}} l^2m^2x^2y^2 - 2l^2mnx^2yz = 0. \tag{6}$$

2. The g-parallelian inconic I cannot touch g for any suitable choice of P, i.e., *P may not lie on the sides of the g-anticomplementary triangle $\Delta_a^\star = \{[A,A^\star],[B,B^\star],[C,C^\star]\}$.*

Proof. 1. We compute the resultant of $\mathcal{P}$'s equation (2) and g's equation with respect to any of the variables x, y, or z. The determinant of the coefficient matrix of the remaining quadratic form is the product of the fourth power of g's equation and the quadratic form

$$\sum_{\text{cyclic}} l^2\xi^2 - 2mn\eta\zeta$$

which (set equal to zero) yields the equation of $\mathcal{S}$ after replacing ξ, η, ζ by x, y, z.

The regularity of $\mathcal{P}$ is equivalent to the regularity of its coefficient matrix $\mathbf{P}$. Hence, $\mathcal{P}$ is regular if the homogeneous coordinates $\xi:\eta:\zeta$ of P do not satisfy

$$\underbrace{\xi\eta\zeta}_{=\Delta^\star}\cdot\underbrace{(lm\xi\eta+mn\eta\zeta+nl\zeta\xi)}_{=\mathcal{S}'}\cdot\underbrace{(l\xi+m\eta+n\zeta)^4}_{=g}=0.$$

Since admissible positions of P are off $\Delta^\star$ and off g, P may only be chosen on $\mathcal{S}'$. With the parametrization of $\mathcal{S}' = n(\alpha l+\beta m)\alpha : n(\alpha l+\beta m)\beta : -lm\alpha\beta$ $(\alpha:\beta\neq 0:0)$ inserted of $\xi:\eta:\zeta$ into the first equation of (2), we are able to factor $\mathcal{P}$'s equation and find

$$\begin{aligned}&\mathcal{P}_{\text{singular}}:\\ &\left(\beta^2m^2(\alpha l+\beta m)x-\alpha^2\beta lm^2y-\alpha n(\alpha l+\beta m)^2z\right)\cdot\\ &\left(\alpha\beta^2l^2mx-\alpha^2l^2(\alpha l+\beta m)y+\beta n(\alpha l+\beta m)^2z\right)=0.\end{aligned}$$

The latter equation describes a pair of lines (as long as $l:m:n\neq 0:0:0$) that always intersect in

$$\alpha^2ln(\alpha l+\beta m)^2 : \beta^2mn(\alpha l+\beta m)^2 : \alpha^2\beta^2l^2m^2$$

which parametrizes the quartic $\mathcal{S}'$ given by (6).

2. In the same way, we proceed with I and find

$$\underbrace{(n\zeta+l\xi)(n\zeta+m\eta)(m\eta+l\xi)}_{=\Delta_a^\star}\underbrace{(l\xi+m\eta+n\zeta)}_{=g}=0$$

relating the coordinates of the pivot point P such that it yields a parallelian inconic I touching g. If we replace ξ, η, ζ with x, y, z, the first three factors are the equations of the sides of Δ's g-anticomplementary triangle $\Delta_a^\star$ and the fourth factor yields the equation of the line g. □

If g is the ideal line of the projectively closed Euclidean plane, the inconic $\mathcal{S}$ (4) described in Thm. 4 becomes the Steiner inellipse and the corresponding parallelian conics are then parabolas, cf. [1]. Therefore, $\mathcal{S}$ can be considered the g-Steiner inconic.

Here, we shall also remark that the g-Steiner deltoid Q is the image of g-Yff inconic $\sum_{\text{cyclic}} x^2-2yz=0$ under the g-isogonal transformation $x\to mnyz$, $y\to nlzx$, $z\to lmxy$. Fig. 5 shows the g-Steiner circumconic $\mathcal{S}'$ and its g-isogonal image Q.

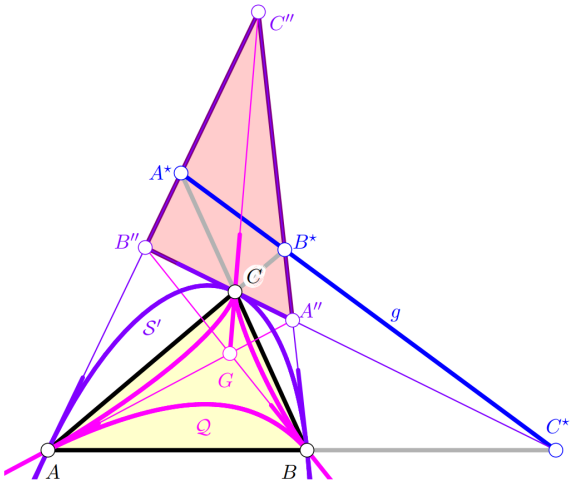

Figure 5: *The g-anticomplementary triangle $\Delta_a = A''B''C''$, the g-Steiner circumconic $\mathcal{S}'$, and its g-isogonal image Q (the g-Steiner deltoid).*

The intersections of subsequent tangents t_i to $\mathcal{P}$ at points P_i define (among others) the six points

$$\begin{aligned}&T_{23}:=t_2\cap t_3,\quad T_{36}:=t_3\cap t_6,\quad T_{61}:=t_6\cap t_1,\\ &T_{14}:=t_1\cap t_4,\quad T_{45}:=t_4\cap t_5,\quad T_{56}:=t_5\cap t_6,\end{aligned} \tag{7}$$

which lie on a single conic $\mathcal{T}$ with the equation

$$\begin{aligned}\mathcal{T}:\sum_{\text{cyclic}} lmn(m\eta+n\zeta)(3l\xi+m\eta+n\zeta)\eta^2\zeta^2x^2 =\\ \sum_{\text{cyclic}} l\xi^2\left((2mn\eta\zeta)^2+\left(\sum_{\text{cyclic}} lm\xi\eta((l\xi+m\eta)^2+6mn\eta\zeta)\right)\right)yz.\end{aligned} \tag{8}$$

We call $\mathcal{T}$ the *g-parallelian tangent conic* of P. It is obvious that $\mathcal{T}$ is the polar image of $I^\star$ (*i.e.*, the dual of the conic I or the set of tangents of I).

2.3 An elliptic sextic

In a way similar to the proof of Thm. 4, we can show that $\mathcal{T}$ is tangent to g if the pivot point P is chosen on the sextic

$$\mathcal{S}_\mathcal{T}: \sum_{\text{cyclic}} l^2m^2x^2y^2(lx-my)^2 + 2l^3mnx^3yz(lx-my-nz) = 6l^2m^2n^2x^2y^2z^2. \quad (9)$$

An example of such a sextic $\mathcal{S}_\mathcal{T}$ is displayed in Fig. 6. The sextic is shown together with a certain pivot point P, the corresponding parallelian conic $\mathcal{P}$, and the parallelian tangent conic $\mathcal{T}$ which touches g since the pivot P is chosen on the sextic $\mathcal{S}_\mathcal{T}$ in Fig. 7.

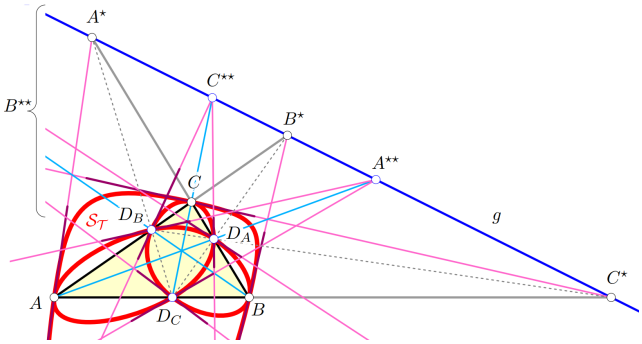

Figure 6: *The sextic $\mathcal{S}_\mathcal{T}$ as the locus of pivot points P whose g-parallelian tangent conic $\mathcal{T}$ touches g.*

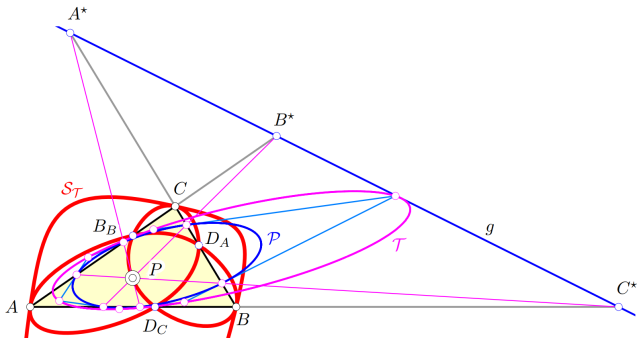

Figure 7: *The g-parallelian tangent conic $\mathcal{T}$ touches g, since it corresponds to a pivot point $P \in \mathcal{S}_\mathcal{T}$.*

The curve $\mathcal{S}_\mathcal{T}$ has three ordinary double points at the vertices of Δ. Further, it carries three tacnodes at the vertices D_A, D_B, D_C of the Cevian triangle of the triangle pole of g with respect to Δ. At any of these tacnodes, two linear branches emerge. For one of them, the node is a flat point (*i.e.*, it has a local expansion of the form $(t, t^4 + O(t^5))$, cf. [2, 4], only for the flat point branch). The lines $[A, A^\star]$ (cyclic) are the tangents at the flat points A (cyclic). $\mathcal{S}_\mathcal{T}$'s tangents to the linear branches at the ordinary double points $D_C \in [A, B]$ (cyclic) pass through the points $A^{\star\star} := [A, D_A] \cap g$ and $B^{\star\star} := [B, D_B] \cap g$ (cyclic). Moreover, any pair of ordinary double points on $\mathcal{S}_\mathcal{T}$ is collinear with a *star point*, *i.e.*, D_A, D_B, $C^\star$ (cyclic) are collinear (see Fig. 6).

2.4 The iteration of the porism

If $\mathbf{I}$, $\mathbf{P}$, and $\mathbf{T}$ denote the coefficient matrices of the conics I, $\mathcal{P}$, and $\mathcal{T}$, we first note that they are regular, provided the proper choice of the pivot point P, *i.e.*, P not on any side of Δ or $\Delta_a^\star$ and also not on the g-Steiner circumconic $\mathcal{S}'$. Further, we can verify the following matrix identity

$$\mathbf{P}\mathbf{I}^{-1}\mathbf{P} = \lambda\mathbf{T}$$

with

$$\lambda = -\frac{\sum_{\text{cyclic}} l\xi}{4lmn \prod_{\text{cyclic}} l\xi + m\eta}$$

which depends on P and g solely. (The cyclic product is explained in nearly the same way as the cyclic sum.) This expresses what is clear from the construction: The conic $\mathcal{T}$ is the polar image of I with respect to $\mathcal{P}$. Moreover, from I and $\mathcal{P}$, we can construct the "next" circumscribed conic, say $\mathcal{U}$, by repeating the polarization, or in more simple terms, by once again intersecting neighboring tangents of $\mathcal{T}$ in order to obtain a further sextuple of conconic points. Hence, we can state:

Theorem 5 *The parallelian inconic I and the parallelian conic $\mathcal{P}$ span an exponential pencil of conics in which any pair of subsequent conics allows for a poristic family of hexagons.*

Proof. We have already found that $\lambda\mathbf{T} = \mathbf{P}\mathbf{I}^{-1}\mathbf{P}$ holds (with some λ depending on P and g). According to [13], the coefficient matrices $\mathbf{M}$ of the conics in the exponential pencil spanned by I and $\mathcal{P}$ are obtained from $\mathbf{I}$ and $\mathbf{P}$ as

$$\mathbf{M}(k) = \mathbf{P}(\mathbf{I}^{-1}\mathbf{P})^{k-1}, \quad k \in \mathbb{Z}.$$

For any integer k, $\mathbf{M}(k)$ and $\mathbf{M}(k+1)$ are the coefficient matrices of two conics that allow for the same kind of porism as I and $\mathcal{P}$ or $\mathcal{P}$ and $\mathcal{T}$ do:

We use the Cayley criterion [12, p. 432, Thm. 9.5.4] in order to show that the type of porism is preserved when tracing the discrete exponential pencil. If the coefficients of the power series $\sqrt{\det(\mathbf{P}\cdot t + \mathbf{I})} = a_0 + a_1 t + a_2 t^2 + a_3 t^3 + \ldots$ fulfill $a_2 = 0$, I and $\mathcal{P}$ define a poristic triangle family; $a_3 = 0$ guarantees for a poristic family of interscribed quadrangles. If $\det\begin{pmatrix} a_2 & a_3 \\ a_3 & a_4 \end{pmatrix} = 0$ or $\det\begin{pmatrix} a_3 & a_4 \\ a_4 & a_5 \end{pmatrix} = 0$, then

the conics I and $\mathcal{P}$ allow for poristic families of pentagons or hexagons. In any case, I serves as the inconic (touched by the sides of the polygons) and $\mathcal{P}$ is the circumconic (carrying the vertices of the polygons).

Now, we show that these conditions are valid for any pair of subsequent conics in the exponential pencil spanned by I and $\mathcal{P}$. For that purpose, we write down the discriminant of the Cayley function for $\mathbf{M}(k+1)$ and $\mathbf{M}(k)$ and find

$$\begin{aligned}&\det(\mathbf{M}(k+1)\cdot t+\mathbf{M}(k))=\\&\det(\mathbf{P}(\mathbf{I}^{-1}\mathbf{P})^k\cdot t+\mathbf{P}(\mathbf{I}^{-1}\mathbf{P})^{k-1})=\\&\det(\mathbf{P}\cdot t+\mathbf{P}(\mathbf{I}^{-1}\mathbf{P})^{-1})\det\left((\mathbf{I}^{-1}\mathbf{P})^k\right)=\\&\det(\mathbf{P}\cdot t+\mathbf{I})\det\left((\mathbf{I}^{-1}\mathbf{P})^k\right),\end{aligned}$$

which shows that the above written power series is only multiplied by a constant factor $\det\left((\mathbf{I}^{-1}\mathbf{P})^k\right)$. The same is true for the coefficients, and since the determinants (used in the Cayley criterion) for the porisms are homogeneous in the power series' coefficients, they are vanishing independent of the choice of k. □

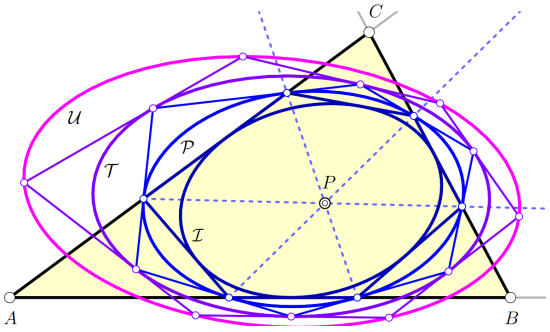

Figure 8: *The g-parallelian conic $\mathcal{P}$ and the g-parallelian inconic I constitute an exponential pencil of conics and set the basis for an infinite chain of nested poristic families of hexagons.*

Fig. 8 shows some conics out of the chain in the discrete exponential pencil spanned by I and $\mathcal{P}$. The conic $\mathcal{U}$ is the next in line: The coefficient matrix of its equation equals $\mathbf{U}=\mathbf{P}(\mathbf{I}^{-1}\mathbf{P})^2=\mathbf{T}\mathbf{I}^{-1}\mathbf{P}$, *i.e.*, $\mathcal{U}^\star$ ($\mathcal{U}$ considered as its set of tangents) is the polar image of $\mathcal{P}$ with regard to $\mathcal{T}$. The interscribed hexagons are also displayed. The order of the base conics I and $\mathcal{P}$ does not matter. Interchanging the matrices I and $\mathcal{P}$ in the usual parametrization of the exponential pencil as given in [13] means traversing the pencil in the opposite direction.

3 Tangent triangles

3.1 The triangle porism

There are two triples of tangents of the parallelian conic $\mathcal{P}$ that form two triangles $\Delta_U:=U_1U_2U_3$ and $\Delta_V:=V_1V_2V_3$ with a common circumconic $\mathcal{D}$. The vertices of the triangles are defined by

$$\begin{aligned}&U_1:=t_3\cap t_5,\ \ U_2:=t_5\cap t_1,\ \ U_3:=t_1\cap t_3,\\&V_1:=t_2\cap t_4,\ \ V_2:=t_4\cap t_6,\ \ V_3:=t_6\cap t_2.\end{aligned}\tag{10}$$

Note that the triangle $U_1U_2U_3$ and $V_2V_3V_1$ (note the different orientation) are perspective to P, while the corresponding trilaterals are perspective to p given by (3).

The common circumconic $\mathcal{D}$ of the triangles Δ_U and Δ_V can be described by the homogeneous equation

$$\begin{aligned}&\mathcal{D}:\\&\sum_{\text{cyclic}} l^2mn\xi\eta^2\zeta^2(m\eta+n\zeta)x^2+l\xi^2\Big(2l^2\xi^2(m^2\eta^2+n^2\zeta^2)+\\&\sum_{\text{cyclic}} lm\xi\eta(l^2\xi^2+m^2\eta^2)+4l^2mn\xi^2\eta\zeta\Big)yz=0.\end{aligned}\tag{11}$$

Now, it is near to formulate the following result:

Theorem 6 *The pair $(\mathcal{P},\mathcal{D})$ of conics allows for a triangle porism.*

Proof. The existence of the triangle porism is clear by the same reasoning as used in the proof of Thm. 3. □

We can deduce some more porisms out of the previously described one:

Theorem 7 *The pair of conics $(\mathcal{P},\mathcal{D})$ allows for a hexagon porism, and $3n$-gon porisms with $n\in\mathbb{N}\setminus\{0\}$.*

Proof. Like in the proof of Thm. 5, we use the Cayley criterion [12, p. 432, Thm. 9.5.4] in order to show the existence of porism with $3n$-gons inconic $\mathcal{P}$ and circumconic $\mathcal{D}$. For that purpose, we extract the coefficient matrices $\mathbf{D}$ and $\mathbf{P}$ from the equations of $\mathcal{D}$ and $\mathcal{P}$, and expand the function $\sqrt{\det(t\cdot\mathbf{D}+\mathbf{P})}$ in a power series $S=a_0+a_1t+a_2t^2+\ldots$. The criterion for the existence of a triangle porism is $a_2=0$ (which is clearly fulfilled). According to CAYLEY, the criteria for the existence of poristic families of hexagons, nonagons, ... equal

$$\det\begin{pmatrix}a_3&a_4\\a_4&a_5\end{pmatrix}=0,\ \ \det\begin{pmatrix}a_2&a_3&a_4&a_5\\a_3&a_4&a_5&a_6\\a_4&a_5&a_6&a_7\\a_5&a_6&a_7&a_8\end{pmatrix}=0,\ldots$$

which also turns out to be satisfied, as do the further criteria. □

Poristic families of quadrangles or other polygons with a vertex number that is not a multiple of 3 interscribed between $\mathcal{D}$ and $\mathcal{P}$ cannot occur for admissible choices of P (see also Tab. 2).

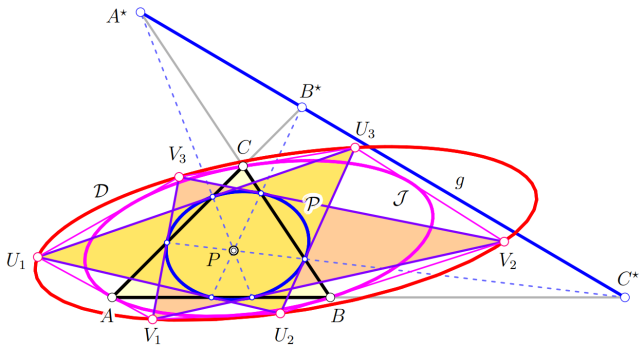

Figure 9: *The conic $\mathcal{D}$ through the vertices of the tangent triangles Δ_U and Δ_V of $\mathcal{P}$ and the inconic $\mathcal{J}$ of the hexagon $U_1V_1U_2V_2U_3V_3$ both give rise to two independent families of porisms.*

Here, we shall state explicitly that (in general) the existence of a poristic family of triangles does not necessarily imply the existence of a poristic family of hexagons, and *vice versa*.

The union of the two triangles Δ_U and Δ_V can be viewed as a degenerate hexagon. In that respect, $\mathcal{P}$ and $\mathcal{D}$ can already serve as a base of the pencil of conics allowing for a poristic family of hexagons. Indeed, the hexagon $H_2 := U_1V_1U_2V_2U_3V_3$ (alternately chosen vertices of Δ_U and Δ_V) is tangent to a single conic:

Theorem 8 *The hexagon H_2 has an inconic $\mathcal{J}$ with the trilinear equation*

$$\mathcal{J}: \sum_{\text{cyclic}} \frac{l\xi^2}{x} = 0 \tag{12}$$

which is at the same time a circumconic of the base triangle Δ.

Proof. We use the trilinear representation (10) of the vertices of Δ_U and Δ_V in order to compute the trilinear coordinates of the sides s_i of the hexagon. In order to find an equation of the inconic $\mathcal{J}$ of H_2, we compute the kernel of the 6×6 matrix whose columns (or rows) are the Veronese images of the trilinear coordinates of the six lines s_i (see [12, p. 241]). This kernel is one-dimensional (provided that the six lines are tangent to single conic) and a base vector of the kernel yields the coefficients of the equation

$$\mathcal{J}^\star: \sum_{\text{cyclic}} l^2\xi^4x^2 - 2mn\eta^2\zeta^2yz = 0$$

of a line conic (quadratic set of lines) containing the six sides s_i of H_2. The corresponding point conic $\mathcal{J}$ is the dual to $\mathcal{J}^\star$, and thus, the respective matrices are related by $\mathbf{J} = \mathbf{J}^{\star -1}$ (cf. [12, p. 273]). Hence, $\mathcal{J}$ is the inconic given in (12) and it is clearly seen that the vertices of Δ are contained in $\mathcal{J}$. □

We can also show:

Theorem 9 *The pair of conics $(\mathcal{J}, I)$ allows for poristic families of 3n-gons.*

Proof. We use the Cayley criterion (cf. [12, p. 432]) in order to verify the contents of this theorem. □

With the help of the Cayley criterion (cf. [12, p. 432]), we can show that the pair $(\mathcal{D}, \mathcal{J})$ allows for a poristic family of hexagons and even dodecagons.

The conics $\mathcal{D}$ and I span a pencil of the third kind. The pivot point P equals the common pole and the common polar line is already found as the common polar line of I and $\mathcal{P}$ with the trilinear representation (3).

As a consequence of Thms. 6, 7, 8, and 9 we can state a result on infinitely many poristic families of triangles and hexagons:

Theorem 10
1. The pair of conics $(\mathcal{D}, \mathcal{P})$ spans an exponential pencil of conics and any pair of subsequent conics in the pencil allows for a poristic family of 3n-gons.
2. The pair of conics $(\mathcal{D}, \mathcal{J})$ spans an exponential pencil of conics and any pair of subsequent conics in the pencil allows for a poristic family of hexagons.
3. The pair of conics $(\mathcal{J}, I)$ spans an exponential pencil of conics and any pair of subsequent conics in the pencil allows for a poristic family of 3n-gons.

4 Special assumptions and cases

In this section, we shall discuss the previously mentioned porisms in case of special choices of P and/or g. It is clear that the choice $g = a : b : c$ leads to the elementary geometric parallelians and the related porisms which are studied in detail in [1]. Another even more special and in some sense simpler case is obtained if $P = 1 : 1 : 1$ and $g = 1 : 1 : 1$. In terms of elementary triangle geometry, P is the incenter and g the anti-orthic axis. Moreover, g is the triangle polar of P (with respect to the base triangle Δ).

4.1 g antiorthic axis, $P = X_1$

The choice of $P = 1 : 1 : 1 = g$ yields

$$\mathcal{J}: \sum_{\text{cyclic}} xy = 0 \quad \text{and} \quad I: \sum_{\text{cyclic}} x^2 - 2yz = 0. \tag{13}$$

Conics with equations of that particular form belong to the family of Yff conics (cf. [19, 22]). The porism between I

and $\mathcal{J}$ are already studied even for various finite projective planes (see [22]) and turned out to be *Universal Porisms* in the sense of N. WILDBERGER [30]. In any case, I and $\mathcal{J}$ as given in (13) admit $3n$-gon porisms according to Thm. 9. The conics $\mathcal{P}$, $\mathcal{T}$, and $\mathcal{D}$ are not contained in the exponential pencil spanned by $\mathcal{J}$ and I.

4.2 g is the triangle polar line of P with respect to Δ

P is given by the homogeneous coordinates $\xi : \eta : \zeta \neq 0 : 0 : 0$, $\xi\eta\zeta \neq 0$, and P not on any side of the g-anticomplementary triangle, then P's triangle polar line is given by $\eta\zeta : \zeta\xi : \xi\eta$. The latter together with P comprises the pair of common pole and polar line of any two out of the five g-parallelian conics we have seen so far. This special assumption does not change the porisms that we have discovered in the previous sections. The Cayley criterion makes clear that no porisms other than such with triangle and hexagon families will occur.

The same holds true if we choose $P = \xi : \eta : \zeta = g$.

4.3 g ideal, pivot P a triangle center

If the line g is chosen as the ideal line of the plane of Δ, *i.e.*, $g = a : b : c$, then we deal with the case of Euclidean parallelians as described in [1]. However, in this case the centers of the conics $\mathcal{P}$, $\mathcal{T}$, I, $\mathcal{J}$, and $\mathcal{D}$ coincide with known triangle centers if we choose a triangle center for the pivot point. We do not aim at a complete list, some centers can be read off from Tab. 1. The numbers X_i given to the centers correspond to the list of triangle centers in [17, 18].

P	$C(\mathcal{P})$	$C(\mathcal{T})$	$C(I)$	$C(\mathcal{J})$	$C(\mathcal{D})$
X_1	X_{1001}	?	X_{1125}	X_3	?
X_2	X_2	X_2	X_2	X_2	X_2
X_3	X_{182}	?	X_{140}	X_{1147}	?
X_4	X_{10002}	?	X_5	X_{6523}	?
X_5	X_{10003}	?	X_{3628}	X_{6663}	?
X_6	X_{182}	?	X_{3589}	X_{206}	?
X_7	X_{10004}	?	X_{142}	X_{17113}	?
X_8	X_{10005}	?	X_{10}	X_{6552}	?
X_9	X_{1001}	?	X_{6666}	X_{6600}	?
X_{10}	X_{3842}	?	X_{3634}	X_{4075}	?
X_{11}	X_{1006}	?	X_{6667}	X_{64440}	?
X_{12}	?	?	X_{6668}	?	?
X_{19}	?	?	X_{40530}	X_{15259}	?
X_{20}	X_{47381}	?	X_3	?	?

Table 1: *The centers of the Euclidean parallelian conics $\mathcal{P}$, $\mathcal{T}$, I, $\mathcal{J}$, and $\mathcal{D}$ depending on certain choices of the pivot point P as a triangle center. The line g equals the ideal line $\omega = a : b : c$ in all cases and the numbers of the centers equal those in [17, 18].*

The question marks indicate yet unnamed triangle centers serving as centers of various g-parallelian conics.

5 Porisms of arbitrary types between different pairings of conics

In the following, we shall derive the conditions on the pivot point P such that poristic families of triangles, quadrangles, pentagons, and hexagons occur between any pair of conics out of the five conics $\mathcal{P}$, $\mathcal{T}$, I, $\mathcal{D}$, and $\mathcal{J}$. It turns out that these conditions are certain algebraic loci in the plane of Δ. In the majority of the cases, these loci are elliptic cubics and elliptic sextics. in some cases, the degrees of the loci are even higher, and then, we simply write $\mathcal{C}^d$ for a degree d curve.

In Table 2, we list the sets of possible pivot points for certain types of porisms. Some of these set occur frequently: We define $\mathbb{P}^{2\star} = \mathbb{P}^2 \setminus \{\Delta^\star, \Delta_a^\star\}$. The cubic curves that show up regularly belong to a certain class of (triangle) cubics. Their equations are of similar shapes and depend on two (homogeneous) parameters:

$$\mathcal{C}^3_{\alpha,\beta} = \alpha \left(\sum_{\text{cyclic}} lm(lx+my)xy \right) + \beta\, lmnxyz = 0, \qquad \alpha : \beta \neq 0 : 0.$$

We note that in this linear one-parameter family of cubics we find three degenerate curves. These are $\mathcal{C}^3_{0,1} = \Delta^\star$, $\mathcal{C}^3_{1,2} = \Delta_a^\star$, and $\mathcal{C}^3_{1,3} = \mathcal{S}' \cap g$. The family also contains the rational cubic $\mathcal{C}_{1,-6}$ with an isolated node at $l^{-1} : m^{-1} : n^{-1}$ with the complex conjugate tangents

$$lx + \varepsilon my + \varepsilon^2 nz = 0 \quad \text{and} \quad lx + \varepsilon^2 my + \varepsilon nz = 0,$$

where ε is a complex (not real) cube root of 1.

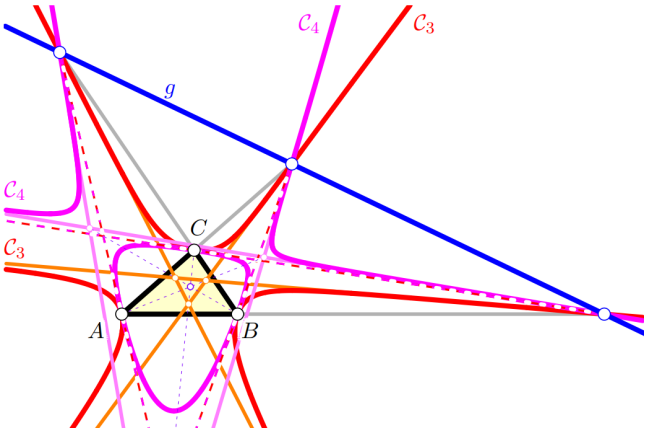

Figure 10: *Two examples of cubics $\mathcal{C}_3$, $\mathcal{C}_4$ housing pivot points for parallelian conics allowing for triangle and quadrangle porisms between $\mathcal{J}$ and $\mathcal{P}$.*

Fig. 10 shows two of the cubics on which a pivot point P is to be chosen such that a triangle or quadrangle porism between two particular conics comes into being.

The loci of pivot points possibly allowing for triangle, quadrangle, pentagon, and hexagon porisms are in some cases sextic curves of the same type as the curve (9) appearing in Section 2.3. These curves form a linear four-parameter family with the equations

$$\mathcal{C}^6_{\alpha,\beta,\gamma,\delta} = \alpha\left(\sum_{\text{cyclic}} l^2m^2(l^2x^2+m^2y^2)x^2y^2\right) + \beta\left(\sum_{\text{cyclic}} l^4mnx^4yz\right) + \gamma\left(\sum_{\text{cyclic}} l^3mn(my+nz)x^3yz\right) + \delta l^2m^2n^2x^2y^2z^2 = 0, \quad \alpha:\beta:\gamma:\delta \neq 0:0:0:0.$$

	triangles	quadrangles	pentagons	hexagons
$(\mathcal{T},\mathcal{P})$	$\emptyset$	$\emptyset$	$\emptyset$	$\mathbb{P}^{2\star}$
$(\mathcal{P},\mathcal{T})$	$\mathcal{C}^{12}$	$\mathcal{C}^3_{1,0}$, $\mathcal{C}^3_{1,0}$, $\mathcal{C}^{12}$	$\mathcal{C}^{36}$	$\mathcal{C}^6_{1,2,10,30}$, $\mathcal{C}^6_{1,2,2,-2}$, 2 $\mathcal{C}^{12}$
$(\mathcal{P},I)$	$\emptyset$	$\emptyset$	$\emptyset$	$\mathcal{P}^{2\star}$
$(I,\mathcal{P})$	$\mathcal{C}^{12}$	$\mathcal{C}^3_{1,1}$, $\mathcal{C}^3_{1,4}$, $\mathcal{C}^{12}$	$\mathcal{C}^{36}$	$\mathcal{C}^6_{1,2,2,2}$, $\mathcal{C}^6_{1,2,2,10}$, 3 $\mathcal{C}^{12}$
$(\mathcal{D},\mathcal{P})$	$\mathcal{P}^{2\star}$	$\emptyset$	$\emptyset$	$\mathcal{P}^{2\star}$
$(\mathcal{P},\mathcal{D})$	$\mathcal{C}^3_{1,1}$, $\mathcal{C}^3_{1,4}$, $\mathcal{C}^6_{1,2,-2,,-10}$	$\mathcal{C}^{12}$, $\mathcal{C}^6_{1,2,2,-2}$	2 $\mathcal{C}^9$, $\mathcal{C}^{18}$	$\mathcal{C}^3_{1,0}$, $\mathcal{C}^3_{1,4}$, $\mathcal{C}^6_{1,2,-2,-10}$, $\mathcal{C}^{12}$, $\mathcal{C}^{24}$
$(\mathcal{P},\mathcal{J})$	$\mathcal{C}^6_{1,2,-4,-5}$	$\mathcal{C}^3_{1,-1}$, $\mathcal{C}^6_{1,2,-2,-7}$	$\mathcal{C}^{18}$	$\mathcal{C}^3_{1,-5}$, $\mathcal{C}^6_{1,2,-4,-5}$, $\mathcal{C}^{12}$
$(\mathcal{J},\mathcal{P})$	$\mathcal{C}^3_{4,3}$	$\mathcal{C}^3_{10,21}$	$\mathcal{C}^9$	$\mathcal{C}^3_{4,3}$, $\mathcal{C}^3_{16,39}$, $\mathcal{C}^6_{64,128,692.1257}$
$(\mathcal{T},I)$	$\mathcal{C}^3_{1,4}$	$\mathcal{C}^3_{3,14}$	$\mathcal{C}^3_{1,5}$, $\mathcal{C}^6_{1,2,13,32}$	$\mathcal{C}^3_{1,4}$, $\mathcal{C}^3_{1,6}$, $\mathcal{C}^9$
$(I,\mathcal{T})$	$\mathcal{C}^3_{1,0}$, $\mathcal{C}^3_{1,4}$, $\mathcal{C}^{12}$, $\mathcal{C}^6_{1,2,14,30}$	$\mathcal{C}^{12}$, $\mathcal{C}^{24}$	2 $\mathcal{C}^9$, $\mathcal{C}^{18}$, $\mathcal{C}^{36}$	?
$(\mathcal{T},\mathcal{D})$	$\mathcal{C}^6_{1,2,-4,-5}$	$\mathcal{C}^3_{1,-1}$, $\mathcal{C}^6_{1,2,-2,-7}$	$\mathcal{C}^{18}$	$\mathcal{C}^3_{1-54}$, $\mathcal{C}^6_{1,2,-4,-5}$, $\mathcal{C}^{12}$
$(\mathcal{D},\mathcal{T})$	$\mathcal{C}^3_{4,3}$	$\mathcal{C}^3_{10,21}$	$\mathcal{C}^9$	$\mathcal{C}^3_{4,3}$, $\mathcal{C}^3_{16,39}$, $\mathcal{C}^6_{64,128,692,1257}$
$(\mathcal{T},\mathcal{J})$	$\emptyset$	$\mathcal{C}^3_{1,1}$, $\mathcal{C}^3_{1,-7}$	$\mathcal{C}^3_{1,-1}$, $\mathcal{C}^3_{1,5}$, $\mathcal{C}^6_{1,2,-2,-7}$	$\mathcal{C}^3_{1,-3}$, $\mathcal{C}^9$
$(\mathcal{J},\mathcal{T})$	$\mathcal{C}^3_{1,0}$, $\mathcal{C}^3_{5,12}$, $\mathcal{C}^6_{3,6,64,66}$	$\mathcal{C}^6_{1,2,-6,-18}$, $\mathcal{C}^{12}$	$\mathcal{C}^9$, $\mathcal{C}^{18}$	$\mathcal{C}^3_{1,0}$, $\mathcal{C}^3_{5,12}$, $\mathcal{C}^3_{3,6,64,66}$, $\mathcal{C}^{12}$, $\mathcal{C}^{24}$
$(I,\mathcal{D})$	$\mathcal{C}^{24}$	$\mathcal{C}^{12}$, $\mathcal{C}^{24}$	$\mathcal{C}^{96}$	?
$(\mathcal{D},I)$	$\emptyset$	$\mathcal{C}^3_{1,4}$	$\mathcal{C}^6_{4,8,35,70}$	$\mathcal{C}^6_{1,2,13,32}$
$(\mathcal{J},I)$	$\mathbb{P}^{2\star}$	$\emptyset$	$\emptyset$	$\mathbb{P}^{2\star}$
$(I,\mathcal{J})$	$\mathcal{C}^3_{1,0}$, $\mathcal{C}^3_{1,4}$, $\mathcal{C}^6_{1,2,-2,-10}$	$\mathcal{C}^3_{1,\pm\sqrt{8}}$, $\mathcal{C}^6_{1,2,\pm\sqrt{8},\pm\sqrt{8}}$	2 $\mathcal{C}^9$, $\mathcal{C}^{18}$	$\mathcal{C}^3_{1,0}$, $\mathcal{C}^3_{1,4}$, $\mathcal{C}^6_{1,2,-2,-10}$ $\mathcal{C}^{12}$, $\mathcal{C}^{24}$
$(\mathcal{D},\mathcal{J})$	$\emptyset$	$\emptyset$	$\emptyset$	$\mathbb{P}^{2\star}$
$(\mathcal{J},\mathcal{D})$	$\mathcal{C}^{12}$	$\mathcal{C}^3_{1,0}$, $\mathcal{C}^3_{1,4}$, $\mathcal{C}^{12}$	$\mathcal{C}^{36}$	$\mathcal{C}^6_{1,2,2,-2}$, $\mathcal{C}^6_{1,2,10,30}$, 3 $\mathcal{C}^{12}$

Table 2: *The porisms and chains of porism between various pairs of g-parallelian conics.*

The sextic curves of this type *that occur as loci of pivot points P* have six double points and are of genus 1. This is not the case for arbitrary choices of $\alpha:\beta:\gamma:\delta$. Three of the six double points are ordinary nodes, the remaining three are tacnodes. The latter carry a flat point on one of the linear branches at the node. For details on tangents, see Sec. 2.3.

The order of the conics in the pairs $(\mathcal{A},\mathcal{B})$ matters: CAYLEY's criterion [12, p. 432, Thm. 9.5.4] uses the coefficients of the power series of $\sqrt{\det(t\cdot\mathbf{A}+\mathbf{B})}$ and it is easily verified that $\det(t\cdot\mathbf{B}+\mathbf{A})=\det(\mathbf{B}\mathbf{A}^{-1}\cdot\mathbf{A}\mathbf{B}^{-1}(t\cdot\mathbf{B}+\mathbf{A}))=\det(\mathbf{B}\mathbf{A}^{-1})\cdot\det(t\cdot\mathbf{A}+\mathbf{A}\mathbf{B}^{-1}\mathbf{A})\neq\det(t\cdot\mathbf{A}+\mathbf{B})$. The first conic, here $\mathcal{A}$, is assumed to be the 'circumconic'. In many cases, this is also justified by the fact that the circumconic contains six points obtained as the intersection of certain tangents of the 'inconic'. This might be of importance in finite geometries or in geometries over algebraically non-closed fields.

6 Conclusion and final remarks

The porisms constructed in the previous sections are objects of projective geometry. Their embeddings in metric (Euclidean or non-Euclidean) geometries can be studied from the projective point of view by prescribing an elliptic or a hyperbolic involution on g. This yields the cases of Euclidean and pseudo-Euclidean parallelians and the related conics. The counterparts in elliptic and hyperbolic geometry are not that near. The algebraic curves given in Tab. 2 are not studied in detail and it is questionable whether these pivot loci allow for an investigation of the corresponding porisms. The rather high algebraic degrees may not be helpful.

References

[1] BOŽIĆ DRAGIN, I., KONCUL, H., ODEHNAL, B., Conics and Transformations defined by the Parallelians of a Triangle. *Mathematics* **13**(21) (2025), https://doi.org/10.3390/math13213424

[2] BRIESKORN, E., KNÖRRER, M., *Plane Algebraic Curves.* Birkhäuser, Basel, 1986.

[3] DEL CENTINA, A., Poncelet's Porism: a long story of renewed discoveries I. *Arch. Hist. Exact Sci.* **70**(1) (2016), 1–122, https://doi.org/10.1007/s00407-015-0163-y

[4] COOLIDGE, J.L., *A Treatise on Algebraic Plane Curves.* Dover Publications, New York, 1959.

[5] FLATTO, L., *Poncelet's theorem.* American Mathematical Society, Providence, RI, 2008, https://doi.org/10.1090/mbk/056

[6] GARCIA, R.A., KOILLER, J., REZNIK, D., Loci of 3-periodics in an Elliptic Billiard: Why so many ellipses? *J. Symb. Comp.* **114** (2023), 336–358, https://doi.org/10.1016/j.jsc.2022.06.001

[7] GARCIA, R.A., ODEHNAL, B., REZNIK, D., Loci of Poncelet Triangles in the General Closure Case. *J. Geom.* **113**, 17 (2022), https://doi.org/10.1007/s00022-022-00629-3

[8] GARCIA, R.A., ODEHNAL, B., REZNIK, D., Poncelet porisms in hyperbolic pencils of circles. *J. Geom. Graph.* **25**(2) (2021), 205–225.

[9] GARCIA, R.A., REZNIK, D., Loci of the Brocard points over selected triangle families. *Intl. J. Geom.* **11**(2) (2022), 35–45.

[10] GARCIA, R.A., REZNIK, D., KOILLER, J., New properties of triangular orbits in elliptic billiards. *Am. Math. Mon.* **128**(10) (2021), 898–910.

[11] GARCIA, R., REZNIK, D., STACHEL, H., HELMAN, M., Steiner's Hat: a Constant-Area Deltoid Associated with the Ellipse. *KoG* **24** (2020), 12–28, https://doi.org/10.31896/k.24.2

[12] GLAESER, G., STACHEL, H., ODEHNAL, B., *The Universe of Conics.* From the Ancient Greeks to 21st century developments (2nd edition), Springer-Verlag, Berlin - Heidelberg, 2024, https://doi.org/10.1007/978-3-662-70306-9

[13] HALBEISEN, L., HUNGERBÜHLER, N., The exponential pencil of conics. *Beitr. Algebra Geom.* **59** (2018), 549–571, https://doi.org/10.1007/s13366-017-0375-1

[14] HELMAN, M., GARCIA, R.A., REZNIK, D., Intriguing invariants of centers of ellipse-inscribed triangles. *J. Geom.* **112**(2) (2021), 28, https://doi.org/10.1007/s00022-021-00586-3

[15] HELMAN, M., LAURAIN, D., GARCIA, R., REZNIK, D., Invariant Center Power and Elliptic Loci of Poncelet Triangles. *J. Dyn. Control Syst.* **29** (2021), 157–184, https://doi.org/10.1007/s10883-021-09580-z

[16] JURKIN, E., Poncelet Porisms and Loci of Centers in the Isotropic Plane. *Mathematics* **12** (4) (2024), 618, https://doi.org/10.3390/math12040618

[17] KIMBERLING, C., *Encyclopedia of Triangle Centers*. Available at: https://faculty.evansville.edu/ck6/encyclopedia

[18] KIMBERLING, C., Triangle Centers and Central Triangles. (*Congressus Numerantium Vol. 129*) Utilitas Mathematica Publishing, Winnipeg, 1998.

[19] KIMBERLING, C., Yff conics., *J. Geom. Graph.* **12**(1) (2008), 23–34.

[20] ODEHNAL, B., Generalized Gergonne and Nagel points. *Beitr. Algebra Geom.* **51**(2) (2010), 477–491.

[21] ODEHNAL, B., Poristic Loci Triangle Centers. *J. Geom. Graph.* **15**(1) (2011), 45–67.

[22] ODEHNAL, B., Universal Porisms and Yff Conics. *KoG* **28**, (2024) 11–24, https://doi.org/10.31896/k.28.3

[23] ODEHNAL, B., REZNIK, D., Circumparabolas in Chapple's porism. In: *ICGG 2022 - Proceedings of the 20th International Conference on Geometry and Graphics*. Cheng, L-.Y. (ed.) Lecture Notes on Data Engineering and Communications Technologies vol. 146, 47–58, Springer, https://doi.org/10.1007/978-3-031-13588-0_4

[24] STACHEL, H., A Triple of Projective Billiards. *KoG* **26** (2022), 44–51, https://doi.org/10.31896/k.26.4

[25] STACHEL, H., Billiard Motions in Ellipses - Invariants of Projective Nature. *Proceedings of the Slovak-Czech Conference on Geometry and Graphics*, Kočovce, Slovakia 2021, 143–148.

[26] STACHEL, H., Isometric Billiards in Ellipses and Focal Billiards in Ellipsoids. *J. Geom. Graph.* **25**(1) (2021), 97–118.

[27] STACHEL, H., On the Diagonals of Billiards. In: Cheng, L.-Y. (ed): ICGG 2022 - *Proceedings of the 20th International Conference on Geometry and Graphics*, São Paulo/Brazil 2022, Springer Nature Switzerland AG 2023, 19–33.

[28] STACHEL, H., On the Motion of Billiards in Ellipses. *Europ. J. Math.* **8** (Special Issue: New Developments in Integrable Systems) (2022), 1602–1622, https://doi.org/10.1007/s40879-021-00524-2

[29] STACHEL, H., The Geometry of Billiards in Ellipses and their Poncelet Grids. *J. Geom.* **112**, 40 (2021), https://doi.org/10.1007/s00022-021-00606-2

[30] WILDBERGER, N.J., *Divine Proportions: Rational Trigonometry to Universal Geometry.* Wild Egg Pty. Ltd., Australia, 2005.

Boris Odehnal
orcid.org/0000-0002-7265-5132
e-mail: boris.odehnal@uni-ak.ac.at

University of Applied Arts Vienna
Oskar-Kokoschka-Platz 2, A-1010 Vienna, Austria

INSTRUCTIONS FOR AUTHORS

SCOPE. "KoG" publishes scientific and professional papers from the fields of geometry, applied geometry and computer graphics.

SUBMISSION. Scientific papers submitted to this journal should be written in English, professional papers should be written in Croatian or English. The papers have not been published or submitted for publication elsewhere.
The manuscript should be sent in PDF format via e-mail to the editor:

Ema Jurkin
ema.jurkin@rgn.unizg.hr

The first page should contain the article title, author and coauthor names, affiliation, a short abstract in English, a list of keywords and the Mathematical subject classification.

UPON ACCEPTANCE. After the manuscript has been accepted for publication authors are requested to send its LaTex file via e-mail to the address:

ema.jurkin@rgn.unizg.hr

Figures should be titled by the figure number that match to the figure number in the text of the paper.

The corresponding author and coauthors will receive hard copies of the issue free of charge.

How to get KoG?

The easiest way to get your copy of KoG is by contacting the editor's office:

Marija Šimić Horvath
marija.simic@arhitekt.unizg.hr
Faculty of Architecture
Kačićeva 26, 10 000 Zagreb, Croatia
Tel: (+385 1) 4639 176

The price of the issue is €15 + mailing expenses €5 for European countries and €10 for other parts of the world.

The amount is payable to:

ACCOUNT NAME:	Hrvatsko društvo za geometriju i grafiku Kačićeva 26, 10000 Zagreb, Croatia
IBAN:	HR8623600001101517436